TECHNISCHE
UNIVERSITÄT
WIEN
Vienna University of Technology

DIPLOMARBEIT

Working point and resonance studies at the CERN Proton Synchrotron

Ausgeführt am

Europäischen Kernforschungszentrum CERN
CH-1211
Genf 23

und am

Atominstitut der Technischen Universität Wien
Stadionallee 2
1020 Wien

unter der Anleitung von
Privatdoz. Dipl.-Ing. Dr.techn. Michael Benedikt

durch
Alexander Huschauer, BSc
Dr. Adolf Schärfstraße 3/7/14
2353 Guntramsdorf

Genf, im September 2012 Alexander Huschauer

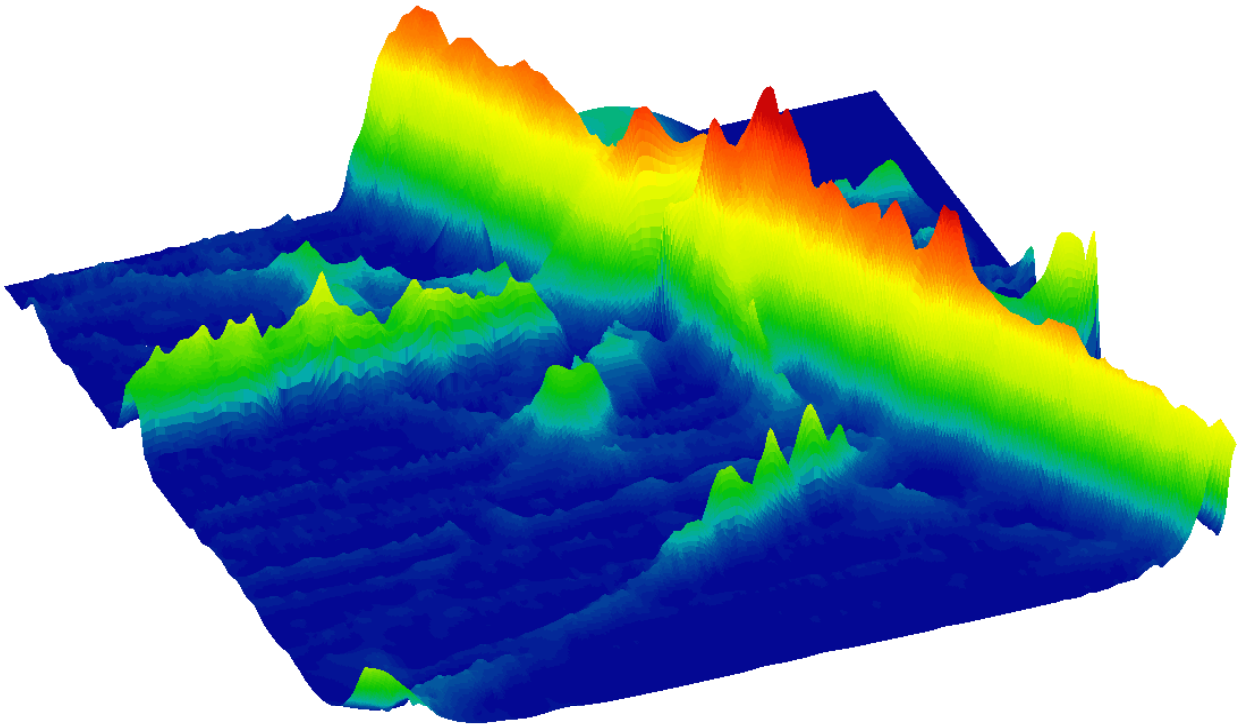

A proton's understanding of resonances.

Abstract

The Proton Synchrotron (PS) is the oldest yet the most versatile particle accelerator operating at CERN. Having accelerated a multitude of different particle species within the last five decades, it is today used to define the longitudinal structure of the proton beams going into collision in the Large Hadron Collider (LHC), and thus constitutes an integral part of the LHC injector chain.

Around 2020 the LHC will be subject to an upgrade to significantly increase the number of collisions at the interaction points. The beam parameters demanded by the High Luminosity LHC (HL-LHC) will, as a result, require substantial improvements of the pre-accelerators, which are currently being studied within the LHC Injectors Upgrade (LIU) project.

The increase of luminosity will be accompanied by an increase of beam intensity, which might result in instabilities appearing on the injection flat bottom of the PS. Transverse Head-Tail instabilities have already been observed on operational LHC beams and an alternative stabilizing mechanism for this type of instability is currently being studied. It consists of reducing the mode number of the transverse oscillation by changing linear chromaticity and in succession completely damping the instability by a damper system with appropriate bandwidth.

However, nowadays at the PS there is no chromaticity correction scheme implemented at low energy. Special circuits mounted on top of the main magnet poles - the Pole Face Windings (PFW) - could account for that, but so far they are only used to control the betatron tunes and linear chromaticities at high energy. The first part of this thesis is therefore dedicated to extensive studies concerning the correction of betatron tunes, linear and higher order chromaticities by exploitation of the intrinsic opportunities these special circuits offer at low energy.

An additional limitation of the PS for high-brightness and high-intensity beams is the presence of beam destructive betatron resonances, which restrict the choice of the injection working point and the maximum acceptable tune spread. This is especially the case for the double batch injection for LHC beams: four bunches are kept at injection energy for 1.2 seconds, leaving enough time for degradation of the transverse beam characteristics in case the space charge induced tune spread causes the beam to touch stop bands of different resonances. Detailed knowledge of the working point plane is thus necessary in order to choose both transverse tunes in an area sufficiently free of resonances. To improve the current working point control scheme, the influence of the PFW on the machine resonances is examined in the second part of this thesis, leading to a deeper understanding of the limits of the PS.

Acknowledgments

Firstly, I would like to thank my university supervisor, Michael Benedikt, for all his support and for establishing contact with my CERN supervisor and, therefore, making this thesis possible in the first place.

I would like to express my gratitude to my CERN supervisor, Rende Steerenberg, who offered me the possibility of conducting the research for my thesis at the Proton Synchrotron. I would like to thank him for his continuous support and guidance, and for all of our professional and personal discussions.

I am greatly indebted to Simone Gilardoni, who never tired of answering my questions and who was always willing to share his extensive knowledge with me.

It has been a great pleasure to be a part of the PS operations crew, and I would like to thank all my colleagues for making me feel welcome from the very first day of my arrival and for all their advice during the many, many days and nights I spent in the CCC. Furthermore, I am grateful to the PSB operations crew, who always found a way to accommodate my particular requirements in terms of beam characteristics.

I would also like to express my gratitude to Giuliano Franchetti, not only for his ideas concerning the identification of betatron resonances, but also for fruitful discussions improving my understanding of space charge effects.

I owe my deepest gratitude to all my friends, family and especially my parents, who have always supported me and, therefore, allowed me to find my own path.

Finally, I wish to thank Tanja for all her love, encouragement and understanding throughout the previous years, and I am looking forward to continuing this journey together.

Contents

1 Basic accelerator physics

The development of the first particle accelerators in the 1920s led to revolutionary possibilities for examination and understanding of the constitution of matter. Nuclear reactions could suddenly be provoked within laboratories by accelerating particles to kinetic energies of a few MeV[1].
At today's high energy frontier, physicists benefit from the Large Hadron Collider (LHC) at CERN[2] with a design beam energy of 7 TeV, an increase of six orders of magnitude compared to the first machines. However, the majority of the 30.000 particle accelerators available worldwide is not used for fundamental physics research, but has instead found application in biology, industry and medicine.
The following introduction to accelerator physics is based on [1–6], where more detailed explanation can be found.

1.1 Guiding particles in an accelerator

Within a particle accelerator, electrically charged particles experience accelerating forces by electric fields while magnetic fields arrange for deflective forces and therefore determine the particles' trajectories. These processes of acceleration and guiding are exclusively based on the Lorentz force[3]

$$\mathbf{F} = q\,(\mathbf{E} + \mathbf{v} \times \mathbf{B}). \tag{1.1}$$

For proton machines the electric charge q simply corresponds to one elementary charge e and $\mathbf{E}$ and $\mathbf{B}$ describe the electric and magnetic fields influencing a particle moving with velocity

[1] 1 eV = 1.602176565·10^{-19} J
[2] European Organisation for Nuclear Research, situated in Geneva, Switzerland
[3] Shown in its non-relativistic representation.

v. At CERN high energies are achieved by accelerating particles in circular machines, so-called synchrotrons. Within these machines, dipole magnets generate homogeneous magnetic fields perpendicular to the direction of motion of the particles to bend them onto circular orbits and electric fields inside radio frequency (RF) cavities provide the necessary acceleration. The synchrotron principle illustrates a necessary synchronization between the magnetic field and the beam energy or the beam momentum p, described by the formula:

$$p\ [\mathrm{GeV/c}] = \frac{B\ [\mathrm{T}]\ \rho\ [\mathrm{m}]}{3.3356}. \tag{1.2}$$

The higher the momentum, the higher the magnetic field needs to be in order to keep the particles on the ideal orbit, which corresponds to the central path through all magnets. Figure 1.1 shows a certain magnetic cycle of the CERN Proton Synchrotron (see Chapter 2), which visualizes this relationship. The particle momentum follows the time dependent programming of the magnetic field in order to comply with (1.2).

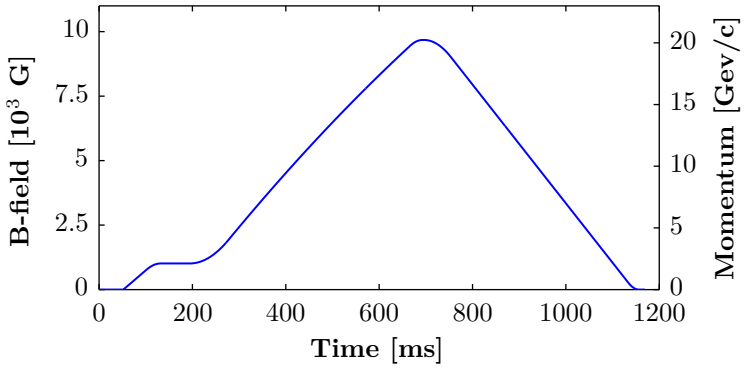

Figure 1.1: Magnetic cycle of the beam sent to the n_TOF[4] facility [7] by the CERN Proton Synchrotron.

The motion of a particle on an ideal orbit with fixed bending radius ρ is characterized by the coordinate system shown in Fig. 1.2. The transverse coordinates x and y correspond to the horizontal and vertical planes and the longitudinal position of a particle is described by the coordinate s.

In reality, bunches containing billions of particles are accelerated within the vacuum chamber of an accelerator and do not behave in the way an ideal particle would. In order to keep the beam inside the chamber, regardless, forces to restrict the transverse motion have to be applied. These are created by quadrupole magnets, which cause focusing around the ideal orbit by a magnetic field, that is no longer homogeneous but depends linearly on the transverse displacement of

[4] Neutron time-of-flight

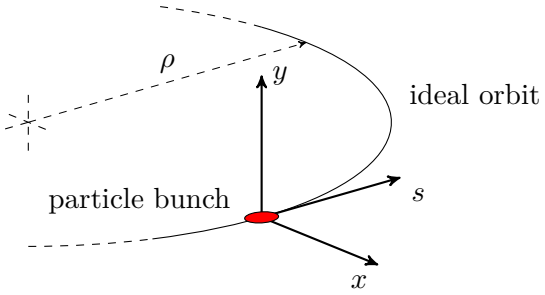

Figure 1.2: Coordinate system within a circular accelerator.

the particles. To obtain this field configuration, the four poles of a quadrupole magnet are hyperbolically shaped, causing a field-free region in its center.

1.2 Transverse motion

A single particle traveling through a short quadrupole magnet encounters a change of transverse divergence angles

$$x' = \frac{dx}{ds} \qquad \text{and} \qquad y' = \frac{dy}{ds} \tag{1.3}$$

due to the divergence kicks

$$\Delta x' = xkl \qquad \text{and} \qquad \Delta y' = -ykl. \tag{1.4}$$

These kicks depend on the current particle position (x,y), the normalized quadrupole gradient

$$k = \frac{1}{B\rho}\frac{dB_y}{dx} \tag{1.5}$$

and the magnet length l.
According to (1.4), it is impossible to apply focusing forces in both transverse planes at the same time. A focusing quadrupole is therefore defined to have a focusing effect in the horizontal and a defocusing effect in the vertical plane. Rotating such an element by 90° about its longitudinal axis, or inverting its excitation currents, leads to a defocusing quadrupole, which is vertically focusing.
In order to provide stable particle motion along an accelerator, an alternating arrangement of focusing and defocusing magnets is required.
The resulting distribution of focusing forces around a machine can be described by a position

dependent gradient $K(s)$ leading to Hill's equation for the transverse motion of a particle:

$$\frac{d^2x}{ds^2} + K(s)x = 0, \tag{1.6}$$

which resembles the one of a harmonic oscillator. Its general periodic solution can be written as

$$x = \sqrt{\varepsilon\beta(s)}\, cos(\phi(s) + \phi_0) = \sqrt{\varepsilon\beta}\, cos(\phi), \tag{1.7}$$

with $\beta(s)$ being the optical beta function and $\sqrt{\varepsilon\beta(s)}$ describing the variation of the maximum particle amplitude around the ring. The particle's phase advance is given by $\phi(s)$ while ϕ_0 represents the initial phase. The derivative of (1.7) yields

$$x' = \frac{\beta'}{2}\sqrt{\frac{\varepsilon}{\beta}}\, cos(\phi) - \sqrt{\varepsilon\beta}\, \phi' sin(\phi) \tag{1.8}$$

and both equations lead to a parametric representation of an ellipse in the transverse phase space $\{x,x'\}$, as the phase advance $\phi(s)$ goes from 0 to 2π. While a particle moves around an accelerator in real space it follows an ellipse in the phase space as shown in Fig. 1.3. Consecutive turns are represented by points and separated according to the phase advance per turn, ϕ_c.

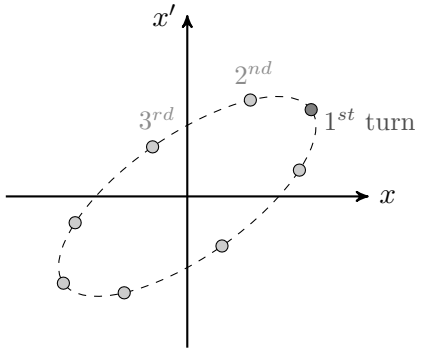

Figure 1.3: Horizontal phase space ellipse for $\phi_c = 45°$ at a constant longitudinal position s. After eight turns the particle returns to its initial conditions.

The orientation and the shape of the ellipse is determined by the lattice, i.e. the arrangement of magnets within an accelerator, and varies depending on the longitudinal position. The ellipse is furthermore characterized by its area $\pi\varepsilon$, which, according to Liouville's theorem, is a constant of motion as long as only conservative forces are present and the energy of the particle remains

constant. The term ε is referred to as emittance with mm·mrad being its unit. Neglecting higher order magnetic fields and other coupling mechanisms, the horizontal, vertical and longitudinal phase space can be treated independently and, therefore, one can define an emittance in each plane.
Concerning a multitude of particles circulating in a machine one then passes on to a statistical approach. Usually, particle beams are described by means of Gaussian distributions and the term emittance then refers to the area in the phase space which is occupied by a certain percentage of particles.
Due to the special choice of the phase space coordinates x and x' - which are not canonic conjugated - Liouville's theorem is not complied with during acceleration.
The particle momentum is given by

$$p = m\,v = m_0\,c\,\beta_{rel}\,\gamma_{rel}, \tag{1.9}$$

where m_0 is the rest mass of the particle, c the velocity of light, $\beta_{rel} = \frac{v}{c}$ and $\gamma_{rel} = \frac{E}{E_0}$, with E representing the particle's total energy and E_0 its rest energy. An increase of momentum occurs exclusively in the longitudinal plane, causing a reduction of transverse divergence angles. This effect of adiabatic damping leads to shrinking transverse emittances and, therefore, these parameters are no longer constants of motion.
Instead of the physical emittance, one therefore defines the normalized emittance

$$\varepsilon^*_{x,y} = \beta_{rel}\,\gamma_{rel}\,\varepsilon_{x,y}, \tag{1.10}$$

by using the relativistic momentum $\beta_{rel}\,\gamma_{rel}$ as normalization factor. ε^* also remains invariant during acceleration and, therefore, allows comparison of transverse beam parameters between different machines.
Another important parameter in accelerator physics is the number of transverse oscillations a particle carries out each turn. This value is obviously closely correlated to the phase advance per turn and defined as the betatron tune

$$Q = \frac{\phi_c}{2\pi} = \frac{1}{2\pi} \oint \frac{ds}{\beta(s)}. \tag{1.11}$$

For two different values of Q the resulting oscillations are shown in Fig. 1.4.

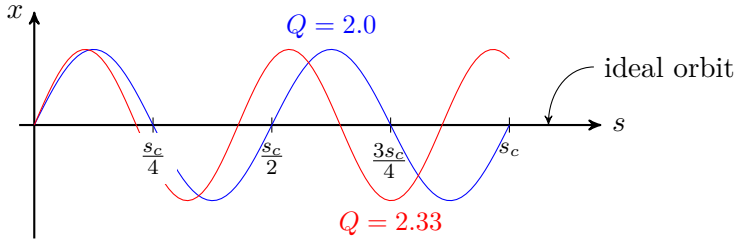

Figure 1.4: Transverse oscillations inside a synchrotron of circumference s_c.

1.3 Longitudinal motion

During the process of acceleration, RF cavities operate at the revolution frequency f_{rev} of the beam forming a certain area - the so-called bucket - in which a particle bunch can be situated. By tuning these cavities to

$$f_{RF} = h \cdot f_{rev}, \tag{1.12}$$

acceleration of h bunches becomes possible, where h is an integer and is called the harmonic number.
The revolution frequency of a particle on the ideal orbit is defined as

$$f_{rev} = \frac{v}{s_c}, \tag{1.13}$$

and its change for a particle with slightly different momentum is described by

$$\frac{df_{rev}}{f_{rev}} = \frac{dv}{v} - \frac{ds}{s_c}. \tag{1.14}$$

This change in revolution frequency is therefore determined by the difference between the change in velocity and the change in orbit length. In order to illustrate the relationship between a change in revolution frequency and a change in momentum, (1.14) can be expressed as

$$\frac{df_{rev}}{f_{rev}} = \left(\frac{1}{\gamma_{rel}^2} - \frac{1}{\gamma_{tr}^2} \right) \frac{dp}{p}, \tag{1.15}$$

where γ_{tr} describes the relative transition energy, which depends on the lattice and is therefore different for each accelerator. For a particle with positive momentum deviation the revolution frequency increases in the same way the momentum does, as long as the particle energy remains below transition energy. Above transition, this is no longer the case and increasing momentum leads to a longer revolution period. The slip factor

$$\eta = \left(\frac{1}{\gamma_{rel}^2} - \frac{1}{\gamma_{tr}^2} \right) \tag{1.16}$$

is therefore positive below, negative above and vanishes at transition.
In the previous section transverse focusing forces were introduced in order to obtain a stable orbit by constraining the motion of particles. In the longitudinal plane, the principle of phase stability allows a similar approach, which is closely correlated to the value of η.

Within a bunch, one particle is defined to be the synchronous particle, meaning that it arrives turn after turn at the same moment with respect to the voltage function in the RF cavity and, therefore, always gains the same amount of energy. In Fig. 1.5 this particle and the corresponding synchronous phase φ_s are indicated by the black dot on the rising edge of the sine wave. A second particle with the same energy entering the cavity late with respect to the synchronous one - indicated by the white dot - experiences a higher voltage and is therefore accelerated more, leading to higher particle velocity and higher revolution frequency. Turn by turn, this particle approaches φ_s until it arrives at the cavity at exactly the same moment as the synchronous particle, but with a revolution frequency that remains higher. One turn later it will arrive early with respect to φ_s, where it sees less voltage. Once this particle has the same revolution frequency as the synchronous particle it will reapproach φ_s leading to an oscillatory motion around the synchronous phase. Accordingly, operation on the rising edge of the voltage function provides a means for longitudinal stabilization provided an increase of energy leads to higher revolution frequency and, therefore, only for $\eta > 0$.
Above transition particles are traveling almost at the speed of light and the energy gain mainly increases the relativistic mass of the circulating particles, enhancing the length of the orbit of particles with a positive momentum deviation, while decreasing the revolution frequency. This necessitates a change of the synchronous phase to $\pi - \varphi_s$, causing acceleration on the falling edge (see Fig. 1.5).

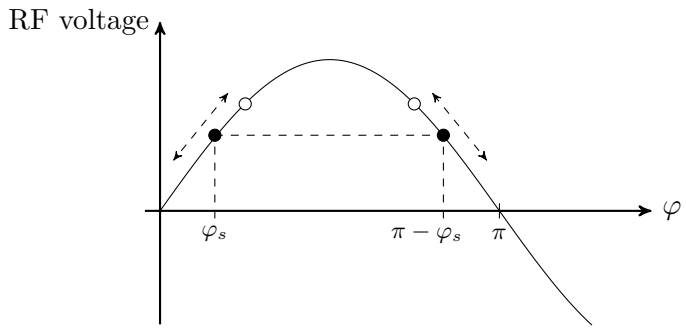

Figure 1.5: Stable phases for operation below (left) and above (right) transition.

Similar to the transverse betatron oscillations particles oscillate around the synchronous phase with the synchrotron tune

$$Q_s = \sqrt{\frac{\eta e h V_0 \cos\varphi_s}{2\pi E_0 \beta_{rel}^2 \gamma_{rel}}}, \tag{1.17}$$

where V_0 is the RF voltage according to $V = V_0 \sin\varphi$. (1.17) reveals that the oscillation frequency vanishes at transition and the motion in the longitudinal phase space is therefore "frozen".

The energy difference between an arbitrary particle and the synchronous one can be used to define the longitudinal phase space $\{\Delta E, \varphi\}$ - or equivalently $\{\Delta E, \Delta t\}$ - and the longitudinal emittance is thus measured in eVs. Oscillations in this phase space occur at a timescale of ms, which is very long compared to the transverse motion where particles carry out several oscillations per turn, leading to oscillation periods in the order of μs.

1.4 Chromaticity

Chromaticity is one of the outcomes of coupling between the longitudinal and the transverse planes and its concept is closely related to the betatron tune. A Taylor expansion of the tune with respect to the relative momentum offset $\frac{\Delta p}{p}$ leads to

$$Q\left(\frac{\Delta p}{p}\right) = Q_0 \; + \; Q' \, \frac{\Delta p}{p} \; + \; Q'' \left(\frac{\Delta p}{p}\right)^2 \; + \; \ldots, \tag{1.18}$$

where Q' is the linear and Q'' the second order chromaticity[5].
The linear chromaticity describes the variation of the tune with energy and the following definition is frequently used:

$$\xi = \frac{\Delta Q / Q_0}{\Delta p / p}. \tag{1.19}$$

Therefore, a large value of ξ obviously causes a large tune spread ΔQ and may lead to particle losses if, for example, resonances are crossed (see Section 1.6). Furthermore, the sign and the absolute value of ξ have to be controlled as they directly influence the rise time of collective instabilities.

1.5 Space charge forces

Up until now the interaction between particles in a circulating beam has been completely neglected. This assumption is no longer valid for high-intensity beams concentrated in small emittances.
Two equally charged particles experience a repulsive Coulomb force acting similar to a defocusing quadrupole in both transverse planes. However, the movement of these particles with a certain velocity v leads to two parallel currents and, thus, to an attractive force due to the magnetic fields generated. The total influence of these two opposite effects remains repulsive as long as $\beta < 1$, and exactly cancels out once the particles are traveling at the speed of light.
This effect of direct space charge reduces the number of transverse oscillations per turn and,

[5] The factor $\frac{1}{2}$ has been included into Q''.

therefore, the tune. In case of a non-uniform transverse distribution such as a Gaussian density, which is indeed the case for the majority of proton beams, the defocusing effect depends on the particle amplitude and induces a tune spread inside the beam, which has been first derived by Laslett:

$$\Delta Q_{x,y} = -\frac{r_0 N}{4\pi \varepsilon^*_{x,y} \beta_{rel} \gamma^2_{rel}}. \tag{1.20}$$

It is proportional to the classical particle radius r_0 and the beam intensity N, and is reduced with increasing normalized emittance ε^* and increasing momentum $\beta_{rel}\gamma^2_{rel}$. As quadrupole magnets apply focusing forces only in one plane, they are clearly not capable of curing space charge effects. For given intensity and emittance, the only remaining means to reduce ΔQ is to increase energy (see also Section 2.3).
By numerical integration around the circumference of a synchrotron, a value for the Laslett tune spread can be calculated and is given by

$$\Delta Q_{x,y} = -\frac{r_0 N}{(2\pi)^{3/2} \beta^2_{rel} \gamma^3_{rel} \sigma_z} \oint \frac{\beta_{x,y}(s)}{\sigma_{x,y}(s)[\sigma_x(s) + \sigma_y(s)]} ds, \tag{1.21}$$

where σ_z is the bunch length and

$$\sigma_x(s) = \sqrt{\varepsilon_x \beta_x(s) + D^2(s) \left(\frac{\Delta p}{p}\right)^2} \qquad \text{and} \qquad \sigma_y(s) = \sqrt{\varepsilon_y \beta_y(s)} \tag{1.22}$$

describe the transverse beam dimensions. The lattice of a machine determines the variation of the beam size along the circumference and this effect is taken into account by the integral in (1.21). The dispersion function $D(s)$ accounts for an increase of the beam size in the horizontal plane as particles with higher or lower momentum than the ideal particle are deflected differently within dipole magnets. In the vertical plane this effect does not appear as it is unusual to install vertical bending magnets in a synchrotron.
Nevertheless, also indirect space charge effects caused by image currents in the equipment constituting the accelerator such as the vacuum pipe, magnets, etc. and their interaction with the circulating beam have to be considered. In contrast to the direct effects, these do not cancel out when reaching $\beta = 1$.

1.6 Resonances

A single particle carrying out transverse oscillations with a phase advance per turn of $\phi_c = 0$ - corresponding to an integer value for the tune Q - will return to a given point in a synchrotron with exactly the same angle and amplitude each turn. By the presence of a perturbation of the

dipole field at this position, the particle receives a kick, causing a larger orbit the next time it passes by. Repetition of this process over several turns leads to loss of the particle due to the continuously increased oscillation amplitude. This can be overcome by changing the integer tune to a half integer value resulting in a stable oscillation as the divergence kicks cancel out every second turn (see Fig. 1.6).

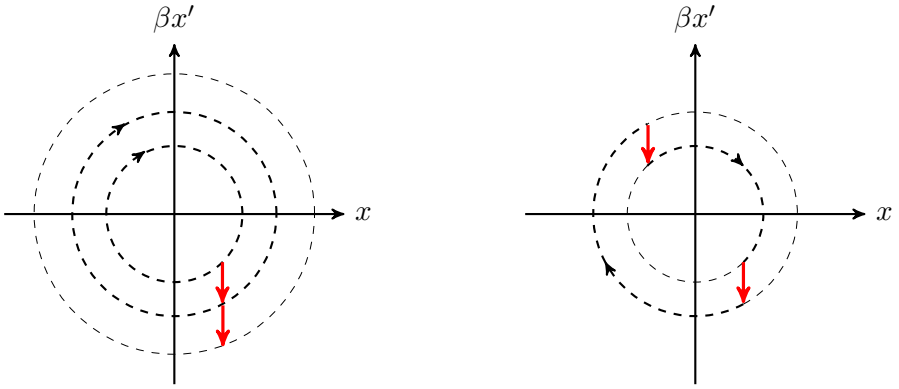

(a) An integer value of the tune such as $Q = 6.00$ leads to an infinitely growing oscillation amplitude.

(b) For a half integer value such as $Q = 6.50$ the oscillation remains stable.

Figure 1.6: Influence of a dipole error and the resulting position-independent kick on the particle oscillation. The vertical axis is multiplied by β in order to transform the phase space ellipses into circles.

However, this approach is only valid for dipole errors. Once a quadrupole error is present, particles will be lost due to half integer resonances as the strength of the kick depends on the displacement. The second kick in Fig. 1.6b would therefore act in the opposite direction leading to a resonant behavior as in the case of an integer tune in the presence of a dipole error. It then becomes necessary to change the tune to a third integer value to stabilize the motion.
In practice perturbations of the magnetic fields cannot be avoided as magnets are manufactured and aligned with certain tolerances. Therefore, stable particle motion in a circular accelerator is closely correlated to an appropriate choice of transverse tunes defining the working point (Q_x, Q_y) and detailed knowledge of resonances which could spoil the beam quality.
The entity of all possible working points leads to tune diagrams as shown in Fig. 1.7 and the classification of resonances is based on the formula

$$mQ_x + nQ_y = l \tag{1.23}$$

where m, n and l are integers and $|m| + |n|$ gives the order of the respective resonance[6]. 1^{st} order resonances are excited by dipole errors, 2^{nd} order by quadrupole errors, and non-linear perturbations of the magnetic field cause higher order resonances. Nevertheless, 3^{rd} and 4^{th} order resonances are often excited on purpose by additionally installed sextupoles and octupoles, which are used to correct certain physics parameters such as chromaticity.
Naturally, the number of resonances makes it difficult to choose an off-resonance working point, especially as the interplay of chromaticity and space charge effects with the particle motion causes the beam to cover a certain area in the tune diagram instead of merely a single point.
The red "neck tie" in Fig. 1.7 represents a space charge tune spread according to (1.21) and is similar to the one of LHC beams (see Section 2.2) in the PS today. Particles oscillate at betatron frequencies very different from the programmed working point (6.21, 6.24) and, therefore, cross several resonances, even the integer. In case the linear chromaticity ξ is different from zero, this occurs periodically as the longitudinal and the transverse motions are coupled. The motion around the synchronous particle causes a continuous change of energy and, depending on the value of ξ, the tune is also modified.

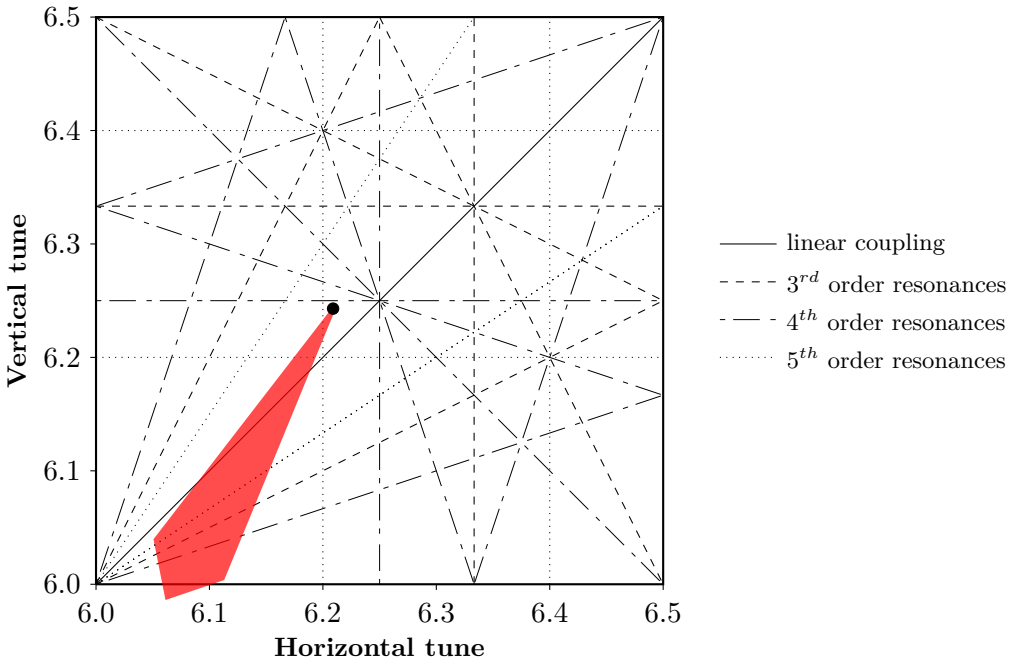

Figure 1.7: Typical tune diagram of the CERN Proton Synchrotron with space charge footprint.

Furthermore, resonance lines are not infinitely thin but have a certain width, described by the stop band. As soon as the tune of a particle falls inside this stop band, the resonant behavior becomes visible and the oscillation amplitude increases. However, this, at the first glance,

[6] Frequently the fractional tune q is used instead of Q, resulting, for example, in a nomenclature of (0.25, 0.28) for the working point (6.25, 6.28).

negative effect can also be beneficial if transverse instabilities are to be cured. One possibility is then to transfer energy from the stable to the unstable plane by means of skew quadrupoles. These are normal quadrupoles rotated by 45° around its central axis and, therefore, couple both transverse oscillations. This effect reaches the maximum if the working point is set in the vicinity of the linear coupling resonance (as in Fig. 1.7).
Another positive contribution from resonances is often exploited within synchrotrons for medical applications such as cancer treatment. By programming one transverse tune on a 3^{rd} order resonance a slow extraction over several hundred milliseconds can be achieved.

2 The CERN Proton Synchrotron

In 1959 the Proton Synchrotron (PS) started operation at CERN as the world's first synchrotron based on the alternating-gradient focusing principle [8]. Since then the PS has been used to accelerate a variety of particles, namely protons and deuterons for the Intersecting Storage Rings[1], antiprotons for the Super Proton-Antiproton Synchrotron-collider[2] and electrons and positrons for the Large Electron Positron-collider.
Today the PS holds a key position within the LHC injector chain (see Section 2.2), sending proton and lead ion beams to the LHC. Additionally, several fixed target experiments are connected to the PS complex, receiving proton beams with a wide range of different beam characteristics.

2.1 The main magnet unit

In order to guide particles around the $2{\cdot}\pi{\cdot}100$ m long accelerator, 100 combined-function main magnets, separated by magnetic field-free straight sections, are installed in the PS tunnel. In total there are four different types of main magnets, all of them being composed of one focusing and one defocusing half unit. The complete magnet unit is subdivided into ten C-shaped blocks - five per half unit - with two different layouts (see Fig. 2.1) to provide the alternating gradient. The application of combined-function magnets necessitates the use of special pole profiles in order to bend and focus the particles at the same time. Figure 2.2a shows the hyperbolic pole shape and several auxiliary windings.
These windings are directly mounted on top of the magnet poles and are therefore called Pole Face Windings (PFW). Together with the Figure-of-Eight Loop (F8L) they provide means to control the betatron tune and the chromaticity. In particular, these five circuits are necessary for the tune control, since the quadrupole component generated by the main magnet poles is -

[1] The world's first p-p collider.
[2] This is today the Super Proton Synchrotron (SPS).

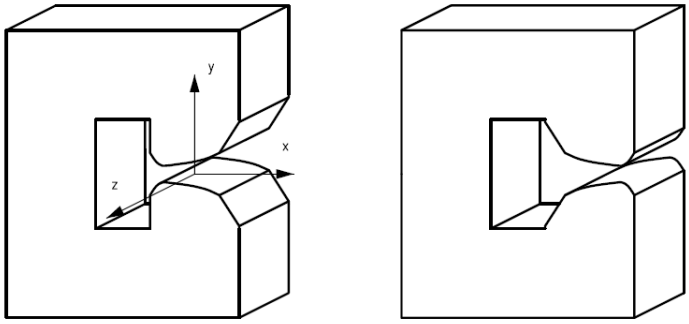

Figure 2.1: Open and closed single block of the main magnet units [9].

due to the special geometry of the poles - fixed by the dipole component.
The top view in Fig. 2.2b describes the arrangement of the auxiliary windings. For each half unit the PFW are divided into narrow and wide windings, which corresponds to the width of the air gap at their respective position.
The F8L owes its name to the fact that it crosses between the two half units giving it the corresponding shape. It is used to increase the quadrupole field in one and decrease it in the other half unit, leaving the overall dipole component unchanged.

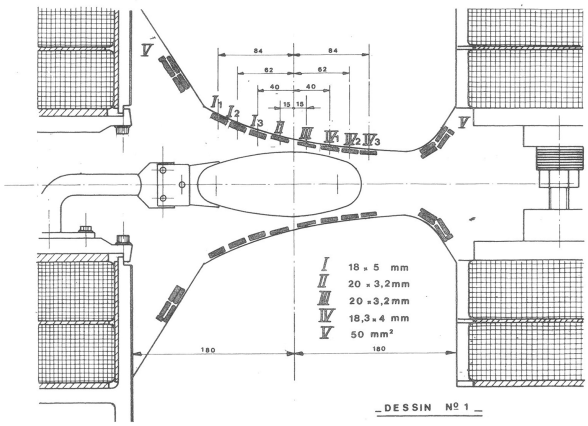

(a) Pole shape [10]

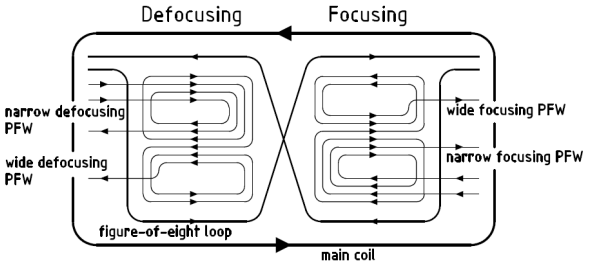

(b) PFW and F8L [11]

Figure 2.2: Main magnet and auxiliary windings.

The available circuits to influence the magnetic field and therefore the beam parameters are the Defocusing Narrow (DN), Defocusing Wide (DW), Focusing Narrow (FN), Focusing Wide (FW) and the F8L[3]. Since the refurbishment of the dedicated power supplies [10], it has become possible to operate each of these windings independently resulting in the so-called five current mode (5CM). This offers higher flexibility in operating the machine compared to the previously used 3CM, where narrow and wide windings of each half unit had been connected in series (see also Section 3.2).

[3] The notation PFW will from now on refer to all these windings, including the F8L.

2.2 Production scheme of LHC beams

With a circumference of almost 27 km, the Large Hadron Collider at CERN is the world's largest particle accelerator and offers unique opportunities to examine the constituents of matter and to increase our understanding of nature.
The LHC consists of two synchrotrons sharing the same twin-aperture magnets. In the two separated vacuum pipes particles circulate in opposite directions, guided, basically, by a common magnetic field. In order to make these two beams collide, the pipes cross at four defined interaction points, where vast detectors are situated to collect as much information as possible about the collision products [12].
The particle beams sent to the LHC are prepared within the LHC injector chain, where one has to distinguish between the proton and the ion chain. Proton beams are produced and accelerated in the LINAC[4] 2 up to a kinetic energy of 50 MeV and are then transfered to the Proton Synchrotron Booster (PSB), a machine comprising four rings on top of each other. From the PSB protons are injected into the PS at 1.4 GeV and extracted at 25 GeV to the SPS, where they receive further acceleration to the LHC injection energy of 450 GeV. Ion beams are not considered within this thesis and information about the ion chain can be found in [13].
The nominal filling scheme of the LHC allows to inject 2808 bunches into each ring, the bunches being separated by 25 ns [14]. However, due to a variety of reasons, including electron cloud issues in the LHC [15], the bunches of the operational beam in 2012 are spaced by 50 ns, leading to a total of 1374 bunches per ring.
In each of the PSB rings one bunch with an intensity of 1.10 10^{12} protons within 1σ normalized transverse emittances of 1.3 mm·mrad is accelerated [16]. The resulting four bunches are injected into the PS at 170 ms after the start of the magnetic cycle and are kept on the 1.4 GeV injection flat bottom for 1200 ms until two additional bunches from the PSB arrive (see Fig. 2.3). All six bunches are captured on harmonic number $h = 7$ and one bucket is left empty to provide a time window for the PS extraction kicker to rise. After the second injection, the bunches receive special longitudinal treatment by the RF-cavities in order to generate the required bunch spacing [17].
These RF-gymnastics consist of a triple splitting already at the flat bottom, producing 18 bunches on $h = 21$. After acceleration to 26 GeV/c, an additional double splitting occurs and the 36 resulting bunches - 1.7 10^{11} ppb[5] within $\varepsilon^*_{x,1\sigma} = 1.12$ mm·mrad and $\varepsilon^*_{y,1\sigma} = 1.39$ mm·mrad [18] - are then rotated in longitudinal phase space shortly before extraction to comply with the 4 ns bunch length required by the SPS.
For LHC-beams $h = 21$ is an essential harmonic as bunches are spaced by 100 ns and spacings of 50 or 25 ns can be easily achieved by additional splittings. The advantage of the splitting scheme mentioned above is therefore, that by applying a second double splitting on the flat top

[4] LINear ACcelerator
[5] protons per bunch

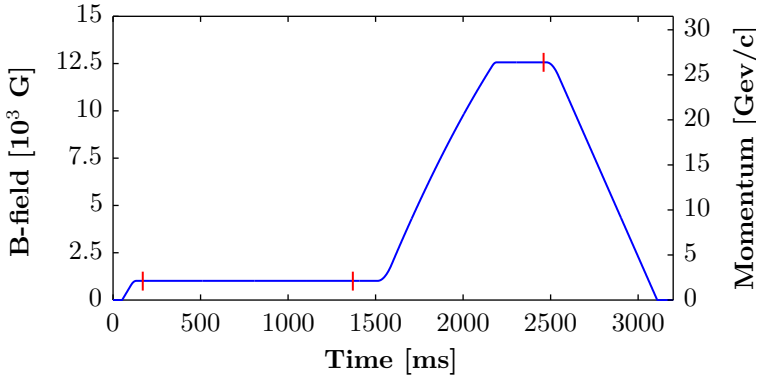

Figure 2.3: Magnetic cycle of the nominal LHC beam in the PS. The red lines on the flat bottom indicate the two injections at 170 ms and 1370 ms, while the red line at top energy corresponds to the extraction timing of 2460 ms.

a bunch spacing of 25 ns is generated.

2.3 The LHC Injectors Upgrade project

After 2019, with the current design of the LHC, it will become a long lasting process to further reduce the statistical error in the measurements that are carried out by the experiments situated at the four interaction points. This error is proportional to $\frac{1}{\sqrt{N}}$, with N being the number of observations for a given event. Several years of LHC operation will have provided the experiments with a vast amount of collisions by 2019, requiring an increase of N in order to improve the statistical significance of the data.
The necessary changes to the machine in order to meet this requirement of an increased number of collisions per second are at present being studied within the High Luminosity LHC (HL-LHC) project [19].
The luminosity L [$\mathrm{cm}^{-2}\mathrm{s}^{-1}$] is the figure of merit for a particle collider as it directly connects beam parameters and N_{event}, the resulting number of collisions per second for the event of interest,

$$N_{event} = \sigma_{event} \cdot L. \tag{2.1}$$

σ_{event} [b][6] is the cross section for the respective event and is, obviously, given by nature. Hence, the number of events can only be increased by increasing the luminosity, which is defined as

$$L = \frac{N_p^2 n_b f_{rev} \gamma_{rel}}{4\pi\sqrt{\varepsilon_x \beta_x^* \varepsilon_y \beta_y^*}} \cdot F, \tag{2.2}$$

[6] 1 barn = 10^{-24} cm^2

with N_p being the number of protons per bunch[7], n_b the number of bunches, f_{rev} the revolution frequency, $\sqrt{\varepsilon_i \beta_i^*}$ the transverse beam dimension at the interaction point and F a reduction factor due to the crossing angle between the colliding beam trajectories [20].
In the first half of 2012 the peak luminosity reached in the LHC was $6 \cdot 10^{33}$ cm^{-2} s^{-1} for a beam energy of 4 TeV, and the integrated luminosity $\int L\, dt$ over this period amounted to 5.8 fb^{-1} and 5.3 fb^{-1} for the ATLAS and CMS experiments at the LHC [21, 22]. In contrast to these values the aim of the HL-LHC is to provide 250-300 fb^{-1} per year, achieving this by a luminosity of 10^{35} cm^{-2} s^{-1}, which is ten times more than the design value of the LHC.
The parameters demanded by the HL-LHC will not be reached without a major upgrade of the LHC injector chain. Therefore the LHC Injectors Upgrade (LIU) project has been started and examines the necessary changes and their implementation, with the aim of providing the beam characteristics to meet the HL-LHC luminosity goal [23].
The injectors can account for an increase of luminosity by producing more intense beams within constant or even smaller transverse emittances and hence increasing the beam brightness. However, especially at injection into the PS, space charge forces play a non-negligible role as the first batch of four bunches from the PSB is kept at injection energy for 1.2 seconds. Due to the Laslett tune spread, the beam is likely to cross several resonances resulting in a transverse emittance blow up. One topic the LIU project investigates is an increase of the PS injection energy from 1.4 GeV to 2 GeV, decreasing the tune spread as $\Delta Q \propto 1/\beta\gamma^2$ (see Section 1.5). This fact, together with a well chosen working point (Q_x, Q_y), enables to conserve transverse beam parameters along the injection flat bottom.
Another important point treats the cure of transverse Head-Tail instabilities, which may lead to beam loss [24]. The wake field left behind by the head of the bunch influences its tail and, due to the presence of synchrotron motion, these two parts continuously exchange positions. The coupling between the longitudinal and the transverse planes may then lead to increasing transverse oscillation amplitudes and therefore to an unstable beam. In the PS the linear coupling resonance - excited by skew quadrupoles - is currently exploited to stabilize the particle motion by transferring energy between the stable and the unstable plane. However, this might not be sufficient for future high-brightness beams as the appearance of this instability depends on the beam intensity. In this case, controlling chromaticity along the flat bottom could be used to decrease the mode number of the arising instability [25] and together with a fast transverse damper this approach might be able to stabilize the beam.
Within the following chapters, extensive studies concerning control of tune, chromaticity and higher order effects as well as betatron resonances will be presented. While these have been carried out within the framework of the LIU project, the obtained results are nevertheless applicable to all other types of beams produced at the CERN PS, allowing deeper understanding of this remarkable machine.

[7] This definition is only valid where both beams have the same intensity.

3 Working point control

The choice of an appropriate working point is an essential aspect of stable particle motion and therefore accelerator operation in general. However, apart from determining the transverse tunes by quadrupole fields, higher order components of the magnetic field need to be controlled as well to allow correction of linear and second order chromaticity. This is usually achieved by distribution of additional magnets along the accelerator or by using special auxiliary windings such as the PFW in the PS.

3.1 The bare machine

In the CERN PS the main magnet units already provide bending and focusing forces and therefore small intensity beams can nearly be accelerated to top energy, even without additional auxiliary magnets. At 2 GeV this bare machine leads to a natural working point of (6.253, 6.285) as shown in the tune diagram in Fig. 3.1a and is known to behave completely linear at low energy, i.e. in the absence of any saturation effects of the main magnet yoke.
In order to measure the frequency of the betatron oscillations the Base Band Tune (BBQ) measurement system has been implemented at CERN and is currently used throughout the whole injector chain and at the LHC. The transverse oscillations of the beam are enhanced by application of a kick and a position sensitive pick-up detects the evaluation of the beam position over several turns. A spectral analysis by means of a Fast Fourier Transform (FFT) of the pick-up signal then leads to determination of the tune [26]. The intrinsic error of this procedure is proportional to $1/N_{turns}$, with N_{turns} being the number of turns during which the beam position has been observed [27].
The linearity of the bare machine is verified by measuring the tune in dependence of the

momentum error[1]. For this, an offset is applied to the radial position of the circulating beam causing a difference in revolution frequency and energy. A value of $\frac{\Delta p}{p} = 5 \cdot 10^{-3}$ corresponds to about 10 mm displacement of the mean radial position of the beam with respect to the center of the machine defined by the pick-ups of the PS orbit measurement system ($\frac{\Delta p}{p} = 0$). This has to be compared to the typical dimensions of the elliptical vacuum chamber of $x = 72.5$ mm and $y = 35$ mm.

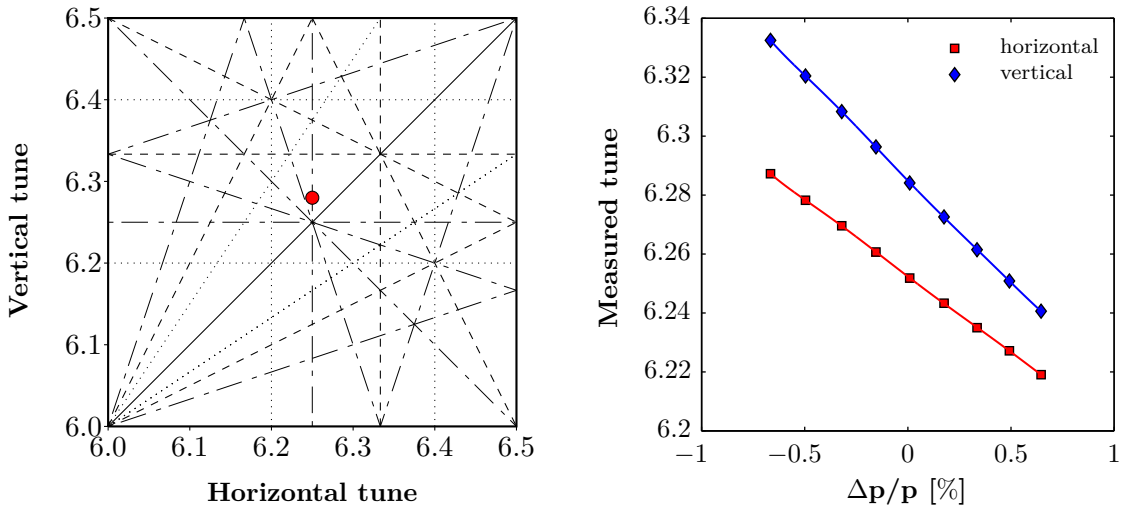

(a) Working point (6.25, 6.28) **(b)** Chromaticity ξ_x=-0.83, ξ_y=-1.12[2]

Figure 3.1: Bare machine at 2 GeV.

The linear chromaticities of the bare machine can be extracted from Fig. 3.1b, as they are given by the slopes of the fits according to (1.18) and (1.19). The negative values of ξ_x=-0.83 and ξ_v=-1.12 correspond to typical values of other synchrotrons without chromaticity control.
However, the sole use of the combined function magnets does not allow to move the working point to areas in the tune diagram which might be more beneficial regarding resonances. Thus, additional quadrupoles are distributed along the machine and installed at the end of the main magnets. These low energy quadrupoles (LEQ) are alternately positioned to provide a pattern of focusing-defocusing magnets and are used to control the tunes from injection up to a kinetic energy of about 3.5 GeV.
The relationship between the currents flowing through these magnets and the measured tunes can be easily established by setting up the matrix equation

$$\begin{pmatrix} \Delta Q_x \\ \Delta Q_y \end{pmatrix} = \begin{pmatrix} 0.02045 & -0.01117 \\ -0.01089 & 0.02078 \end{pmatrix} \begin{pmatrix} \Delta I_F \\ \Delta I_D \end{pmatrix}, \tag{3.1}$$

[1] The respective beam parameters are found in the Appendix.
[2] For each point data was averaged over three consecutive cycles with resulting standard deviations in the order of 10^{-5} leading to non-visible error bars. This applies also to all further $Q\left(\frac{\Delta p}{p}\right)$-plots within this thesis.

where the Δ refers to an offset with respect to the bare machine value. The matrix is only valid at 2 GeV, as its elements depend on the energy of the beam. This is based on the fact, that with increasing momentum also the quadrupole gradient has to rise proportionally in order to obtain the same divergence kicks as at lower energy (see Section 1.2).
It can be immediately seen that changing one current always influences both tunes and the determination of a working point requires a special configuration of both focusing and defocusing quadrupoles. Inversion of the matrix in (3.1) allows to apply the desired offsets to the tunes as the necessary currents can be calculated.
One disadvantage of the LEQ is that they do not offer any means to correct chromaticitiy. At the moment this does not impose any restrictions on the operation at the PS, as the occurring Head-Tail instability on LHC beams can be cured by linear coupling. However, this instability will become more important for higher intensity beams demanded by the HL-LHC, where linear coupling might no longer suffice to stabilize the beam. A chromaticity correction scheme at injection would therefore become inevitable (see also Section 2.3).
Based on these considerations, the feasibility of controlling tunes as well as the linear and second order chromaticities with the PFW has been examined at the future injection energy of 2 GeV.

3.2 PFW at low energy

In today's operation at the PS, the PFW control tunes and chromaticities above 3.5 GeV. Chromaticity correction becomes especially important when reaching transition at around 5 GeV, where the signs of ξ have to be changed in both planes from negative to positive for the beam to remain stable for Head-Tail [28].
From hardware point of view, all the five circuits are connected to different power supplies providing the 5CM. Nevertheless, changing the signs of ξ still uses 3CM, as this mode has been observed to create less non-linearities within the magnetic field than unbalancing the narrow and wide windings of the respective magnet half unit.
Likewise to (3.1) 3CM can be expressed as matrix relationship

$$\begin{pmatrix} \Delta Q_x \\ \Delta \xi_x \\ \Delta \xi_y \end{pmatrix} = \begin{pmatrix} a_{11} & a_{12} & a_{13} \\ a_{21} & a_{22} & a_{23} \\ a_{31} & a_{32} & a_{33} \end{pmatrix} \begin{pmatrix} \Delta I_F \\ \Delta I_D \\ \Delta I_{F8L} \end{pmatrix}, \tag{3.2}$$

but one has to bear in mind that these three currents only permit control over three parameters and in the case of (3.2) ΔQ_y is left completely free. Depending on the choice of this free parameter, three further relations can be established.
In order to provide a chromaticity correction scheme at injection 3CM is obviously not the appropriate choice as Q_x, Q_y as well as ξ_x, ξ_y have to be controllable to prevent large tune

jumps or change of sign of chromaticity already below transition. To exploit the full potential of the PFW hardware the 5CM can be used and the matrix formalism leads to

$$\begin{pmatrix} \Delta Q_x \\ \Delta Q_y \\ \Delta \xi_x \\ \Delta \xi_y \\ \Delta Q''_{x,y} \end{pmatrix} = \begin{pmatrix} a_{11} & a_{12} & a_{13} & a_{14} & a_{15} \\ a_{21} & a_{22} & a_{23} & a_{24} & a_{25} \\ a_{31} & a_{32} & a_{33} & a_{34} & a_{35} \\ a_{41} & a_{42} & a_{43} & a_{44} & a_{45} \\ a_{51} & a_{52} & a_{53} & a_{54} & a_{55} \end{pmatrix} \begin{pmatrix} \Delta I_{FN} \\ \Delta I_{FW} \\ \Delta I_{DN} \\ \Delta I_{DW} \\ \Delta I_{F8L} \end{pmatrix}, \tag{3.3}$$

allowing to control a fifth parameter, namely either the horizontal or the vertical second order chromaticity. Due to the energy dependence of these matrix elements (see Fig. 3.2), an extensive measurement campaign was conducted in 2008 and 2009 [29], resulting in the operational matrix of today. Special attention was paid to the precise measurements of the circuits' influence on Q_x, Q_y, ξ_x and ξ_y and therefore the values for $Q''_{x,y}$ are not correct in this matrix, giving no possibility to control a fifth parameter.

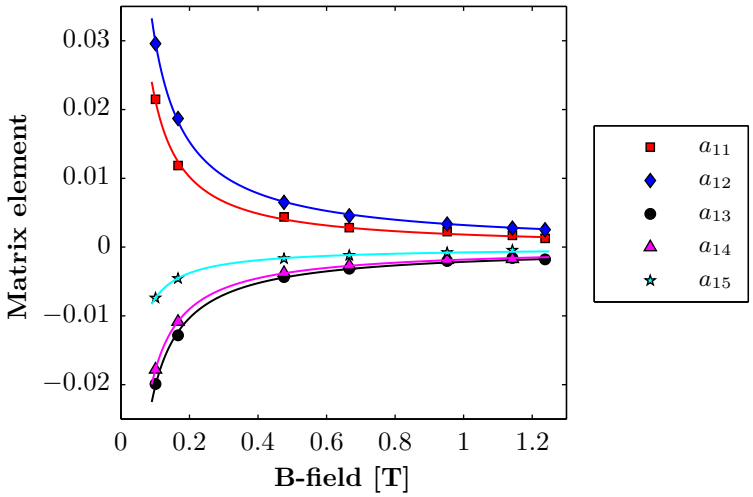

Figure 3.2: Energy dependence of the matrix elements introduced in (3.3). It is clearly visible that the influence of the currents on the horizontal tune Q_x is more important at low energy. Exponential fits in the form of $a{\cdot}\mathbf{B}^b$, with a and b being constants, are applied [29].

For this reason the 4CM has been established and the corresponding matrices can be easily retrieved from (3.3). One out of the five PFW has to be fixed, meaning that the current will remain unchanged in it. This already indicates a choice between five different circuits and, therefore, between five matrices. If, for example, the F8L is chosen to be fixed, the 5×5 matrix is reduced to 4×4 and only the entries within the blue boxes of the following matrix equation remain of interest.

$$\begin{pmatrix} \Delta Q_x \\ \Delta Q_y \\ \Delta \xi_x \\ \Delta \xi_y \\ \cancel{\Delta Q''_{x,y}} \end{pmatrix} = \begin{pmatrix} a_{11} & a_{12} & a_{13} & a_{14} & a_{15} \\ a_{21} & a_{22} & a_{23} & a_{24} & a_{25} \\ a_{31} & a_{32} & a_{33} & a_{34} & a_{35} \\ a_{41} & a_{42} & a_{43} & a_{44} & a_{45} \\ \cancel{a_{51}} & \cancel{a_{52}} & \cancel{a_{53}} & \cancel{a_{54}} & \cancel{a_{55}} \end{pmatrix} \begin{pmatrix} \Delta I_{FN} \\ \Delta I_{FW} \\ \Delta I_{DN} \\ \Delta I_{DW} \\ \cancel{\Delta I_{F8L}} \end{pmatrix} \tag{3.4}$$

3.2.1 Appearance of non-linearities

In the previous section the linearity of the main field was discussed and the LEQ were introduced as elements without influence on this characteristic. To examine the influence of the PFW, the working point (6.10, 6.20) was chosen as the beam intensity remained constant along the 2 GeV measurement plateau. This was important as the quality of the BBQ signal depends on the beam intensity and the mentioned working point provided enough margin to clearly measure the tune even for large radial offsets. The tunes were programmed in 4CM - chromaticities were left to the natural values - by fixing the F8L and a clear separation between the currents in the different circuits is visible in Fig. 3.3.

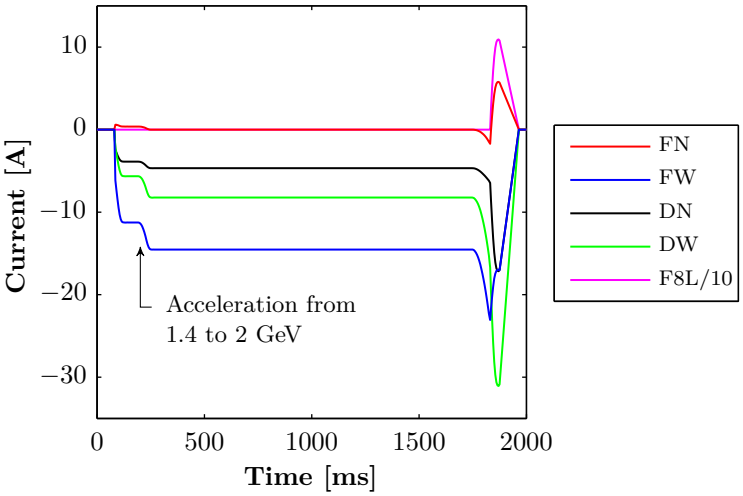

Figure 3.3: Currents to set up the working point (6.10, 6.20).

This setup causes strong non-linearities within the magnetic field, which was already expected due to previous measurements [29]. Figure 3.4b shows the measured dependence of the tune on the radial position of the beam and reveals a completely different behavior than was seen for the bare machine.

One characteristic that immediately attracts attention is an unintentional change of ξ_h to a

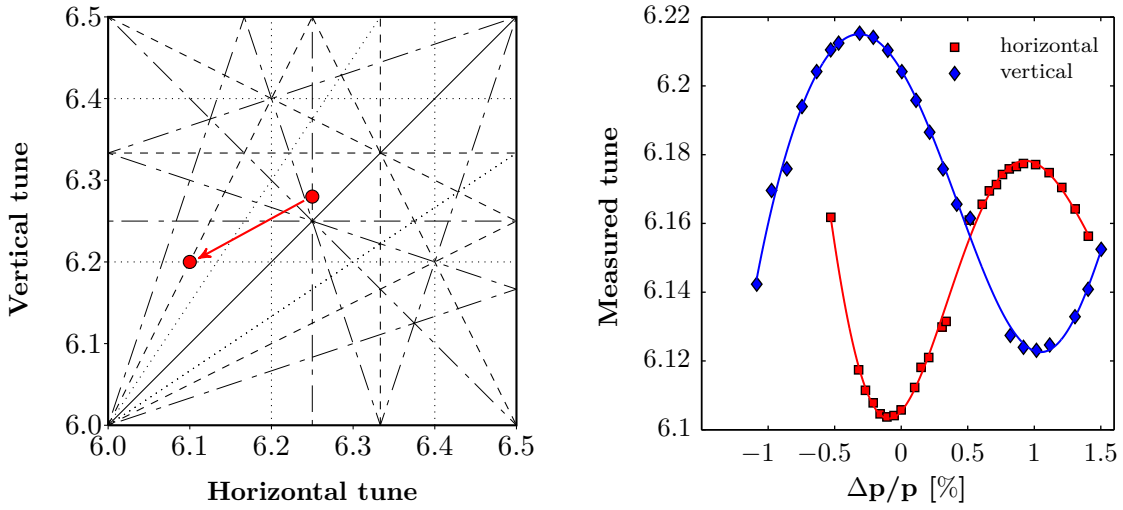

(a) New working point (6.10, 6.20) **(b)** Non-linear behavior

Figure 3.4: Influence of the PFW on the non-linear behavior of the magnetic field.

positive value in close vicinity of the working point. Furthermore, within a beam situated at one of the extrema of the curves, particles may encounter positive or negative chromaticity depending on their momentum spread.
In order to extract the values of Q, ξ and Q'' from Fig. 3.4b, a sixth order polynomial is used to fit the data points in both planes. The respective equations are the following:

$$Q_x = 6.105 + 4.415 \cdot \delta_p + 2105.141 \cdot \delta_p^2 - 1.999 \cdot 10^5 \cdot \delta_p^3 - 5.569 \cdot 10^6 \cdot \delta_p^4 + 9.838 \cdot 10^8 \cdot \delta_p^5 - 25.119 \cdot 10^{10} \cdot \delta_p^6, \tag{3.5}$$

$$Q_y = 6.205 - 6.409 \cdot \delta_p - 874.238 \cdot \delta_p^2 + 4.264 \cdot 10^4 \cdot \delta_p^3 + 3.205 \cdot 10^6 \cdot \delta_p^4 + 2.953 \cdot 10^7 \cdot \delta_p^5 - 7.761 \cdot 10^9 \cdot \delta_p^6, \tag{3.6}$$

with δ_p being the relative momentum error $\frac{\Delta p}{p}$. According to (1.19), this leads to linear chromaticities of $\xi_x = 0.73$ and $\xi_y = -1.03$, indicating the change in the horizontal plane while the vertical value remained almost the same as in the linear case (compare to Fig. 3.1b). In relation to both tunes it can be said that they are in agreement with the programmed values. By comparing both curves in Fig. 3.4b it can be observed that the interval of radial displacement in which data points could be taken is smaller in the horizontal plane. This occurred due to very large negative chromaticity, causing such a tune spread within the bunch that explicit determination of the tune was no longer possible. To confirm this explanation a kick was applied to the beam at two different radial positions, namely the center of the machine and

-6 mm, and the induced oscillation was observed with one pick-up of the PS orbit measurement system. The large tune spread is the reason for a rapid decay of the coherent oscillation leading to a broad peak in the tune spectrum (see Fig. 3.5).

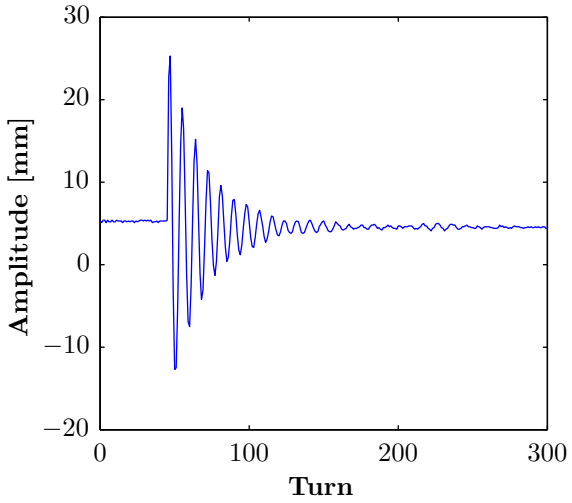

(a) Decay of the oscillation for a beam centered in the machine. The oscillation remains for more than 100 turns after the excitation.

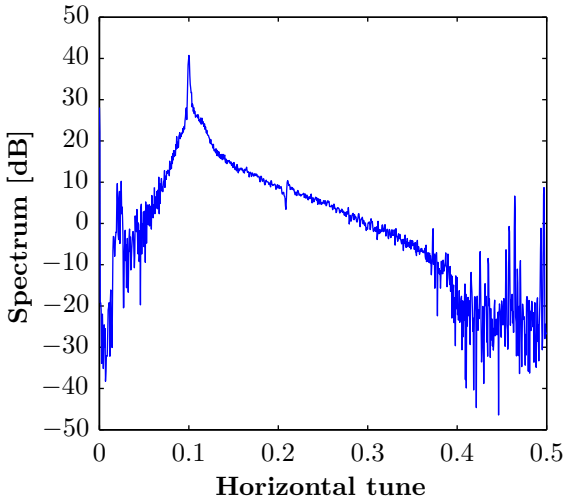

(b) Betatron frequency obtained by application of a FFT to the pick-up signal in (a). The sharp tune peak is caused by small $|\xi_x|$.

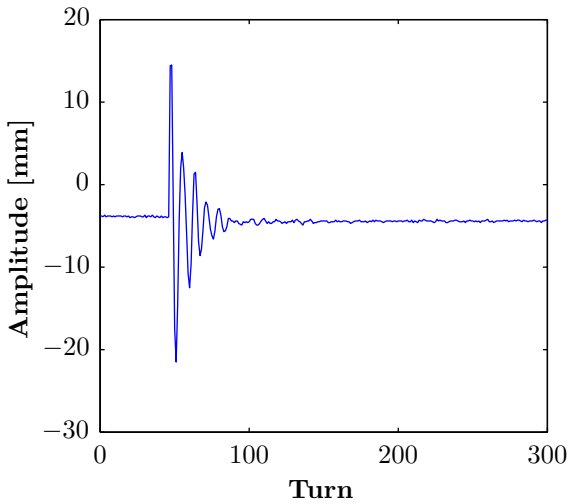

(c) Decay of the oscillation for a beam at a radial position of -6 mm. Around 40 turns after the kick the oscillation has died out.

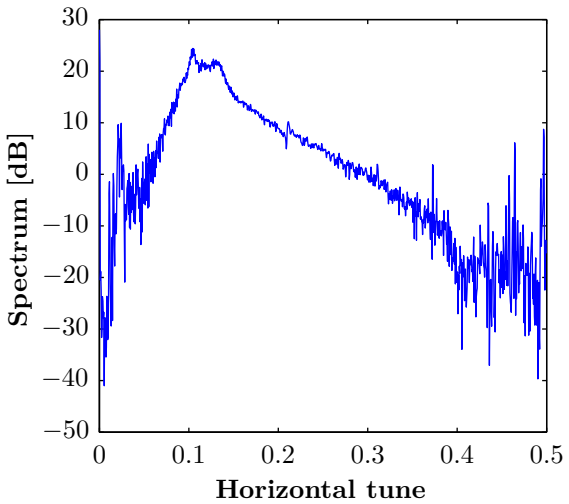

(d) Betatron frequency obtained by application of a FFT to the pick-up signal in (c). The broad peak is the result of the large tune spread within the beam.

Figure 3.5: Influence of chromaticity on the oscillatory behavior of a beam.

3.2.2 Measuring the 5CM matrix

The matrix measurement campaign, which provided today's operational matrix, was carried out by taking tunes and chromaticities of the bare machine as reference. The matrix was then obtained by consecutively applying current offsets to each of the PFW circuits and measuring the response of the beam. This procedure is limited by the stability of the beam, as large offsets applied to single circuits eventually lead to beam loss. Thus, the maximum current offset for which the beam response can still be measured defines the area of validity of the matrix.
In order to extend the current 4CM operation scheme and to provide an additional degree of freedom to the working point control it was decided to measure the 5CM matrix by paying particular attention to the second order chromaticities. In theory, this approach provides an intrinsic method of correction of linear and higher order effects by using the magnetic fields created by the PFW and comes without the necessity for additional quadrupoles or octupoles.
Instead of taking the bare machine working point as reference, the matrix measurement was based on the settings already shown in Fig. 3.3. Since the currents are quite different from zero and cause considerable non-linear effects, the working point (6.10, 6.20) is an eligible candidate to examine the proposed correction scheme.
A measurement plateau was established by applying the necessary current offsets between 500 and 1000 ms (see Fig. 3.6) and several positive and negative values were chosen depending on the stability of the beam (see legends in Figs. 3.7 - 3.11).

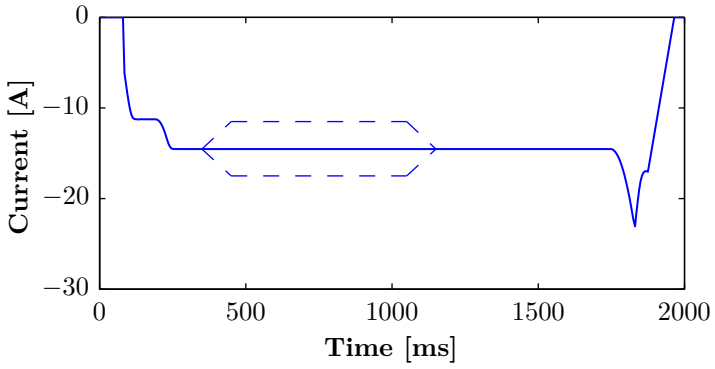

Figure 3.6: Current in the FW circuit to establish the working point (6.10, 6.20). To measure the 5CM matrix several positive and negative offsets were applied, two of which are indicated by the dashed lines.

This process was repeated consecutively for each of the five circuits and, therefore, ten plots describing the influence of these changes on both transverse planes have been obtained.
In Fig. 3.7, measurements using the F8L are shown confirming the expected effect of this special circuit. The F8L was built to increase the magnetic field in one and decrease it in the other

half of the main magnet, influencing only the quadrupole component of the field and therefore the tunes. In the horizontal as well as in the vertical plane it becomes clearly visible that the applied current offsets lead to a proportional shift with respect to the red reference curves (the same as already shown in Fig. 3.4b and defined in (3.5) and (3.6)).
Irrespective of the amount of current flowing through this circuit, the non-linear shape remains the same and the only changing parameters are the tunes.
A very similar response of the beam can be observed by using the wide windings of the focusing and the defocusing magnet half unit. Especially the DW circuit influences the beam parameters

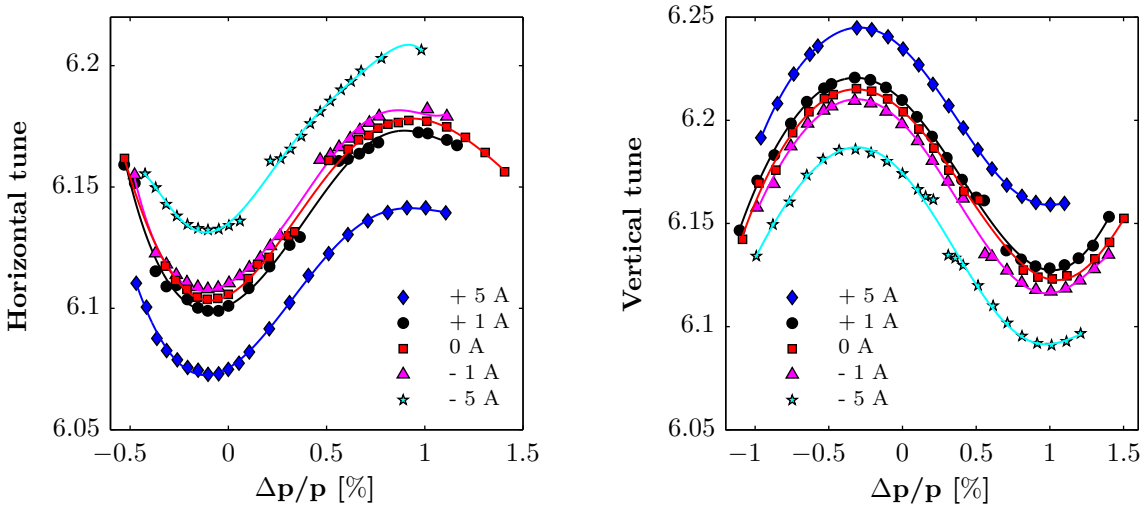

(a) Horizontal plane **(b)** Vertical plane

Figure 3.7: Current offsets applied to the F8L.

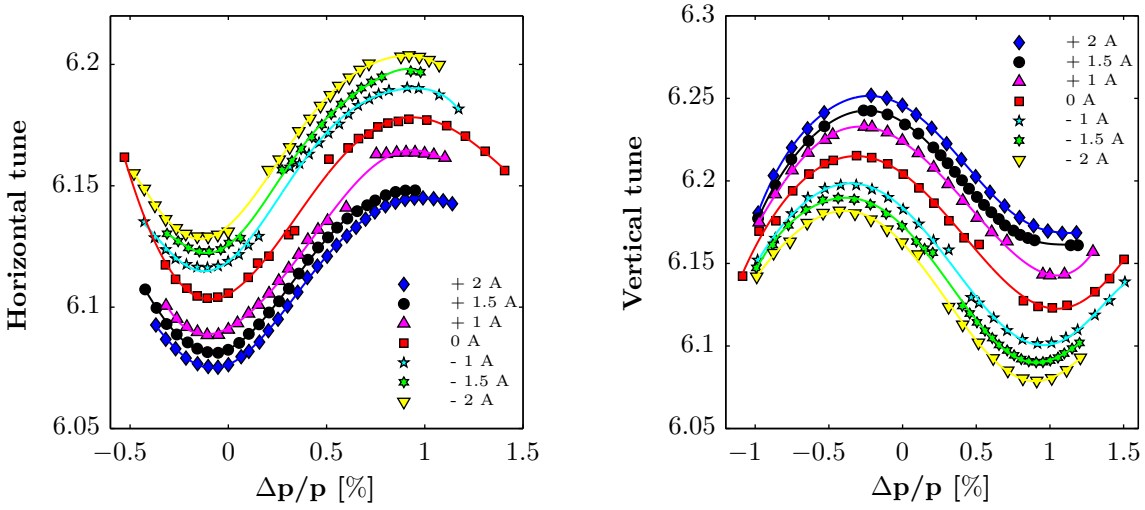

(a) Horizontal plane **(b)** Vertical plane

Figure 3.8: Current offsets applied to the DW.

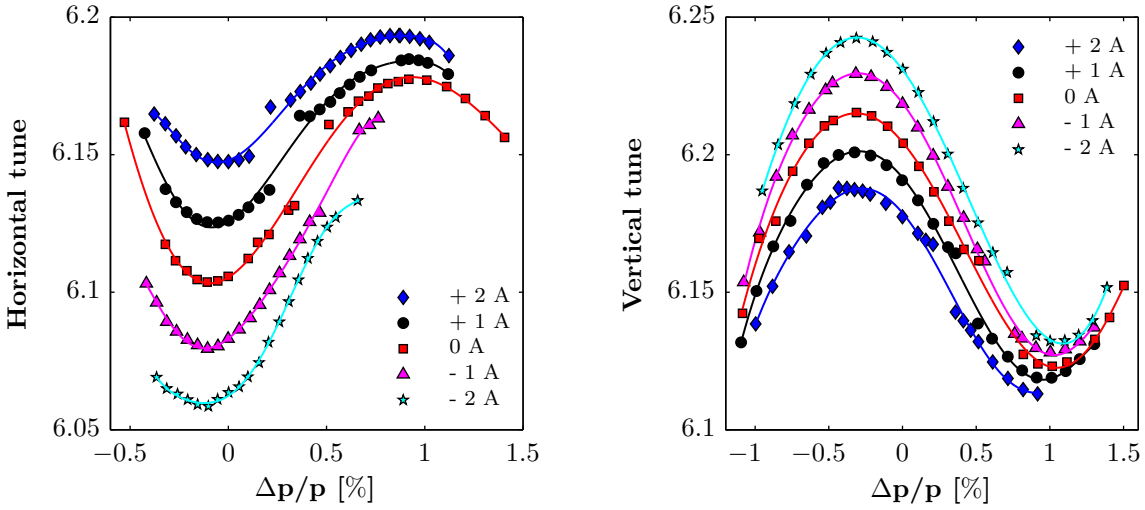

(a) Horizontal plane **(b)** Vertical plane

Figure 3.9: Current offsets applied to the FW.

the same way the F8L does while for the FW slight changes of the slopes and the curvatures of the curves and, therefore, of ξ and Q'', can be identified.

While the F8L, the DW and the FW influence the higher order components of the magnetic field similarly, this is no longer the case for the narrow circuits shown in Figs. 3.10 and 3.11. Both circuits reveal drastic influence on the shape of the curves and, therefore, substantial changes of linear and second order chromaticity. It is striking that, depending on the particular circuit, the point of intersection of the curves lies on different sides with respect to the center of the

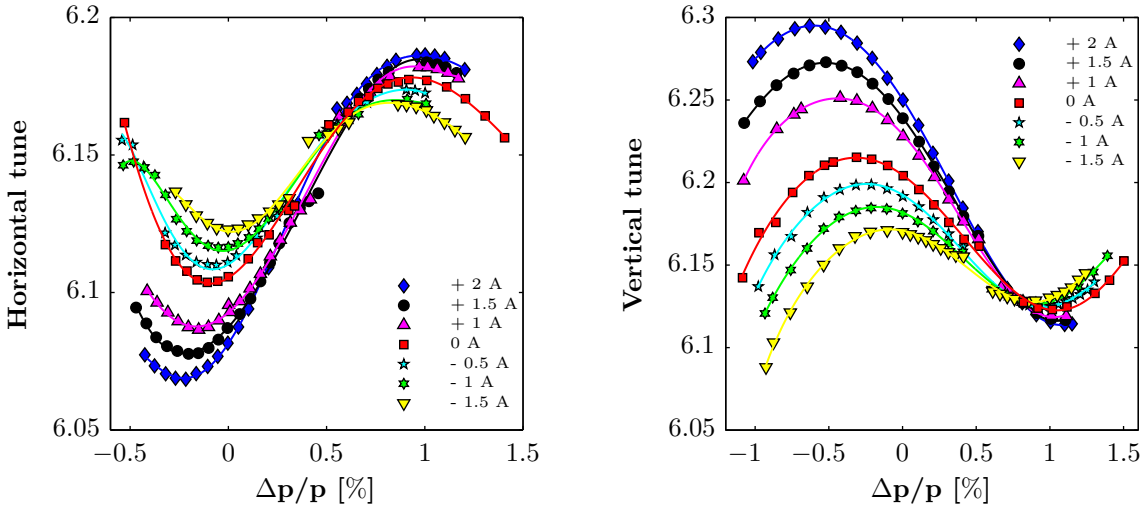

(a) Horizontal plane **(b)** Vertical plane

Figure 3.10: Current offsets applied to the DN.

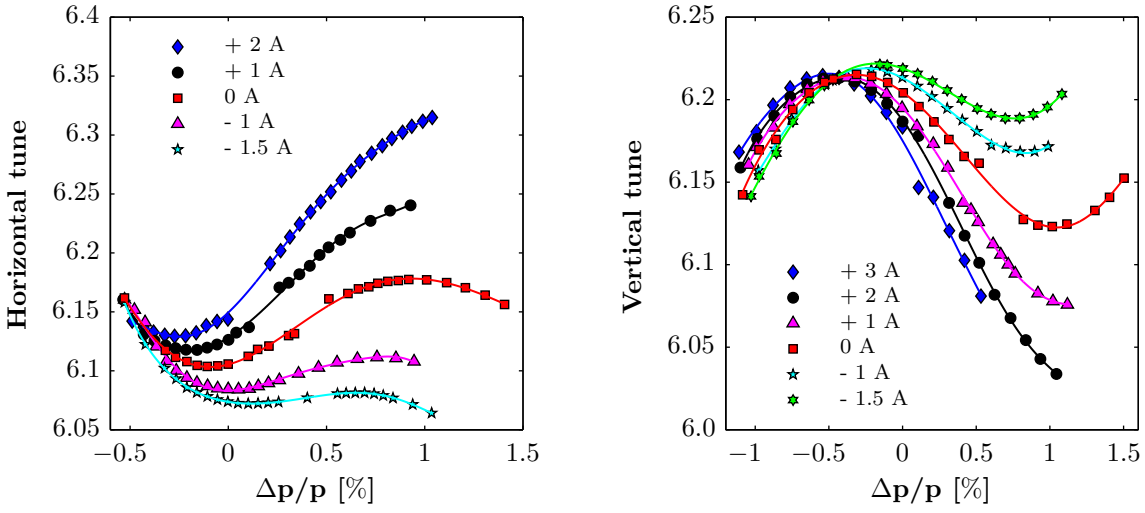

(a) Horizontal plane **(b)** Vertical plane

Figure 3.11: Current offsets applied to the FN.

machine defined by the orbit pick-ups. In order to emphasize the significance of this observation one has to consider the beam going through a sextupole field, which is used to change its linear chromaticitiy and in succession leads to a change of the tune. Only if the particle orbit goes through the center of this sextupole, the tune remains constant. Therefore, the intersection points define the magnetic center of the machine, based on the sextupole contribution produced by the PFW [30]. For the DN this center is found at $\frac{\Delta p}{p} \approx 6 \cdot 10^{-3}$, while for the FN it lies at $\frac{\Delta p}{p} \approx -5 \cdot 10^{-3}$. This difference may arise from the asymmetric alignment of the narrow windings and their localized impact on the magnetic field (see Fig. 2.2b), but remains subject to further studies.

The extracted values of the respective coefficients of the sixth order polynomials can then be used to visualize the evolution of Q, ξ and Q'' depending on the current offset as shown in Figs. 3.12 - 3.16, where the fractional tune q is used in order to plot it together with ξ. The data points are fitted linearly and the resulting slopes describe the relation between currents and beam parameters and are therefore taken as matrix elements.

The plots regarding the F8L and both wide circuits confirm their small influence on the octupole component, while the narrow windings reveal the enormous effect on the linear chromaticities, and the smaller, but nevertheless substantial, effect on the octupole component.

Additionally, it can be observed that the linear chromaticities in the case of the F8L and DW change depending on the programmed current, which was not observed to such an extent by looking at Figs. 3.7 and 3.8. An explanation could be the presence of coupling between the transverse planes, which can directly influence the matrix elements. For clarification Fig. 3.17 shows an enlarged view of the measurement obtained by applying a current offset of -1 A to the DW. The measured points clearly deviate from the polynomial fit and the separation of the tunes due to coupling is visible in both planes.

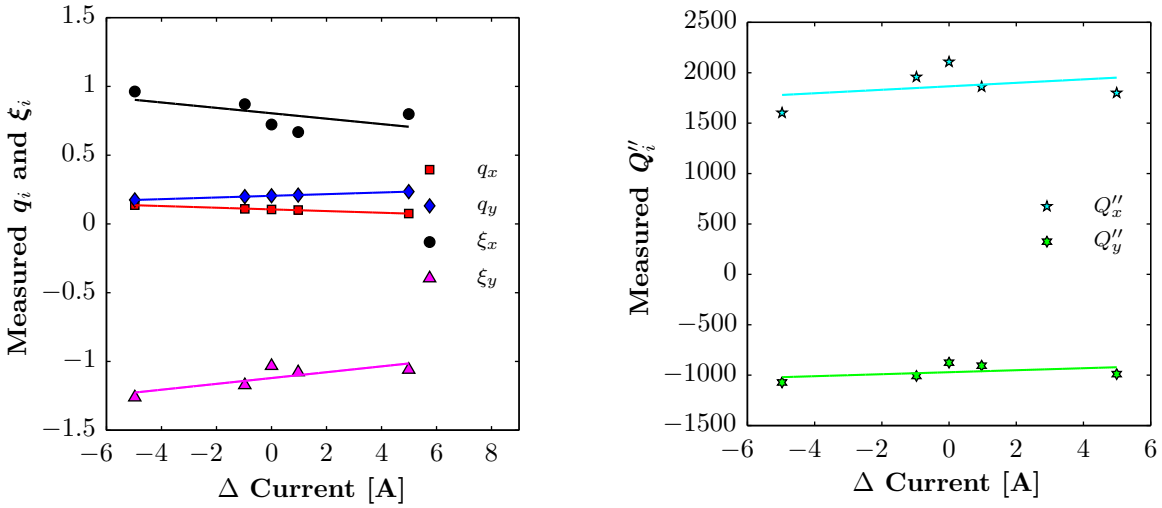

(a) Tune and linear chromaticity **(b)** Second order chromaticity

Figure 3.12: Evolution of the beam parameters depending on the current in the F8L.

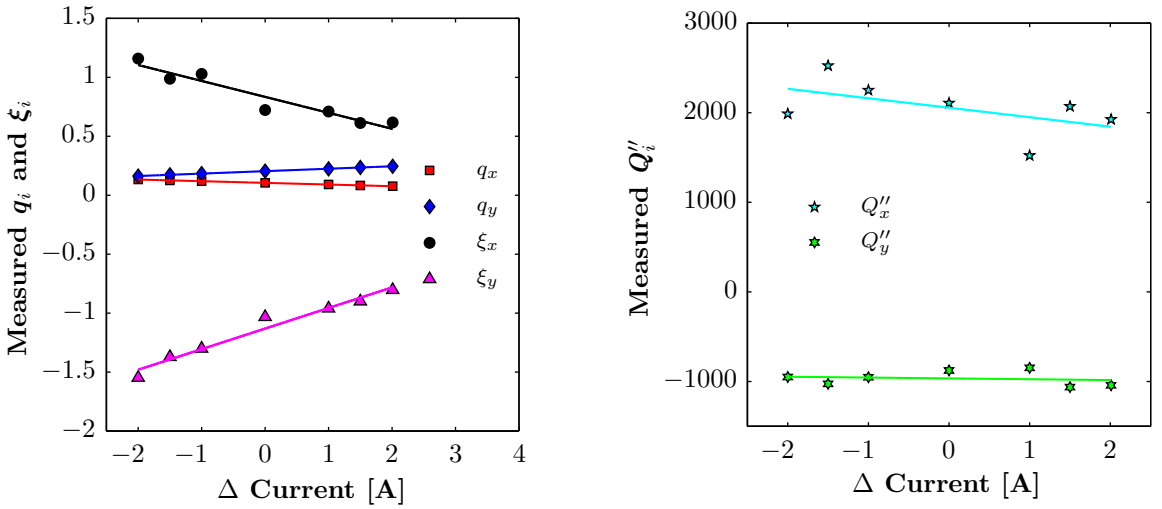

(a) Tune and linear chromaticity **(b)** Second order chromaticity

Figure 3.13: Evolution of the beam parameters depending on the current in the DW.

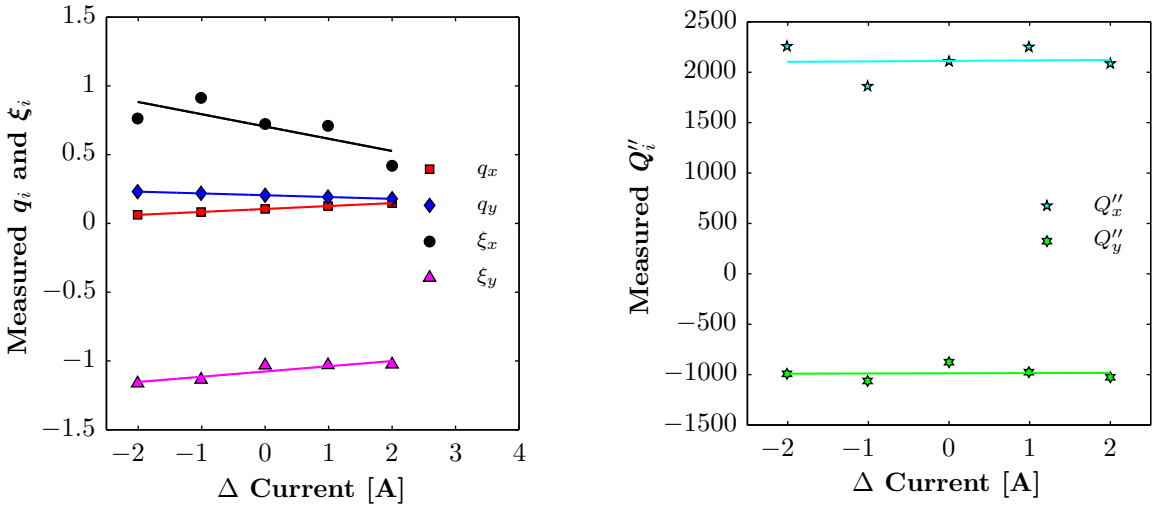

(a) Tune and linear chromaticity **(b)** Second order chromaticity

Figure 3.14: Evolution of the beam parameters depending on the current in the FW.

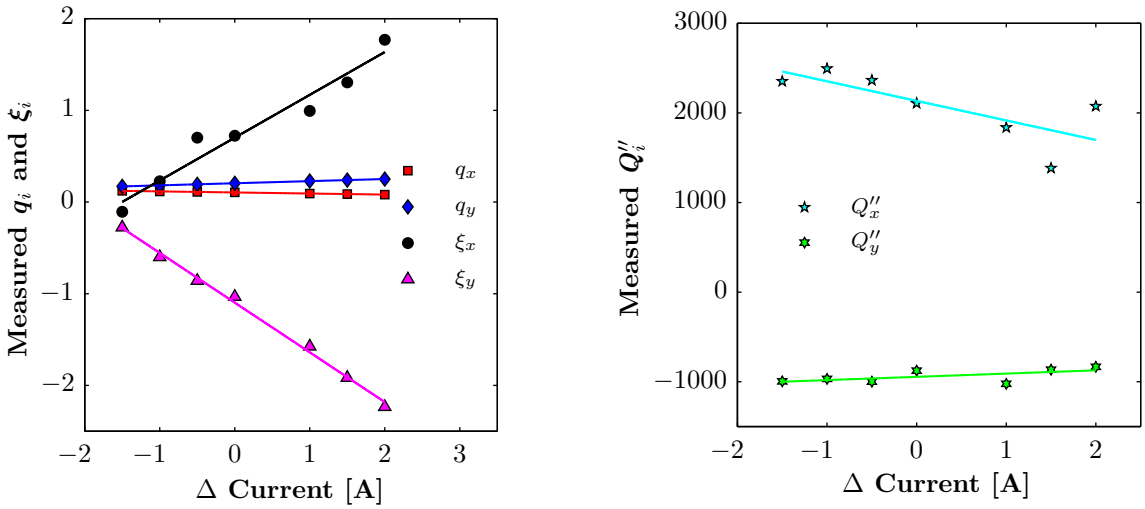

(a) Tune and linear chromaticity **(b)** Second order chromaticity

Figure 3.15: Evolution of the beam parameters depending on the current in the DN.

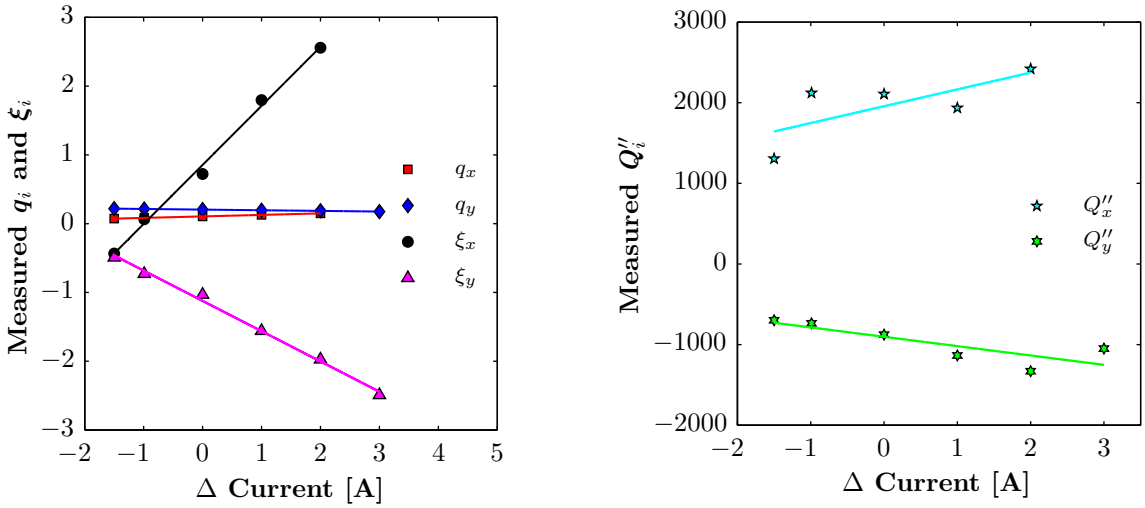

(a) Tune and linear chromaticity **(b)** Second order chromaticity

Figure 3.16: Evolution of the beam parameters depending on the current in the FN.

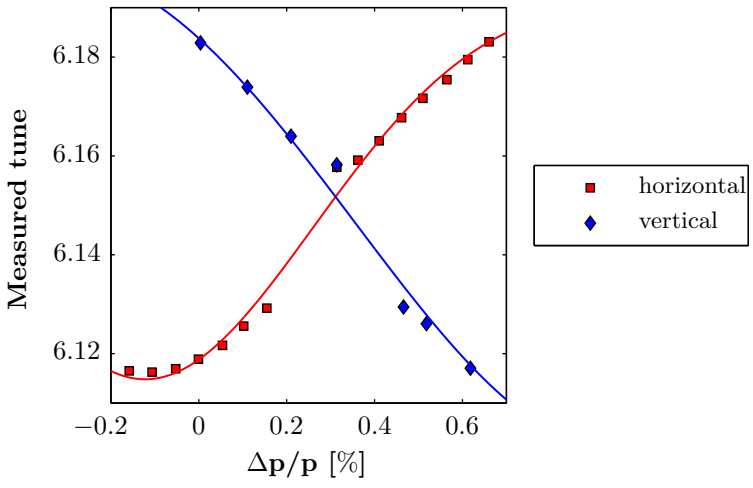

Figure 3.17: Enlargement of Fig. 3.8 displaying the curves -1 A.

With all the resulting matrix elements two different 5CM matrices can be built, containing either Q''_x or Q''_y, as with the available currents only five beam parameters can be determined.
For a kinetic energy of 2 GeV one therefore obtains the non-singular direct matrices

$$\begin{pmatrix} \Delta Q_x \\ \Delta Q_y \\ \Delta \xi_x \\ \Delta \xi_y \\ \Delta Q''_x \end{pmatrix} = \begin{pmatrix} 0.0219 & 0.0213 & -0.0116 & -0.0142 & -0.0061 \\ -0.0094 & -0.0131 & 0.0230 & 0.0207 & 0.0061 \\ 0.8569 & -0.0890 & 0.4671 & -0.1353 & -0.0196 \\ -0.4396 & 0.0380 & -0.5422 & 0.1746 & 0.0212 \\ 207.9130 & 4.6475 & -218.1390 & -105.7302 & 17.2275 \end{pmatrix} \begin{pmatrix} \Delta I_{FN} \\ \Delta I_{FW} \\ \Delta I_{DN} \\ \Delta I_{DW} \\ \Delta I_{F8L} \end{pmatrix}, \tag{3.7}$$

$$\begin{pmatrix} \Delta Q_x \\ \Delta Q_y \\ \Delta \xi_x \\ \Delta \xi_y \\ \Delta Q''_y \end{pmatrix} = \begin{pmatrix} 0.0219 & 0.0213 & -0.0116 & -0.0142 & -0.0061 \\ -0.0094 & -0.0131 & 0.0230 & 0.0207 & 0.0061 \\ 0.8569 & -0.0890 & 0.4671 & -0.1353 & -0.0196 \\ -0.4396 & 0.0380 & -0.5422 & 0.1746 & 0.0212 \\ -115.9633 & 1.9839 & 36.2483 & -9.2980 & 9.8931 \end{pmatrix} \begin{pmatrix} \Delta I_{FN} \\ \Delta I_{FW} \\ \Delta I_{DN} \\ \Delta I_{DW} \\ \Delta I_{F8L} \end{pmatrix}, \tag{3.8}$$

and the respective inverse matrices

$$\begin{pmatrix} \Delta I_{FN} \\ \Delta I_{FW} \\ \Delta I_{DN} \\ \Delta I_{DW} \\ \Delta I_{F8L} \end{pmatrix} = \begin{pmatrix} 9.1950 & 8.3034 & 1.5559 & 1.2855 & 0.0005 \\ 81.2463 & 72.1048 & -3.4521 & -2.8353 & 0.0029 \\ 8.1683 & 13.7911 & -0.9826 & -2.0610 & -0.0005 \\ 19.7073 & 23.6876 & 3.0347 & 4.6650 & -0.0036 \\ 91.4903 & 200.3418 & -11.6632 & -12.2165 & 0.0217 \end{pmatrix} \begin{pmatrix} \Delta Q_x \\ \Delta Q_y \\ \Delta \xi_x \\ \Delta \xi_y \\ \Delta Q''_x \end{pmatrix}, \tag{3.9}$$

$$\begin{pmatrix} \Delta I_{FN} \\ \Delta I_{FW} \\ \Delta I_{DN} \\ \Delta I_{DW} \\ \Delta I_{F8L} \end{pmatrix} = \begin{pmatrix} 8.8553 & 3.9647 & 2.6587 & 2.4701 & 0.0030 \\ 79.3373 & 47.7214 & 2.7459 & 3.8218 & 0.0169 \\ 8.5226 & 18.3158 & -2.1327 & -3.2964 & -0.0031 \\ 22.0787 & 53.9773 & -4.6646 & -3.6046 & -0.0210 \\ 77.4123 & 20.5240 & 34.0444 & 36.8770 & 0.1247 \end{pmatrix} \begin{pmatrix} \Delta Q_x \\ \Delta Q_y \\ \Delta \xi_x \\ \Delta \xi_y \\ \Delta Q''_y \end{pmatrix}. \tag{3.10}$$

Furthermore, a discrepancy observed in [31] can be explained by looking at the data presented in this section, especially the plots in Fig. 3.11. In the mentioned paper the measured matrix elements for the FN were found to be inconsistent with the values expected by simulations. This can be understood by the appearance of non-linearities that make the matrix measurement process strongly dependent on the radial position of the beam. The center of the machine used in simulations therefore has to agree with the one defined by the pick-ups of the orbit measurement system, as a slight radial offset leads to different beam parameters and in succession to different

matrix elements.

3.2.3 Modification of Q''

The inverse matrices in (3.9) and (3.10) allow to calculate the necessary changes of currents in the PFW for a desired change of beam parameters. Vanishing Q''_x should be obtained by applying current offsets according to

$$\begin{pmatrix} \Delta I_{FN} \\ \Delta I_{FW} \\ \Delta I_{DN} \\ \Delta I_{DW} \\ \Delta I_{F8L} \end{pmatrix} = \mathbf{M}_x^{-1}(5\times 5) \begin{pmatrix} \Delta Q_x \\ \Delta Q_y \\ \Delta \xi_x \\ \Delta \xi_y \\ \Delta Q''_x \end{pmatrix} = \mathbf{M}_x^{-1}(5\times 5) \begin{pmatrix} 0 \\ 0 \\ 0 \\ 0 \\ -2105 \end{pmatrix} = \begin{pmatrix} -1.10 \\ -6.18 \\ 1.15 \\ 7.68 \\ -45.59 \end{pmatrix} \tag{3.11}$$

where $\mathbf{M}_x^{-1}(5\times 5)$ represents the inverse matrix in (3.9)[3]. This approach was expected to have a predictable influence on both second order chromaticities, as a chosen value was programmed in the horizontal plane and the change occurring in the vertical plane can be calculated by inserting the currents obtained in (3.11) into (3.8).
Measurements for additional values of $\Delta Q''_x$ have been carried out as well and the complete set of curves is shown in Fig. 3.18, where the legend describes the applied changes. Especially in the center of the machine, contrary to expectations, no change of curvature could be observed. The overall evolution of Q''_x in Fig. 3.19c reveals a behavior, which does not even approximately correspond to the values that have been programmed. Starting from the point $\Delta Q''_x = 0$ the dashed line displays the theoretically expected beam response, while the measured marker positions show a completely opposite trend. Nevertheless, it is interesting that $\Delta Q''_y$ follows the theoretical line although it is the sixth parameter and therefore left free.
Additional problems become apparent from Fig. 3.19b, where a change of both linear chromaticities is seen while they were thought to remain constant as the applied set of currents in the PFW was explicitly chosen to only influence $\Delta Q''_x$. In relation to the evolution of the tunes very good agreement with the expectations can be observed, except for the measurement $\Delta Q''_x = 1000$.
One explanation of the non-predictable effect of the applied changes may be a matrix that is no longer valid for the currents in (3.11). When comparing these values with the currents which were used to obtain the direct matrices (see legends in Figs. 3.7 - 3.11) one finds a difference to the factor of nine for the F8L and a factor of two or three for the wide windings. However, these are exactly the three circuits that mainly influence the quadrupole component and, therefore, even for currents which seem to be far beyond matrix validity, the matrix could still be valid as long as the currents in the DN and FN remain small enough.

[3] The index y will be used for the matrix in (3.10).

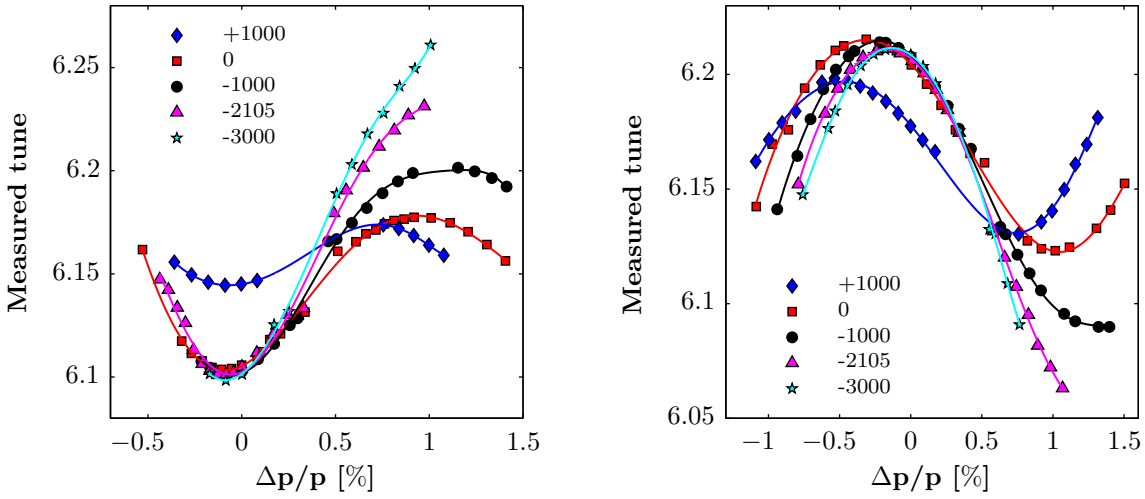

(a) Horizontal plane **(b)** Vertical plane

Figure 3.18: Influence on Q''_x by applying different values of $\Delta Q''_x$.

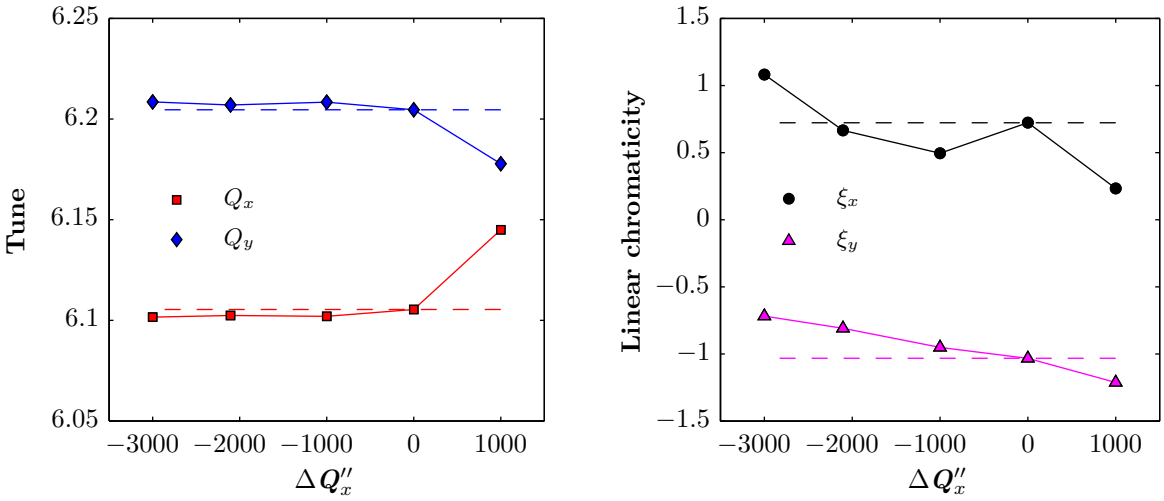

(a) Tunes **(b)** Linear chromaticities

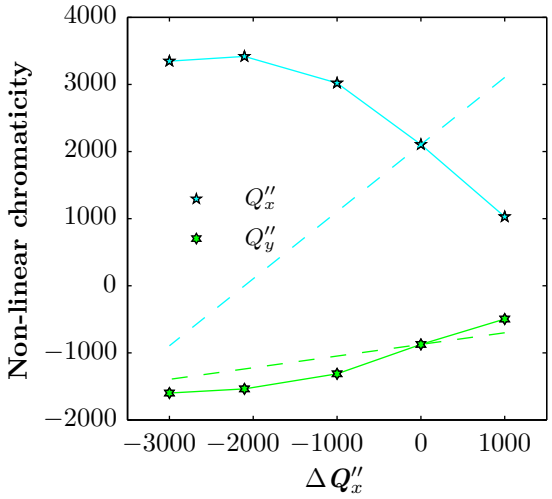

(c) Second order chromaticities

Figure 3.19: Evolution of the beam parameters depending on $\Delta Q''_x$.

In the vertical plane the same process can be applied by using $\mathbf{M}_y^{-1}$, resulting in currents of

$$\begin{pmatrix} \Delta I_{FN} \\ \Delta I_{FW} \\ \Delta I_{DN} \\ \Delta I_{DW} \\ \Delta I_{F8L} \end{pmatrix} = \mathbf{M}_y^{-1}(5\times 5) \begin{pmatrix} 0 \\ 0 \\ 0 \\ 0 \\ 874 \end{pmatrix} = \begin{pmatrix} 2.63 \\ 14.78 \\ -2.74 \\ -18.36 \\ 109 \end{pmatrix}, \tag{3.12}$$

which are even further out of the theoretical matrix validity. Again, several measurements with varying $\Delta Q_y''$ have been carried out and the curves are presented in Fig. 3.20. In this case the evolution of $\Delta Q_y''$ is almost as expected, but an enormous change of ξ_v is observed as well (see Fig. 3.21).

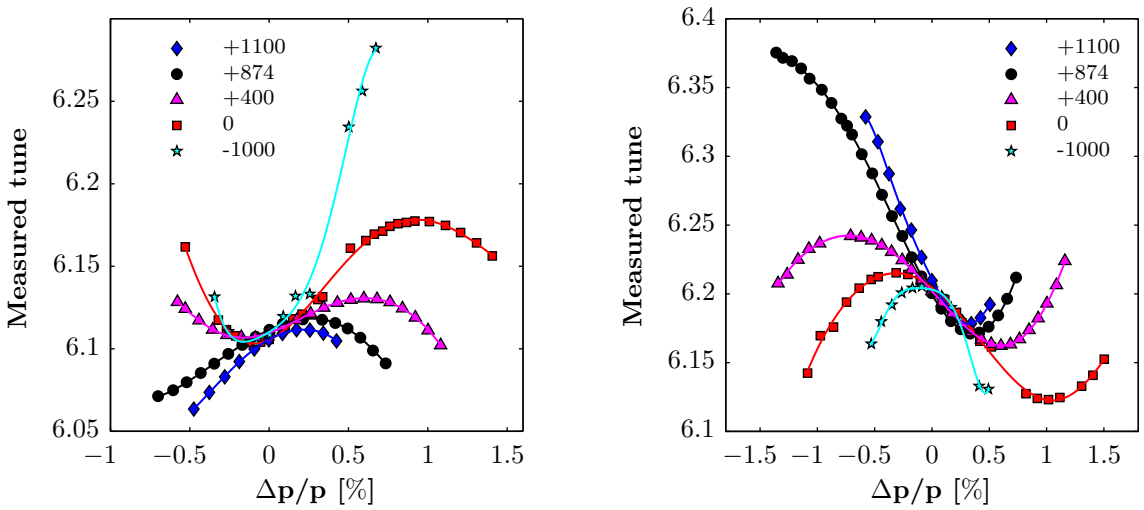

(a) Horizontal plane **(b)** Vertical plane

Figure 3.20: Influence on Q_y'' by applying different values of $\Delta Q_y''$.

In conclusion, it seems that both second order chromaticities are not controllable by the experimentally obtained matrix. A next step would therefore be to obtain the matrices (3.7) and (3.8) from simulations, providing a larger area of validity. Additionally, a different working point should be studied, where there is less corruption of the obtained beam parameters due to linear coupling.

Despite the ineffectiveness of the predictable modification of Q'', additional studies have been carried out to examine the effect of the PFW on the remaining beam parameters.

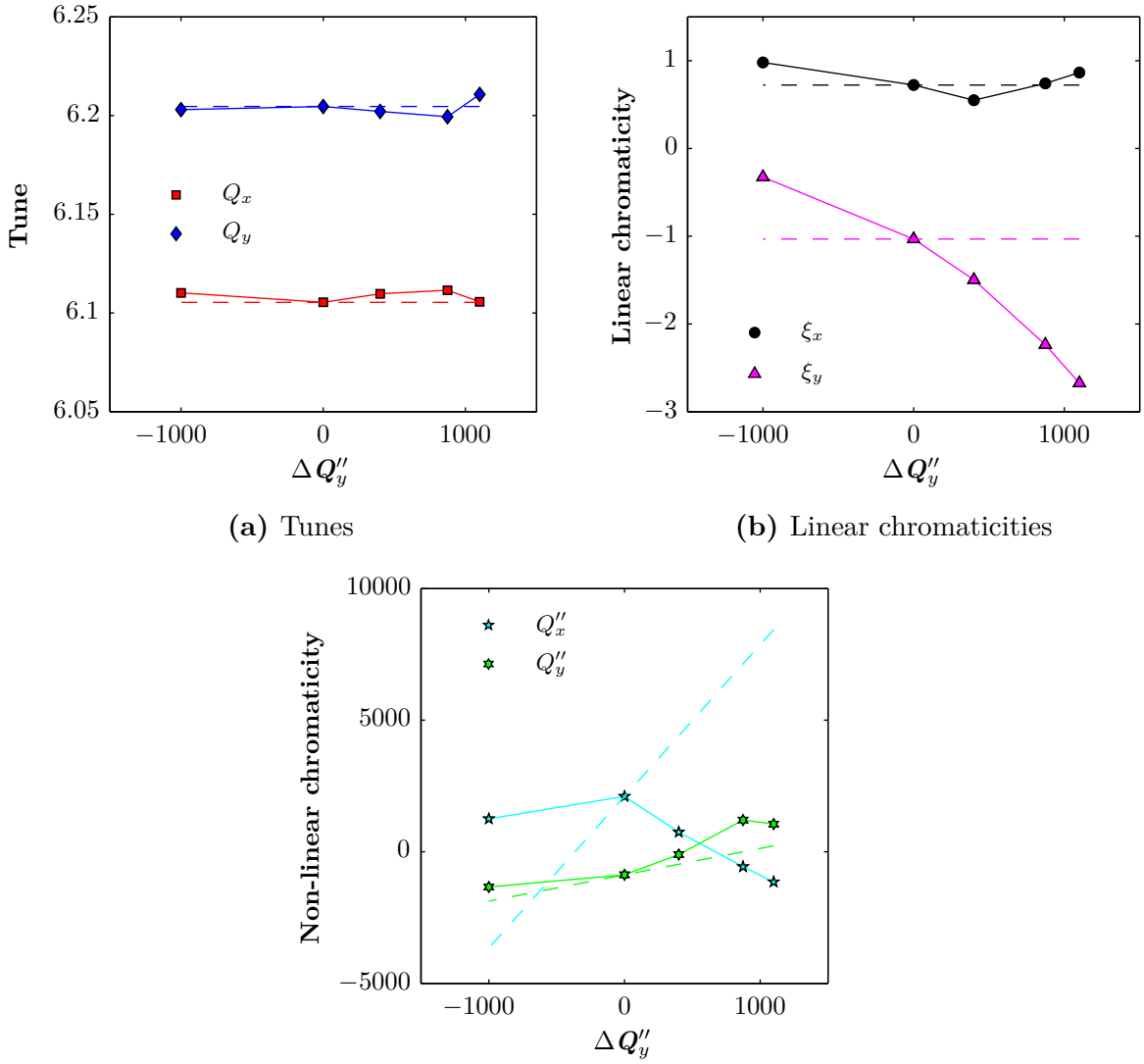

(a) Tunes

(b) Linear chromaticities

(c) Second order chromaticities

Figure 3.21: Evolution of the beam parameters depending on $\Delta Q''_y$.

3.2.4 Modification of Q

Every modification of the tune is expected to result in a shift of the reference measurement in Fig. 3.4b. To examine the influence of both $\mathbf{M}_x^{-1}$ and $\mathbf{M}_y^{-1}$ several values of Q have been programmed and the results show very good agreement between the expected behavior and the measured beam response.

In Figs. 3.22 and 3.23 either the horizontal or the vertical tune was changed by using different matrices in each case. The expected shift with respect to the reference curve is clearly visible and the new values of Q follow the programming very well. Especially important is the fact that the tune which was not changed remains the same in both cases without drastic modification of

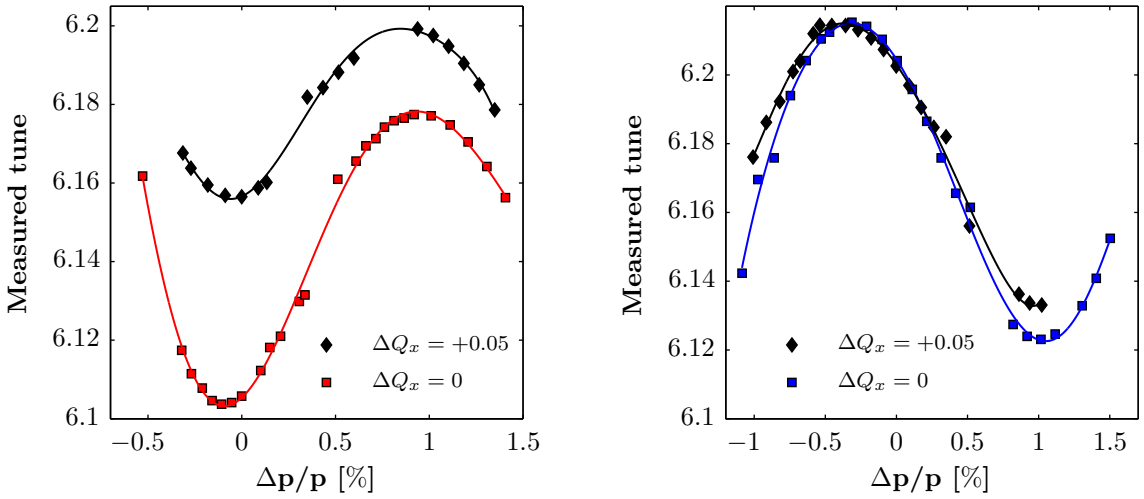

(a) Horizontal plane **(b)** Vertical plane

Figure 3.22: Modification of Q_x with settings being programmed by $\mathbf{M}_x^{-1}$.

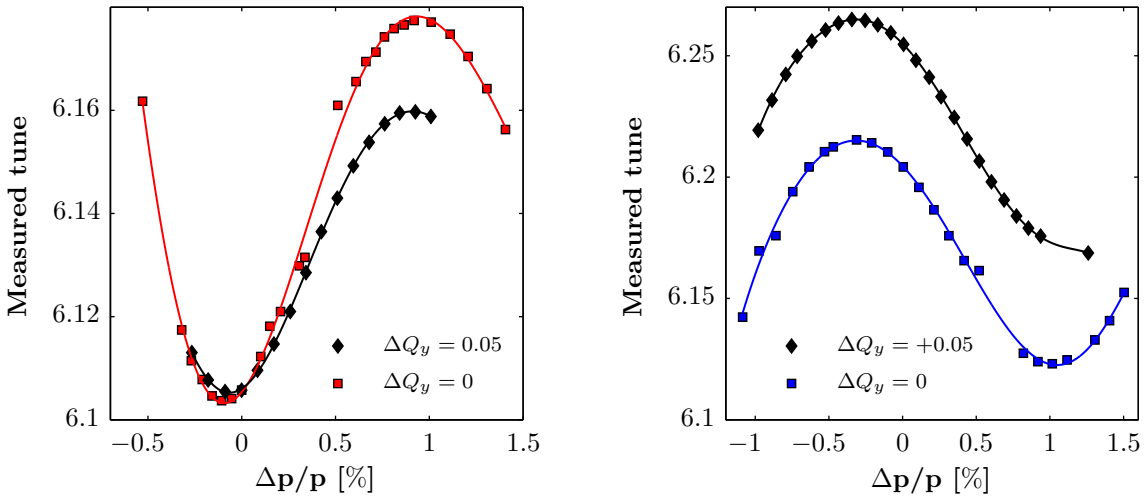

(a) Horizontal plane **(b)** Vertical plane

Figure 3.23: Modification of Q_y with settings being programmed by $\mathbf{M}_y^{-1}$.

the shape of the curve.

In addition, an offset in both planes at the same time has been applied in order to separate the tunes (see Figs. 3.24 and 3.25). Calculation of the currents of the narrow and wide circuits for this case leads to small values with the main contribution comming from the F8L. This, again, reflects the design principle of this circuit, as the modification of the magnetic field causes a separation of both tunes. Therefore, it is also comprehensible that the non-linear shape remains the same.

While the beam followed the applied changes very well in the previous cases, this could not be

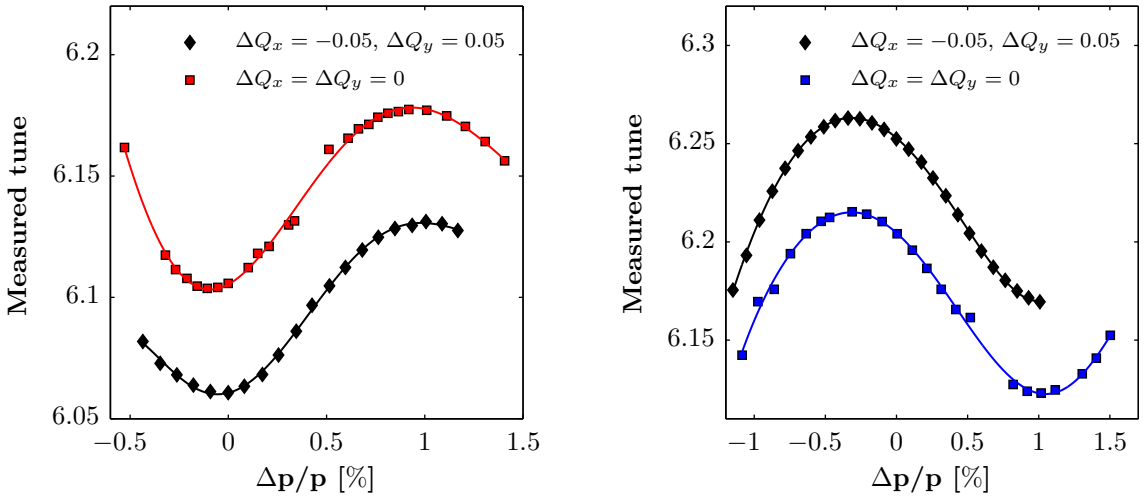

(a) Horizontal plane **(b)** Vertical plane

Figure 3.24: Separation of the tunes programmed by $\mathbf{M}_x^{-1}$.

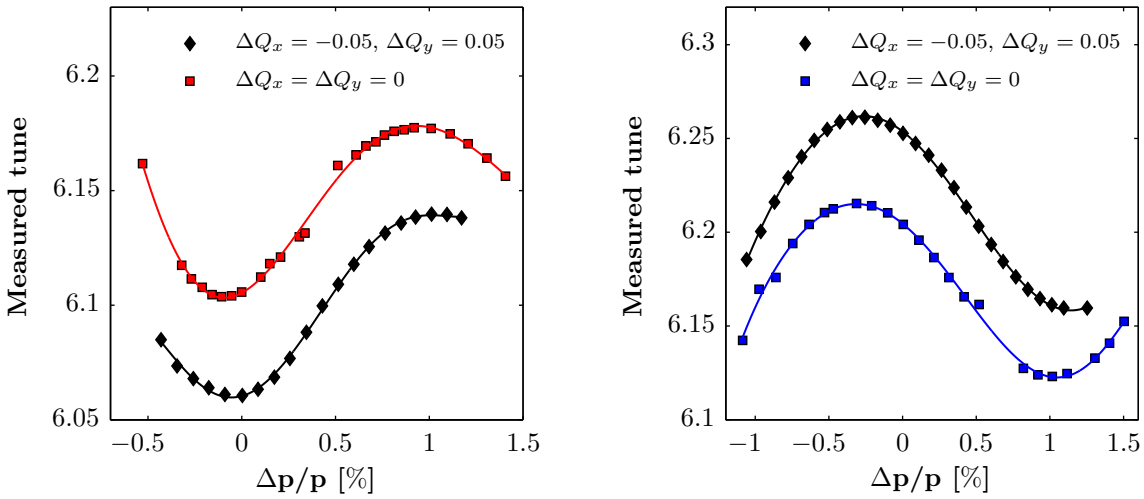

(a) Horizontal plane **(b)** Vertical plane

Figure 3.25: Separation of the tunes programmed by $\mathbf{M}_y^{-1}$.

observed in the following one. Applying an offset of 0.10 to the tunes in both planes suddenly leads to almost vanishing Q'' and ξ_x becomes negative (see Fig. 3.26).
This effect is explained by Fig. 3.27 and the almost equal currents within the narrow and wide circuits of the respective magnet half unit shown there. Such a setup of currents is nearly the same as it would be in 3CM and the far more linear behavior therefore becomes understandable. However, the problematic points about this measurement are the unintentional changes of ξ and Q''. This further restricts the applicability of the measured matrices as they do not account for effects caused by balanced narrow and wide circuits.

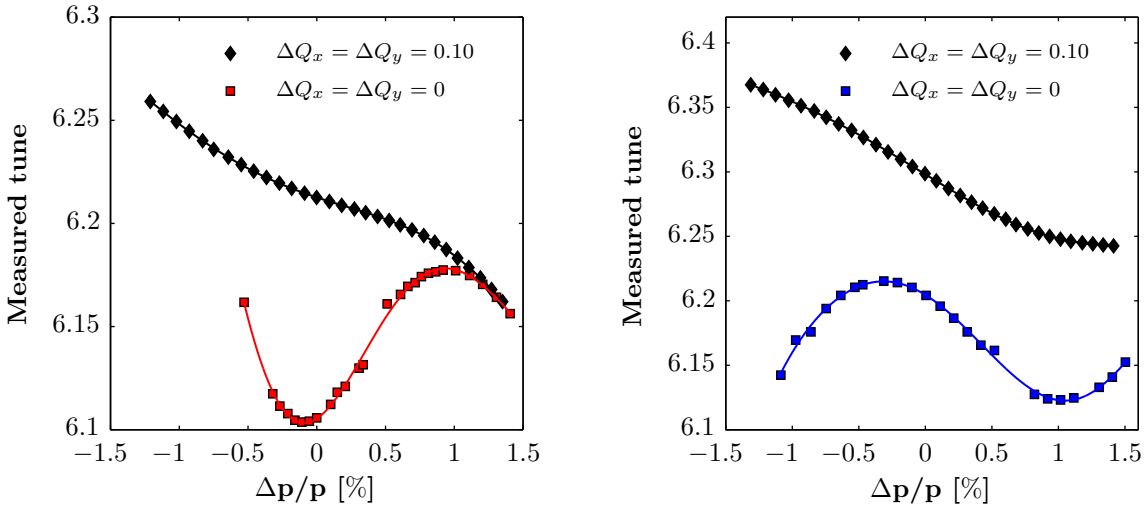

(a) Horizontal plane **(b)** Vertical plane

Figure 3.26: Change of non-linearities by applying the same ΔQ in both planes.

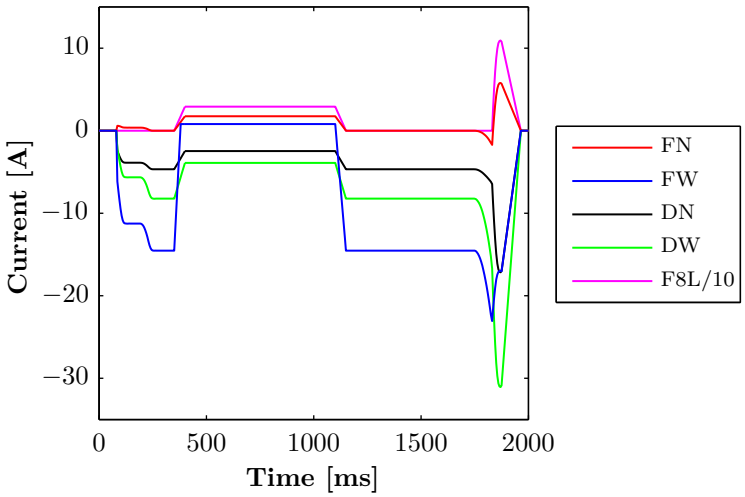

Figure 3.27: Currents to to obtain the measurements in Fig. 3.26.

3.2.5 Modification of ξ

In Sections 2.3 and 3.1 the importance of changing linear chromaticity has already been discussed. Similar to adjusting the tunes linear chromaticities can be programmed either by $\mathbf{M}_x^{-1}$ or $\mathbf{M}_y^{-1}$ and the measurements on the following pages have been conducted to examine the influence of the PFW on these beam parameters.

Figure 3.28 shows a set of measurements where several offsets $\Delta\xi_x$ (values shown in the legend) have been applied to the reference value $\xi_x = 0.73$. Both tunes and linear chromaticities nicely follow the expectations but Q''_x does not remain constant as shown in Fig. 3.29.

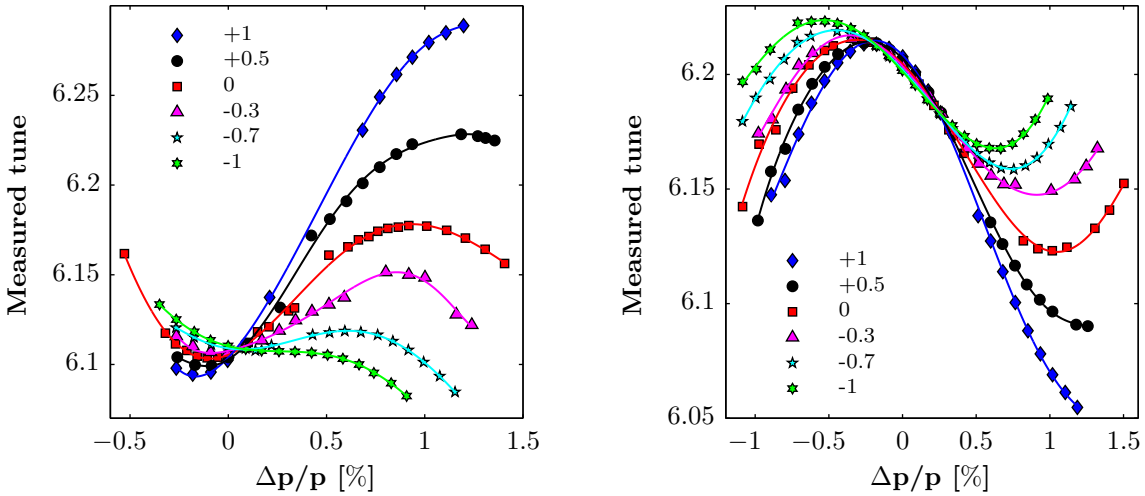

(a) Horizontal plane **(b)** Vertical plane

Figure 3.28: Modification of ξ_x programmed by $\mathbf{M}_x^{-1}$.

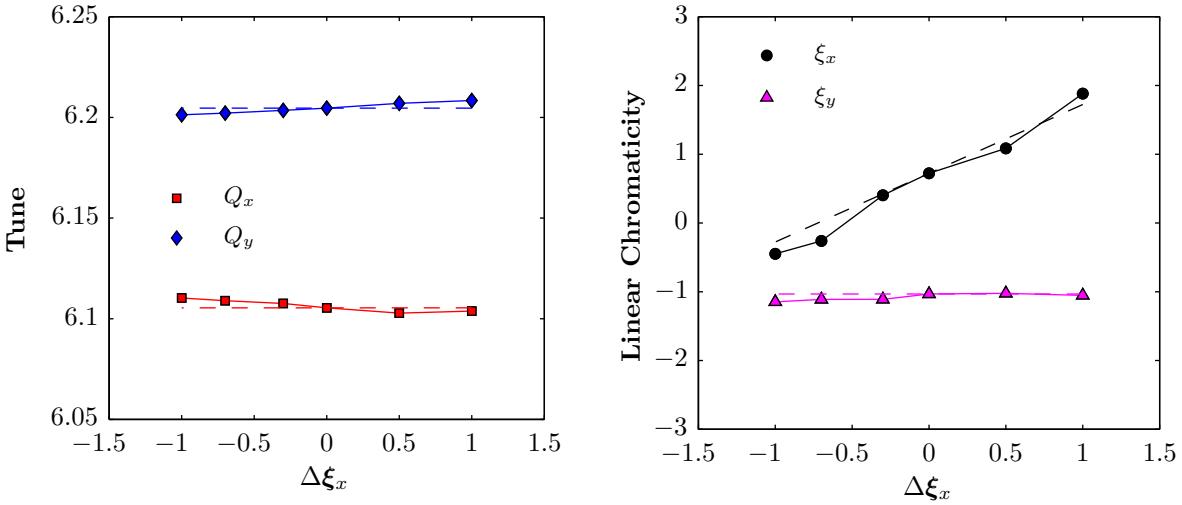

(a) Tunes **(b)** Linear Chromaticities

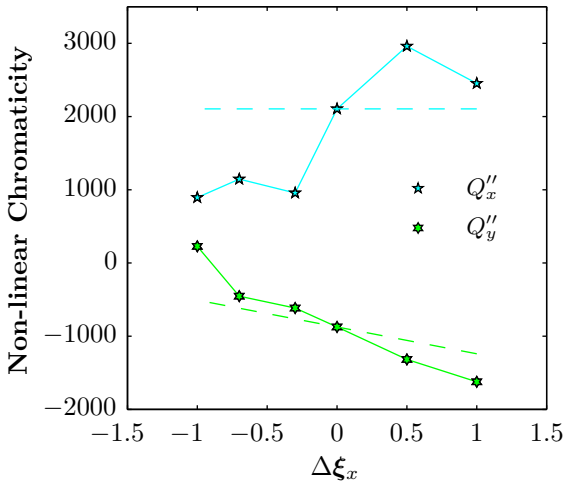

(c) Second order chromaticities

Figure 3.29: Evolution of the beam parameters depending on $\Delta\xi_x$ and $\mathbf{M}_x^{-1}$.

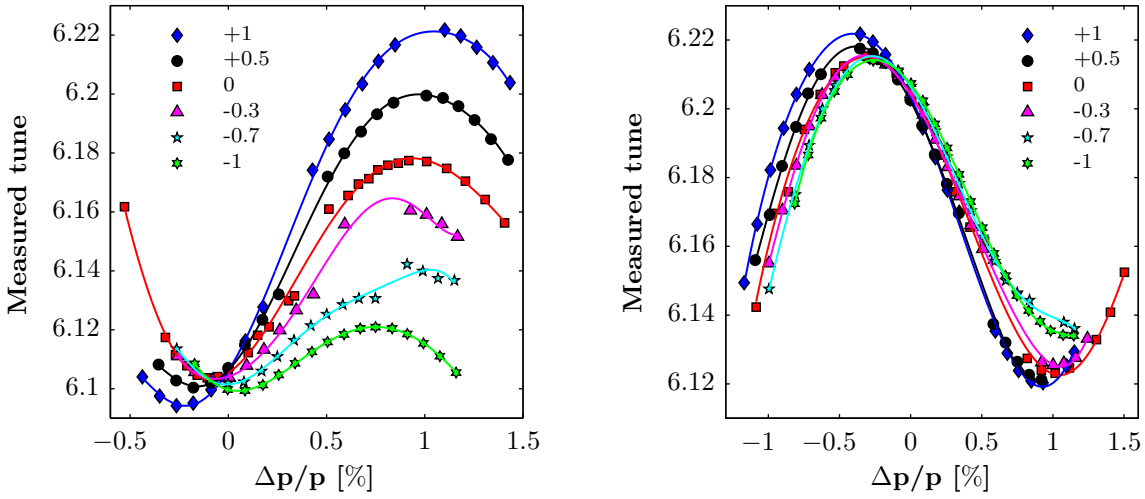

(a) Horizontal plane **(b)** Vertical plane

Figure 3.30: Modification of ξ_x programmed by $\mathbf{M}_y^{-1}$.

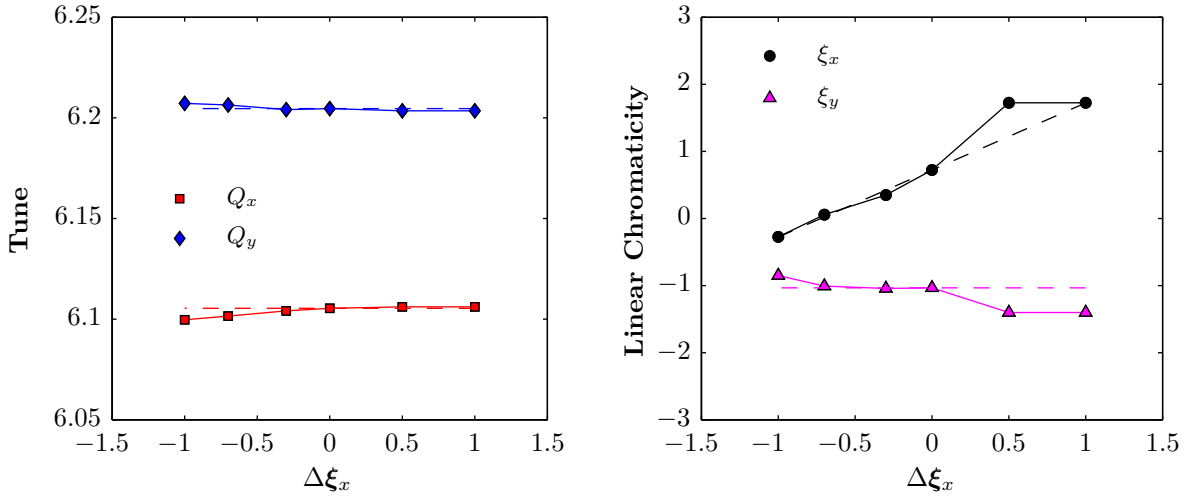

(a) Tunes **(b)** Linear Chromaticities

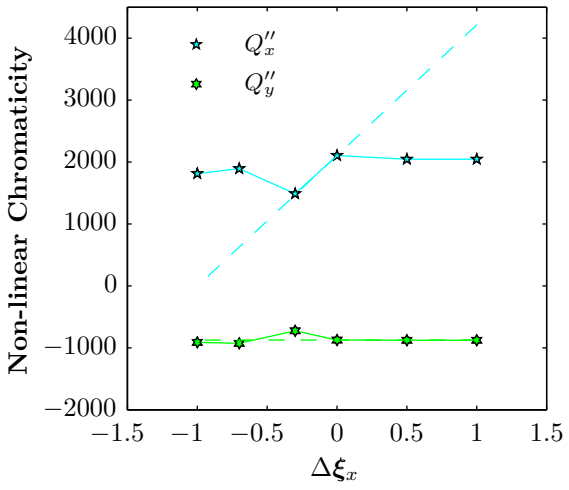

(c) Second order chromaticities

Figure 3.31: Evolution of the beam parameters depending on $\Delta\xi_x$ and $\mathbf{M}_y^{-1}$.

From this point of view the use of $\mathbf{M}_y^{-1}$ leads to an improved possibility for ξ_x-control, as both second order parameters remain constant independent of $\Delta\xi_x$ and also tunes and linear chromaticities behave almost as programmed (see Figs. 3.30 and 3.31).
Furthermore, changes of ξ_y by using both matrices have been subject to a study. Calculation of the correction currents based on $\mathbf{M}_x^{-1}$ reveals serious weaknesses in the horizontal plane compared to the previously shown modifications. Instead of remaining constant even more change of Q_x'' can be observed and, additionally, Q and ξ are significantly different from what the dashed line and, therefore, the theoretical expectations suggest (see Figs. 3.32 and 3.33).
Interestingly, correction of ξ_y is also found to work better by using $\mathbf{M}_y^{-1}$. Figures 3.34 and 3.35 clearly show the constant behavior of all beam parameters except ξ_y, which is exactly the expected behavior.
In a last step correction of both linear chromaticities at the same time has been applied. The measured values stated in the subfigures of Figs. 3.36 and 3.37 and the respective offsets shown by the legends have to be read in relation to the reference values $\xi_x = 0.73$ and $\xi_y = -1.03$. Apart from the case $\Delta\xi = +1$, $\Delta\xi = +0.5$ agreement between measurements based on $\mathbf{M}_x^{-1}$ and $\mathbf{M}_y^{-1}$ and theoretical expectations is very good. In the mentioned exception a large difference in Q_x'' for the $\mathbf{M}_x^{-1}$-case is observed while ξ_y is not changing at all in the other one.

3.3 Summary

Extensive studies have been conducted in order to examine the influence of the PFW on the beam parameters $Q_{x,y}$, $\xi_{x,y}$ and $Q''_{x,y}$ at the future PS injection energy of 2 GeV.
The PFW together with the F8L constitute five individual circuits and should therefore allow control over both tunes and linear chromaticities as well as the second order chromaticity in one plane. A matrix formalism to establish a relationship between these parameters and the currents within the five circuits has been presented and, based on this concept, the 5CM matrix was measured for a specific working point.
It was discovered that this new matrix permits to control both transverse tunes in the expected way, while the situation appeared to be more complex for the linear chromaticities. For these parameters the obtained results differed significantly depending on the matrix that was chosen to calculate the correction currents - $\mathbf{M}_x^{-1}$ or $\mathbf{M}_y^{-1}$ - and results were found to be in better agreement with expectations when using $\mathbf{M}_y^{-1}$.
Concerning both second order chromaticities Q_x'' and Q_y'', the measurements revealed no means to predictably influence these parameters, which might be due to the restricted area of validity of the measured 5CM matrices.

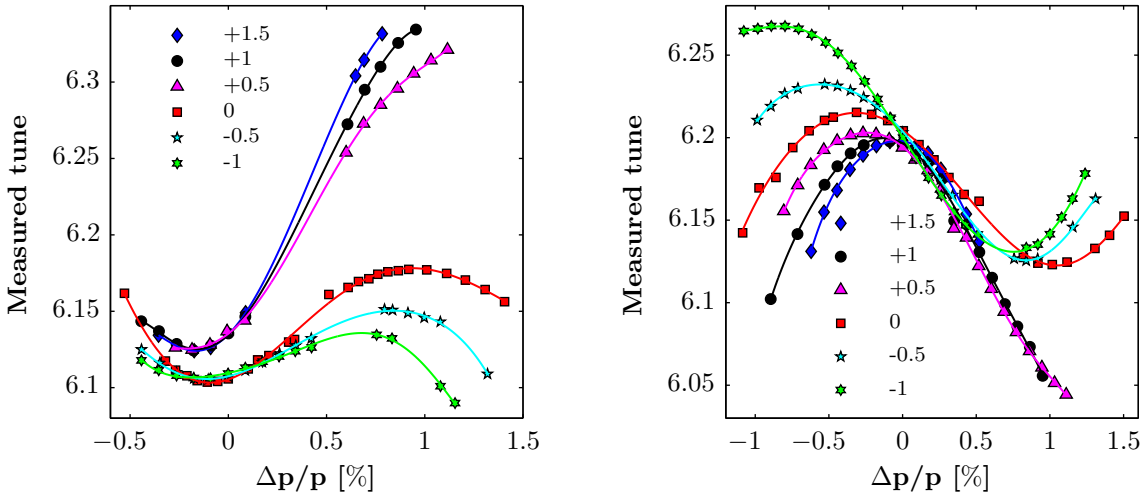

(a) Horizontal plane **(b)** Vertical plane

Figure 3.32: Modification of ξ_y programmed by $\mathbf{M}_x^{-1}$.

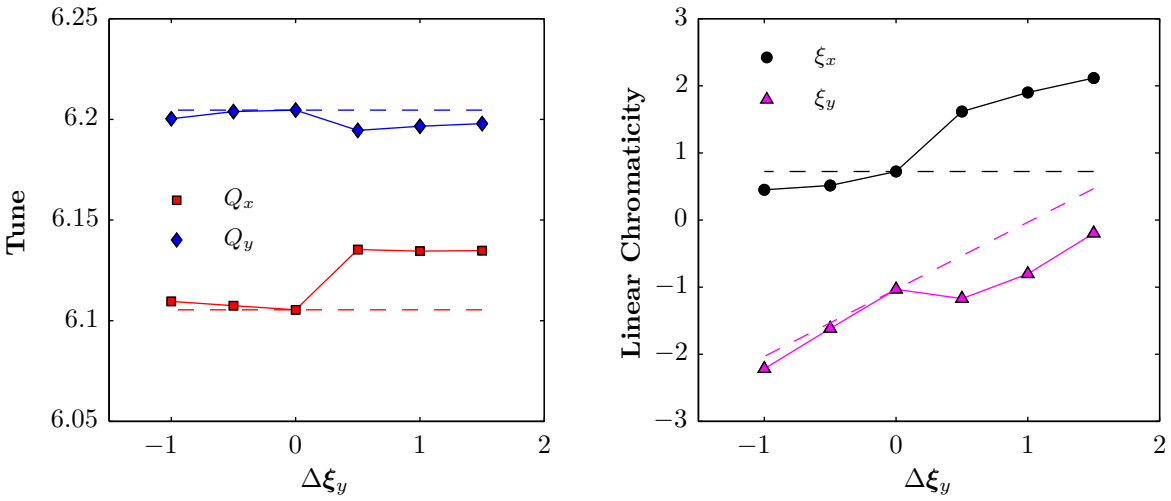

(a) Tunes **(b)** Linear Chromaticities

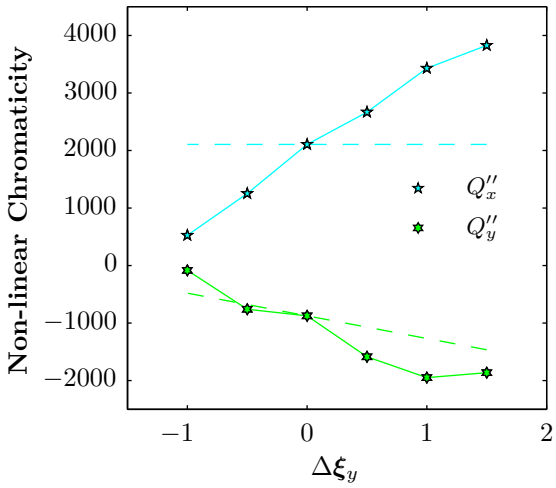

(c) Second order chromaticities

Figure 3.33: Evolution of the beam parameters depending on $\Delta\xi_y$ and $\mathbf{M}_x^{-1}$.

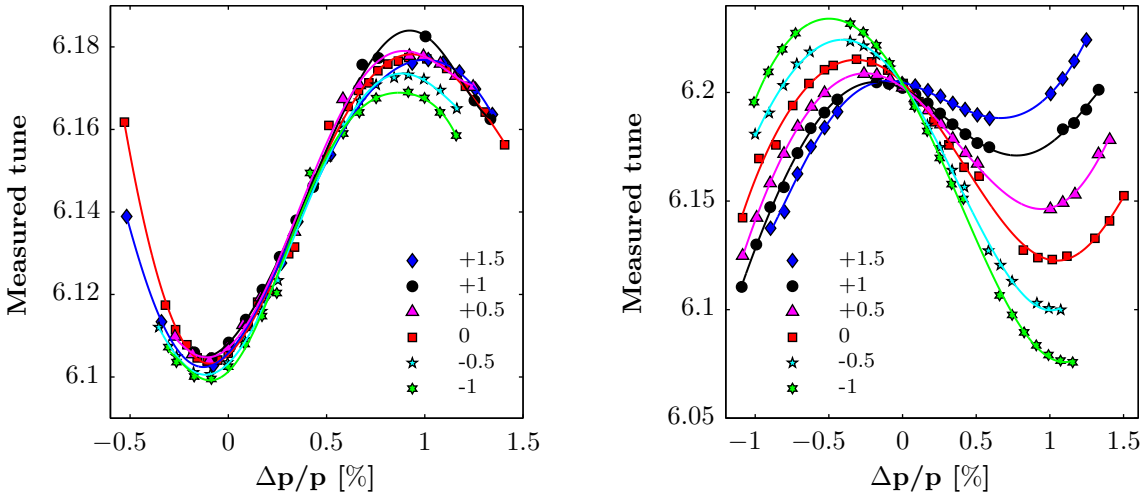

(a) Horizontal plane **(b)** Vertical plane

Figure 3.34: Modification of ξ_y programmed by $\mathbf{M}_y^{-1}$.

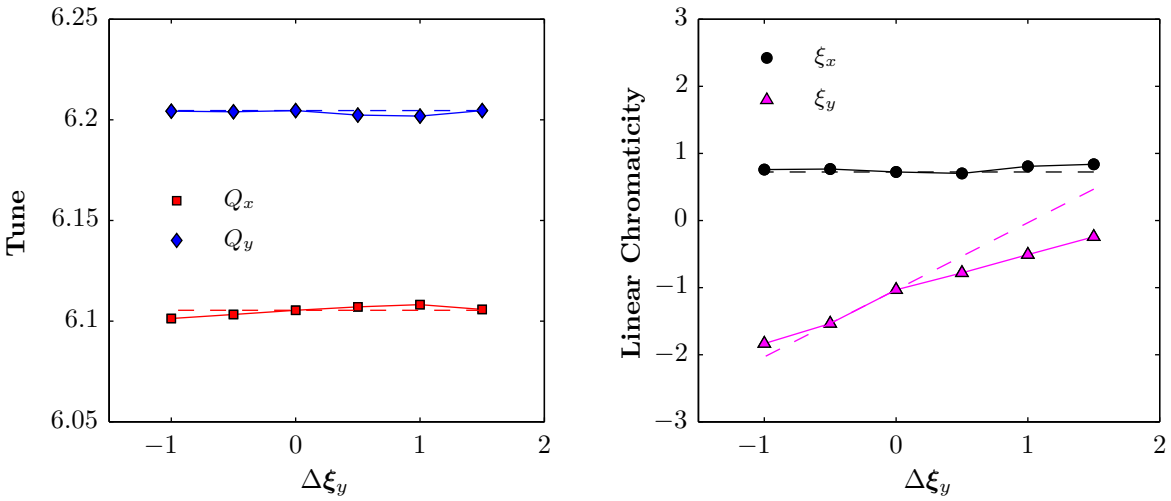

(a) Tunes **(b)** Linear Chromaticities

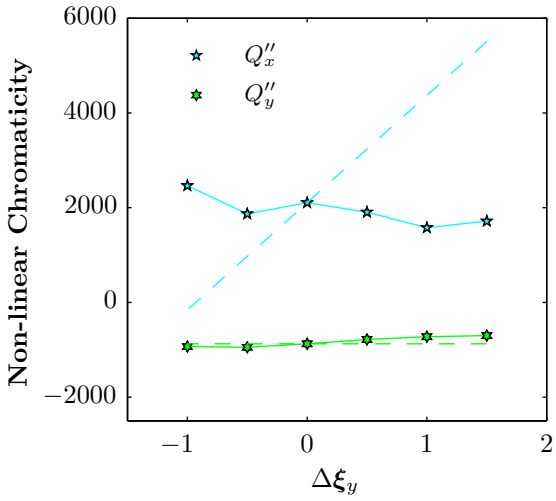

(c) Second order chromaticities

Figure 3.35: Evolution of the beam parameters depending on $\Delta\xi_y$ and $\mathbf{M}_y^{-1}$.

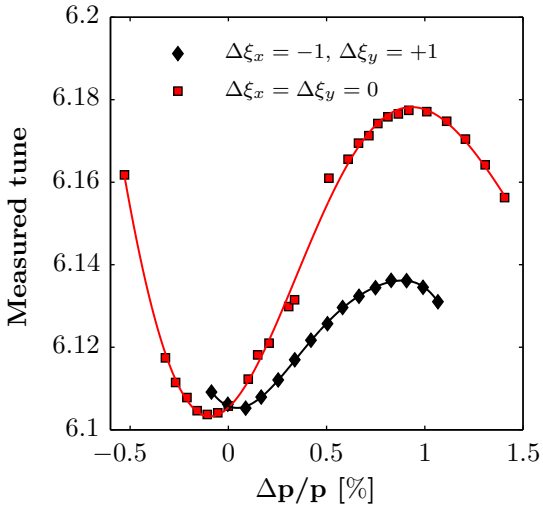

(a) Horizontal plane, measured $\xi_x = -0.32$

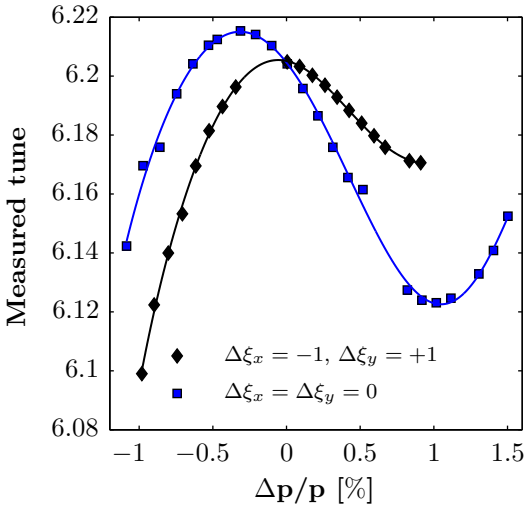

(b) Vertical plane, measured $\xi_y = -0.18$

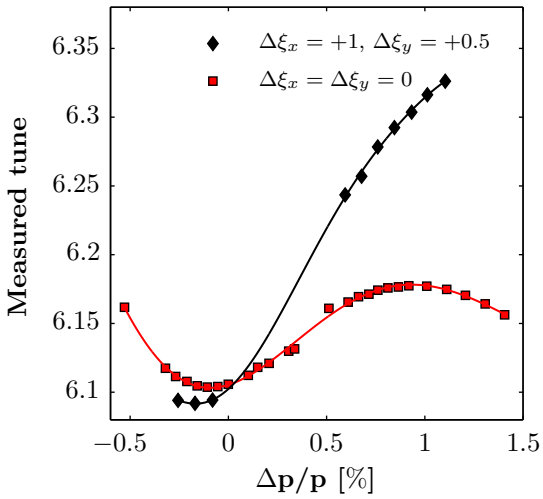

(c) Horizontal plane, measured $\xi_x = 2.11$

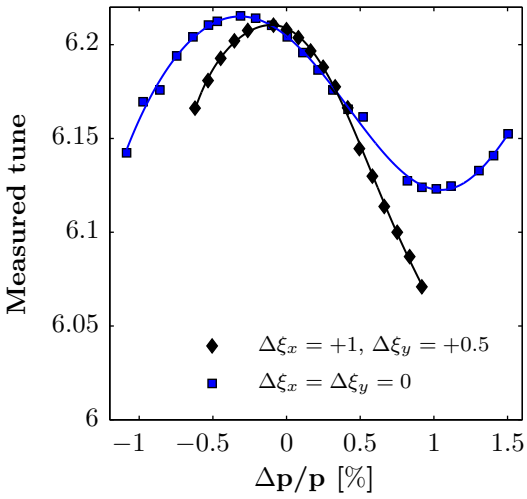

(d) Vertical plane, measured $\xi_y = -0.58$

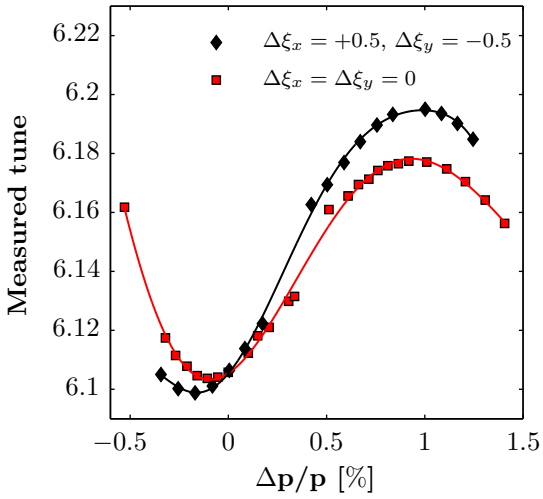

(e) Horizontal plane, measured $\xi_x = 1.30$

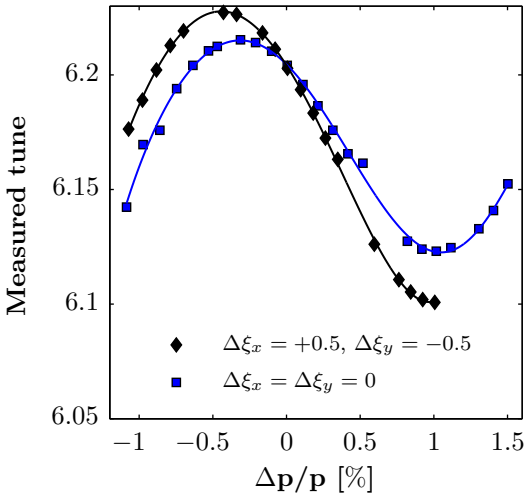

(f) Vertical plane, measured $\xi_y = -1.62$

Figure 3.36: Modification of ξ_x and ξ_y at the same time, programmed by $\mathbf{M}_x^{-1}$.

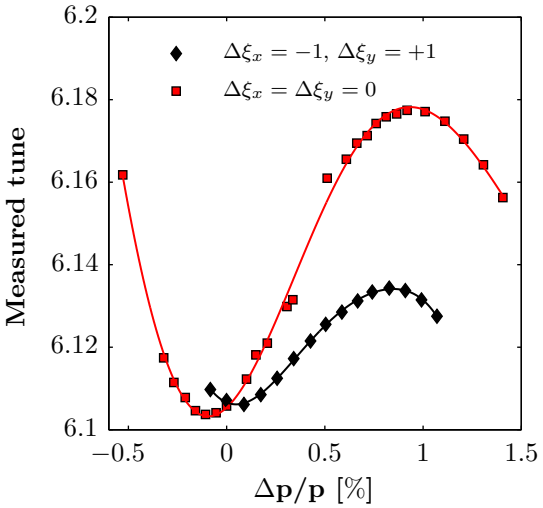

(a) Horizontal plane, measured $\xi_x = -0.33$

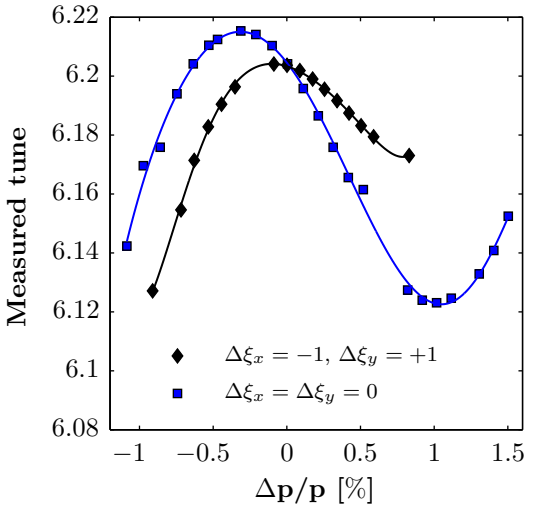

(b) Vertical plane, measured $\xi_y = -0.25$

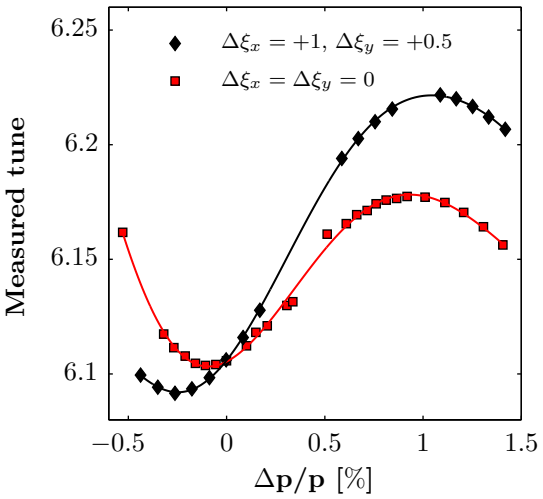

(c) Horizontal plane, measured $\xi_x = 1.77$

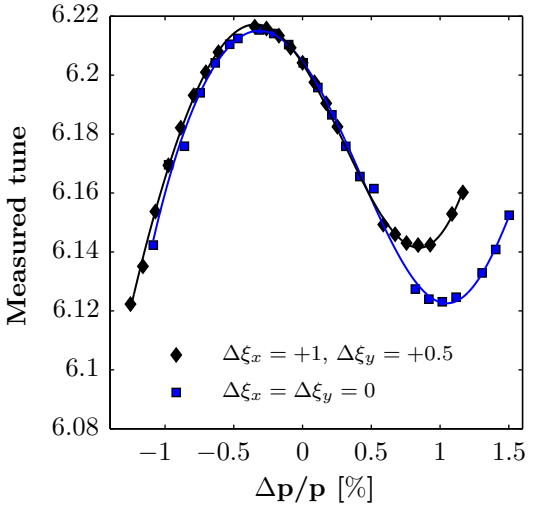

(d) Vertical plane, measured $\xi_y = -1.17$

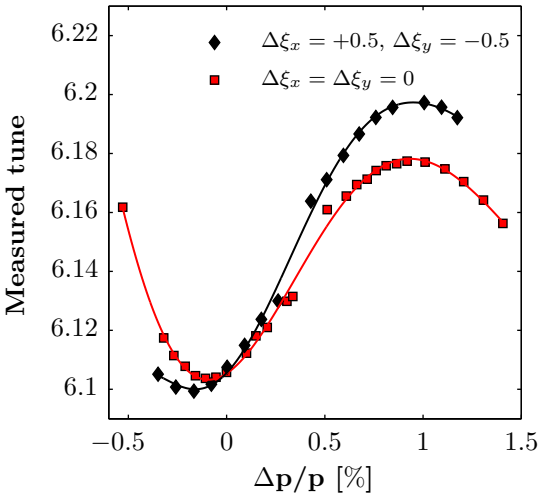

(e) Horizontal plane, measured $\xi_x = 1.15$

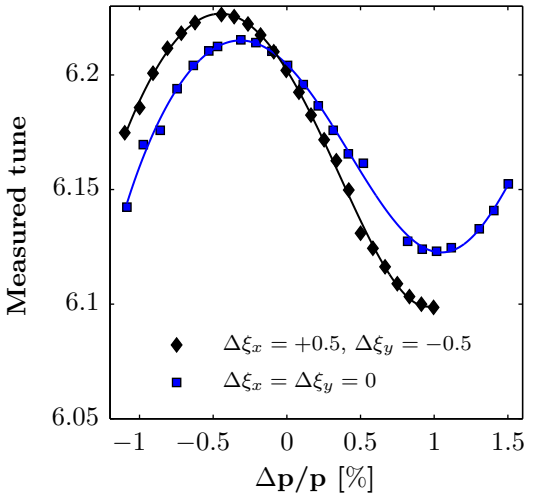

(f) Vertical plane, measured $\xi_y = -1.68$

Figure 3.37: Modification of ξ_x and ξ_y at the same time, programmed by $\mathbf{M}_y^{-1}$.

4 Identification of resonances

At low energy the presence of certain excited betatron resonances is currently the major limitation for future high-brightness and high-intensity beams at the CERN PS. Several machine development sessions that have taken place during previous years (see e.g. [32,33]) as well as operational experience have clearly shown the emittance growth of high space charge beams caused by the vertical integer resonance, $Q_y = 6.0$.

The injection working points of today's operational beams are concentrated in the region $Q_{x,y} \in [6.10, 6.30]$, an area where the linear coupling as well as the vertical 3^{rd} and 4^{th} order resonances are situated. However, for the operational space charge dominated beams such as LHC and TOF - the calculated vertical tune spreads amount to $\Delta Q_y \approx -0.3$ at 1.4 GeV - no degradation of beam quality is observed [34].

The large negative bare machine chromaticity additionally causes a tune spread of $\Delta Q \approx -10^{-2}$, an order of magnitude smaller compared to the effect of space charge. Chromaticity correction at injection to a value closer to zero would therefore not only have a beneficial effect with respect to Head-Tail instabilities (in combination with an operational transverse damper, see also Section 2.3), but also concerning a reduction of ΔQ.

All these aspects have to be considered and the working point has to be carefully adjusted to prevent particles from touching resonances, as this would result in transverse emittance blow up and, consequently, in significant reduction of the beam brightness or even beam loss.

The current production scheme of LHC beams, including the long flat bottom of around 1.2 seconds, has already been addressed in Section 2.2. Keeping a beam with such large ΔQ on this injection plateau requires detailed knowledge of all the appearing resonances in order to continuously optimize the working point and to contribute to the conservation of transverse beam parameters throughout the injector chain. To improve the understanding of the resonances present in the PS, tune diagram measurements have been carried out at the current injection

energy of 1.4 GeV as well as at the injection energy foreseen by the LIU project, 2 GeV. The method that has been used to conduct these measurements is based on an experiment by G. Franchetti et al. at the GSI laboratory in Darmstadt in 2004 [35].

4.1 Measurement principle

In order to efficiently detect resonances, a single bunch with large transverse emittances is injected and kept bunched on a flat bottom for more than one second (see Fig. 4.1). On this plateau both tunes are varied in a defined way, provoking particle oscillations with increasing amplitude as resonances are crossed. Due to the large emittance the beam almost completely fills the vacuum chamber of the machine and losses will be observed once the working point is set close to a resonance. Evaluation of these losses and putting them into correlation with both tunes finally leads to a representation of the tune diagram.

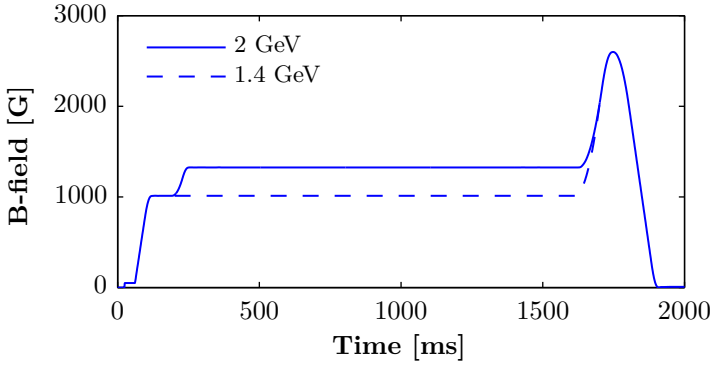

Figure 4.1: Magnetic configurations used for the tune diagram measurements.

The dependence of the measurement sensitivity on the transverse beam characteristics is shown in Fig. 4.2. The intensity profile has been measured by using a beam current transformer (BCT), providing a signal each ms [36]. In the case of a beam with a large average emittance losses are more pronounced as increased particle amplitudes caused by weak resonances already suffice to touch the vacuum chamber. Therefore, the measurements described in this chapter have been carried out with large transverse emittances from the PSB, namely $\varepsilon_x \approx 10$ mm·mrad and $\varepsilon \approx 7.5$ mm·mrad[1,2]. In the PS the transverse emittances are measured by means of wire scanners placed in different straight sections of the machine. These devices flip a thin wire with a velocity of 15 m/s through the circulating beam, creating secondary particles, which are then detected by an arrangement of scintillators and photomultipliers. Correlation of the position of

[1] Detailed beam parameters are found in the Appendix.

[2] These emittances result in 1σ beam sizes of 11 mm in the horizontal and 13 mm in the vertical plane. This is valid for the respective beta-functions in straight sections 54 and 64 of the PS, where horizontal and vertical wire scanners are situated.

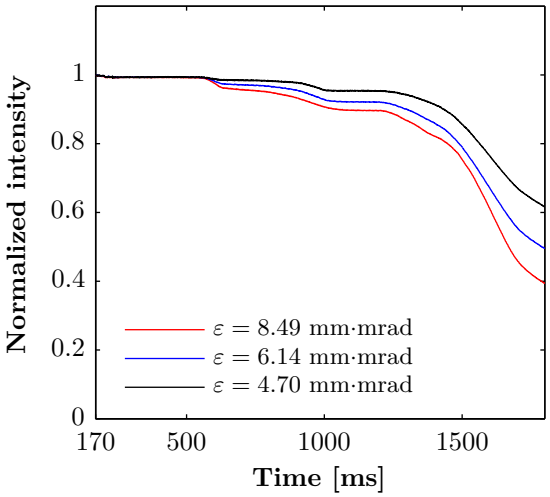

Figure 4.2: Influence of the emittance on resonance crossing. Displayed is the average emittance $\varepsilon = \frac{\varepsilon^*_{x,1\sigma}+\varepsilon^*_{y,1\sigma}}{2}$. The space charge effect remains unchanged in all three cases as a decrease of emittance is obtained by decreasing the beam intensity. Starting at 500 ms the vertical tune has been dynamically changed from 0.1 to 0.4 all along the flat bottom while the horizontal value was fixed to 6.28.

the wire and the respective signal coming from the photomultiplier then allows to calculate the emittance [37].

Furthermore, the space charge tune spread of the beam has to be kept small to avoid multiple resonance crossing as the space charge "neck tie" touches several stop bands at the same time. The large transverse emittance already favors this fact. Additionally, a moderate number of protons per bunch has been chosen.

To obtain knowledge of the whole tune diagram, four steps have to be taken and each of them is shown in Fig. 4.3. The scan of the tune diagram can be conducted either horizontally or vertically, causing one tune to be fixed while a dynamic change occurs in the other plane. In order to fully benefit from the magnetic cycle shown in Fig. 4.1, this scan was programmed over 1300 ms, leaving enough time for the particles to feel the influence of resonances. To measure each of the tunes, data is acquired over three consecutive cycles and only afterwards the beam intensity from the BCT is recorded. This is important in view of the fact that the excitation by the BBQ system provokes additional losses, causing a distortion of the measurement.

The appearing losses already give a qualitative image of the excited resonances. However, by taking the derivative of the intensity curve, losses, and therewith resonances, clearly appear and their strengths and widths can be extracted. In a last step all points describing a certain resonance are normalized by the intensity before crossing this respective resonance in order to account for the different initial conditions due to the reduction of intensity.

Extensive information of the tune diagram can then be obtained by changing the tune which

was kept constant by a defined step size - for all following measurements a step of 0.01 has been chosen - and repeating the four steps. The complete set of tunes and normalized derivatives is then interpolated on an equidistant grid and a two-dimensional plot where color scaling describes beam loss can be produced.

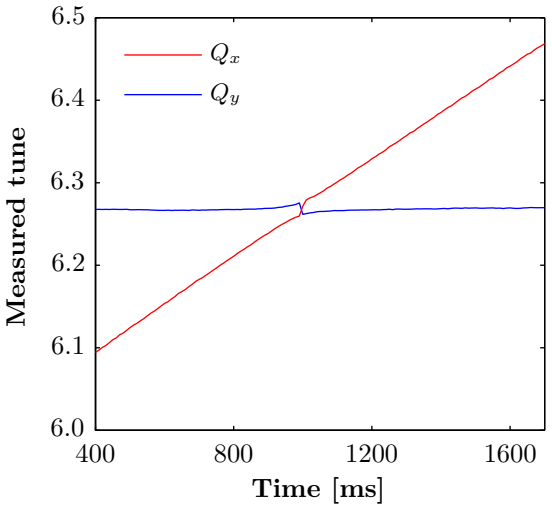

(a) Tunes as measured with the BBQ system. The dynamic change of the vertical tune and the effect of linear coupling when both tunes cross are clearly visible. As mentioned in Section 3.1 the error is in the order of 10^{-3}.

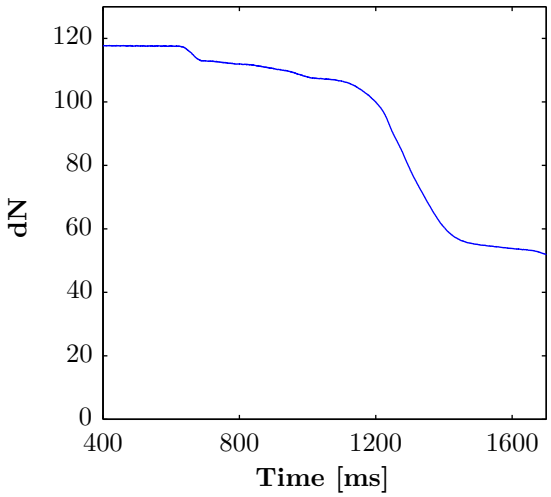

(b) Intensity measured with the BCT, the relative error being less than 1%. The change of the slope is due to different resonances with different strengths.

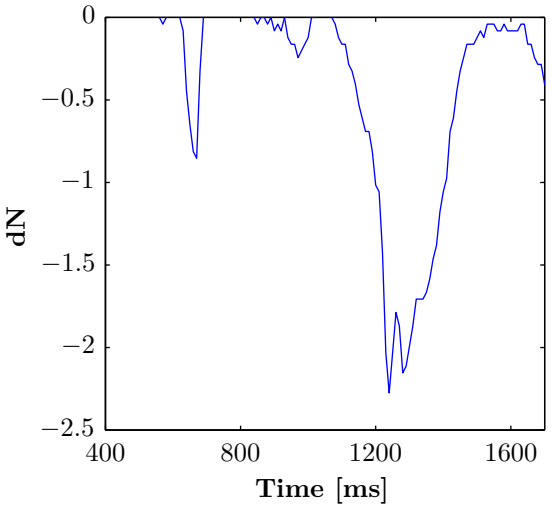

(c) Numerical derivative of the intensity curve representing losses. Several resonances can be clearly identified.

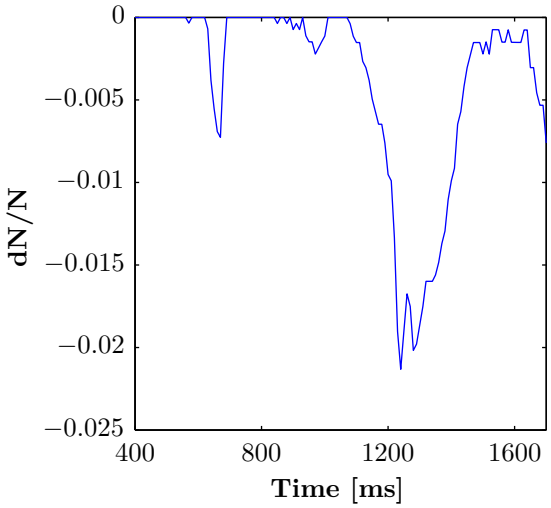

(d) Normalization of all points belonging to a certain resonance to the beam intensity before crossing the respective resonance.

Figure 4.3: Necessary steps to obtain a graphical representation of the working point plane.

4.2 Tune diagram at 1.4 GeV

At current injection energy the LEQ are used to control the tunes. Unfortunately, their RMS[3] current is limited to relatively small values, restricting the reachable area within the tune diagram to approximately 0.1 - 0.4 in both planes. Nevertheless, Fig. 4.4 already shows the appearance of several resonances, especially the linear coupling and the two 3^{rd} order lines $-q_x + 2q_y = 0$ and $2q_x + q_y = 1$, where the fractional part of the tune is used for nomenclature. Blue parts describe the working point settings that do not cause beam loss while the opposite is valid for red areas. The gray colored parts of the tune diagram represent configurations where either the tunes could not be measured or the beam could not even be injected. The overall dimensions of the plot have been chosen in order to be comparable with the measurements at 2 GeV that are going to be described in the following section.
As stated in Section 3.1 above, the LEQ do not introduce non-linearities, and the linear behavior of the bare machine is therefore not altered. However, this does not exclude the presence of non-linearities in general. Alignment and construction of magnets and other elements of the machine is always limited by certain tolerances, successively leading to errors within the magnetic field.

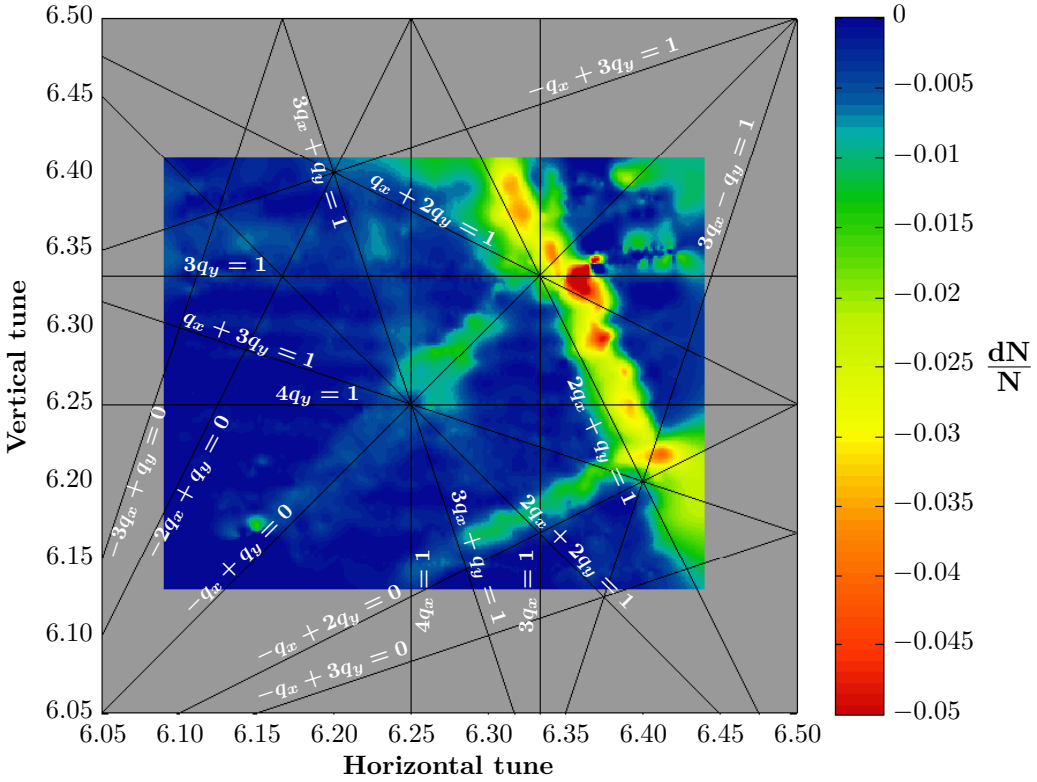

Figure 4.4: Tune diagram of the CERN PS at 1.4 GeV. The tunes have been controlled with the LEQ only.

[3] Root Mean Square

As well as the contribution of the fringe fields of the main magnets and the possible non-linearities within the junctions between the focusing and the defocusing half units, these errors are considered to be the cause of appearing resonances. In order to already see these higher order components in the measurement presented in Fig. 3.1b one would need to go to higher amplitudes where tune changes due to octupole fields and the large radial offset may appear.
The strongest resonance is clearly the 3^{rd} order $2q_x + q_y = 1$ which is a non-linear coupling resonance and, therefore, excited by skew sextupole components. On the other hand, the presence of an octupole component and a large orbit excursion due to a large beta-function at the respective position could also cause this resonance [38, 39].
Another interesting point is the shift of the measured resonances with respect to the resonances expected in theory, which seems to be caused by an interplay of space charge effects and coupling of the longitudinal and transverse motion due to the large uncorrected chromaticities. It has been verified that the shift is not caused by the analysis algorithm, which is plausible, as different resonances are shifted in different directions. This effect is not addressed further in this thesis and, therefore, remains to be fully understood.

4.3 Tune diagrams at 2 GeV

Unlike the measurements at 1.4 GeV, the tune diagrams at the future PS injection energy have been obtained by using only the PFW. This choice was based on the specifications of the LEQ, as their current constraints reduce the reachable area within the working point plane even further at increased energy and, therefore, the LEQ would require a significant upgrade in order to control the tunes of all different types of beams in a reliable way at 2 GeV. For the PFW this is not the case as these circuits have to control the beam parameters up to maximum energy and are therefore designed accordingly.
To program the tunes with the PFW, the operational matrix in 4CM has been used as this approach allows to influence both tunes without changing the bare machine chromaticites (see Section 3.2). The matrix can therefore be used in five configurations where, depending on the choice of the fixed circuit, additional resonances compared to the 1.4 GeV case might be observed due to the arising non-linearities. These effects have to be studied in detail as the requirements of the HL-LHC lead to a tune spread of $\Delta Q_y = -0.32$ at injection [40] which is higher than the values of today's space charge dominated beams.

4.3.1 The fixed narrow windings

The first tune diagram measurements with PFW have been conducted by fixing the narrow windings and programming a scan in the horizontal direction, i.e. keeping the vertical tune constant and dynamically changing the horizontal one from 6.10 to 6.47.

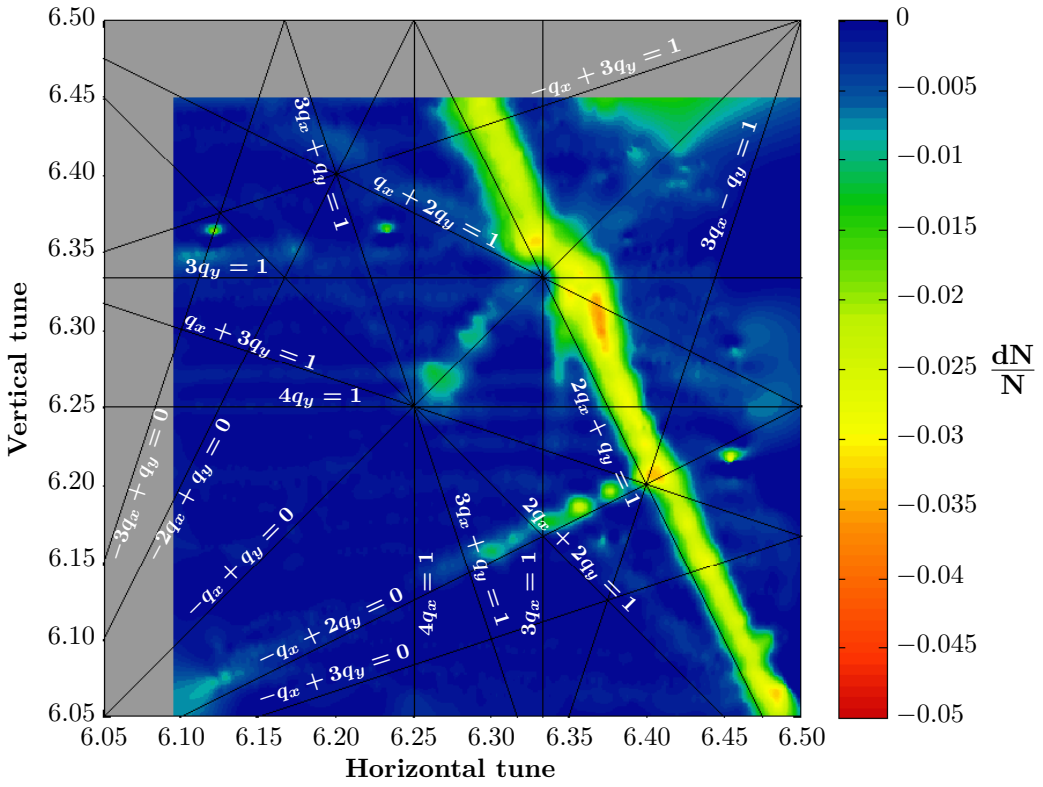

Figure 4.5: Tune diagram at 2 GeV with fixed FN.

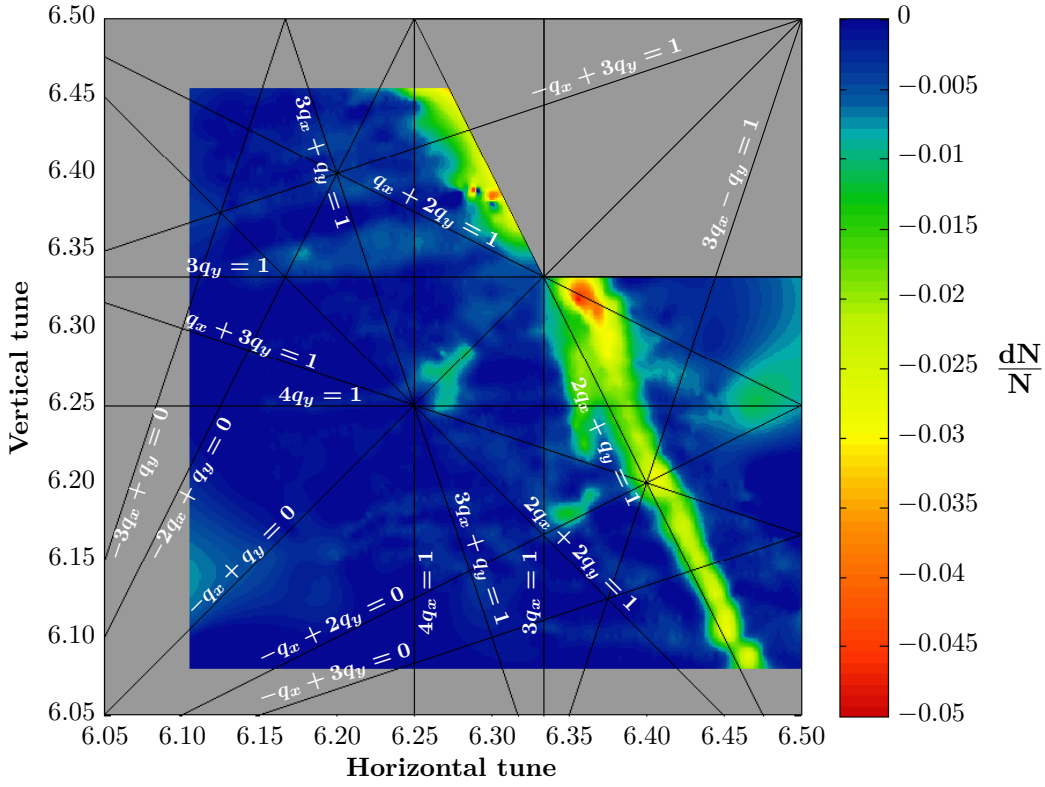

Figure 4.6: Tune diagram with fixed DN. In the upper right corner no clear tune signal could be obtained and the area is therefore not considered.

These programmed values are not necessarily consistent with the presented measurements, which can be traced back to the area of validity of the matrix, as especially the working points in the beginning of the scan are far away from the bare machine tune.
The results in Figs. 4.5 and 4.6 show the same resonances as the scan at 1.4 GeV revealed and furthermore, the extended measurement area is clearly visible. In Fig. 4.5 slight evidence of the 3^{rd} order resonance $3q_y = 1$ also appears.

4.3.2 The fixed wide windings

Scanning the working point plane with fixed wide windings leads not only to the appearance of additional resonances but also to more distinct beam losses compared to previous measurements as shown in Figs. 4.8 and 4.9.
In agreement with the results obtained in Section 3.2.2, this can be explained by the influence of the narrow windings on the non-linear behavior of the machine. In Figs. 3.10 and 3.11 small currents flowing through the narrow windings were shown to significantly change the non-linearities. According to these plots the major change of the magnetic configuration is caused by the DN.
Fixing, for example, the FW at a current of zero ampere causes the tune ramp to be established by the remaining circuits (see Fig. 4.7). Therefore, a non-negligible amount of current is programmed in both the DN and the FN, causing the additional 3^{rd} order resonances and losses as well as the increased width of the stop band of the skew sextupole line.

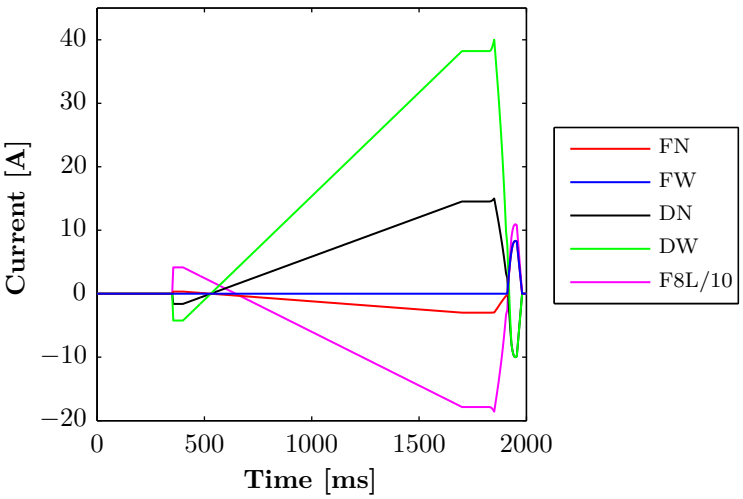

Figure 4.7: Currents in the PFW to scan horizontally at $Q_y = 6.40$ by fixing the FW.

In case the scan is being programmed with a fixed narrow winding, the tune change is mainly based on the currents within the wide windings, leading to less non-linearities as it has already been shown in Figs. 4.5 and 4.6.

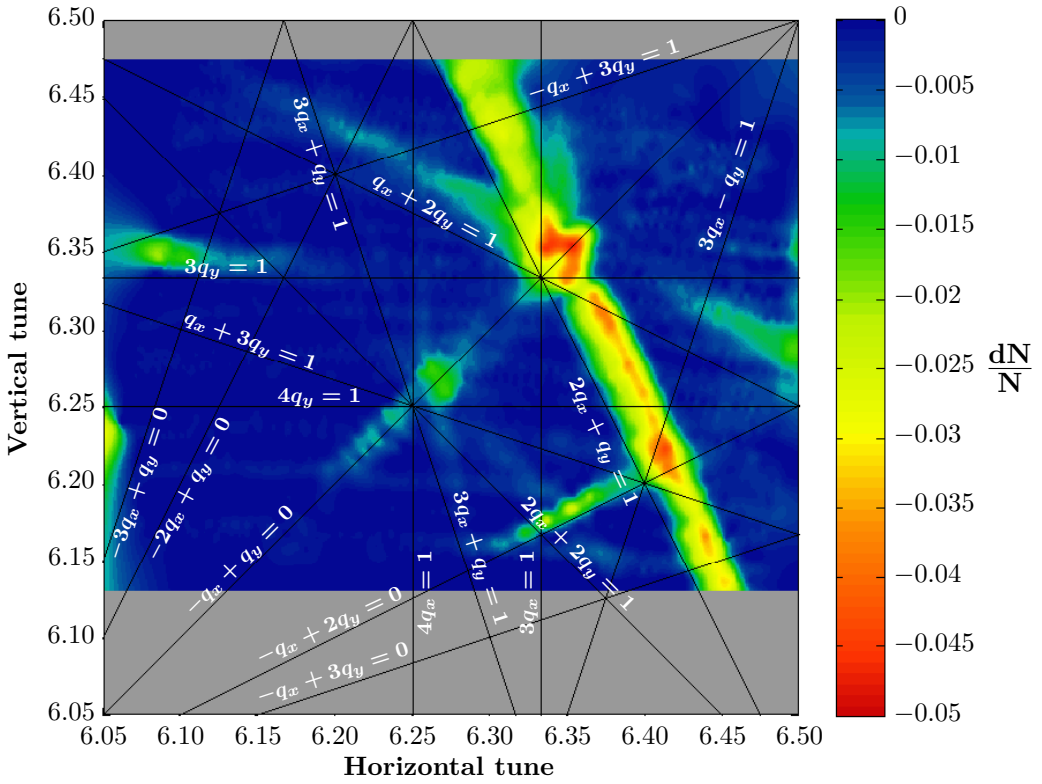

Figure 4.8: Tune diagram with fixed FW. Additional 3^{rd} order lines appear.

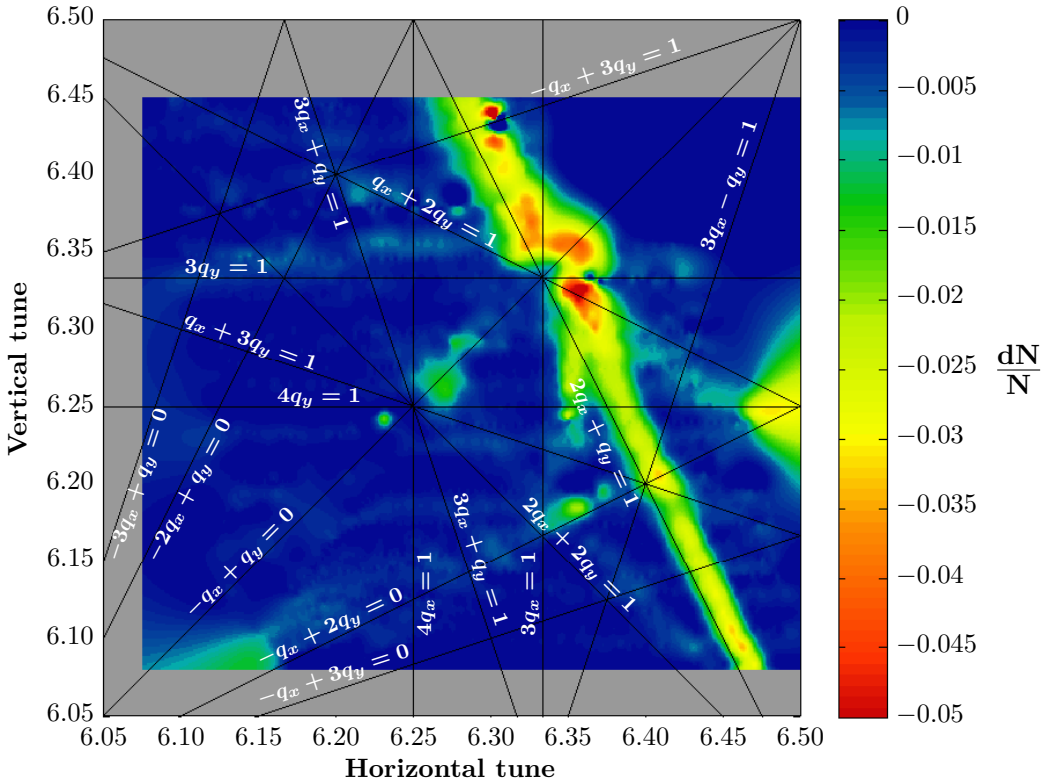

Figure 4.9: Tune diagram with fixed DW.

4.3.3 The fixed F8L

The last possible scan in 4CM can be conducted by fixing the F8L, causing the beam parameters to be controlled exclusively with both narrow and wide circuits. Contrary to Fig. 4.7, Fig. 4.10 shows less current within the DN and also less unbalancing of the defocusing circuits, while the current in the FW is higher than for all the others.

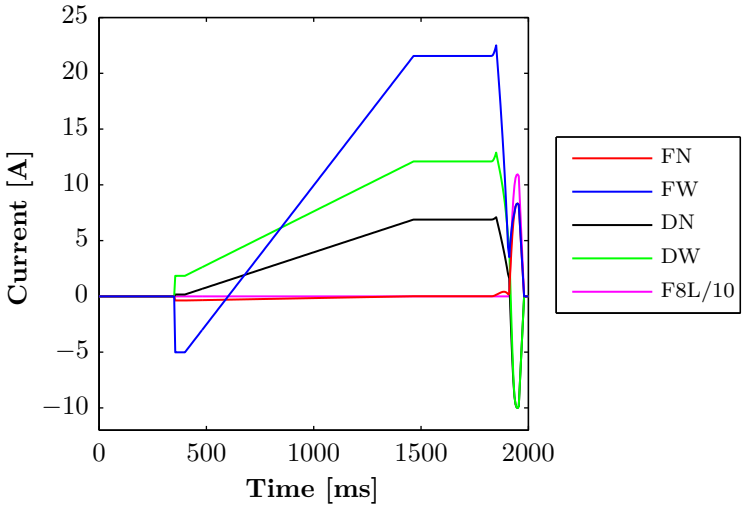

Figure 4.10: Currents in the PFW to scan horizontally at $Q_y = 0.40$ by fixing the F8L.

However, the FW does not seem to severely enhance the higher order components of the magnetic field, as the result of the horizontal scan in Fig. 4.11 does not reveal additional resonance lines. In fact, fixing the F8L seems to be the most interesting configuration for future operation as it causes less beam loss and excitation of resonances compared to all previous scans.
Due to this fact the configuration with fixing the F8L was subject to more detailed examination and the first further step was to conduct a horizontal scan in the inverse direction (see Fig. 4.12). The strong natural resonance is therefore crossed in the beginning of the ramp and the losses are more pronounced as the beam intensity and emittances virtually correspond to the initial conditions. Additionally, the resonance $3q_y = 1$ appears only slightly but was not seen at all when scanning in the normal direction.
In order to gain further insight into and understanding of the working point plane with this special PFW setup, two scans in the vertical direction have been performed and are shown in Figs. 4.13 and 4.14. The skew sextupole resonance is again clearly visible, although weaker than in the normal scan. The most interesting fact is, however, the appearance of the lines $3q_y = 1$ and $q_x + 2q_y = 1$, which have never been so pronounced in previous scans.
To understand this discrepancy between the scans in horizontal and vertical direction an additional study has been conducted and is presented in the following section.

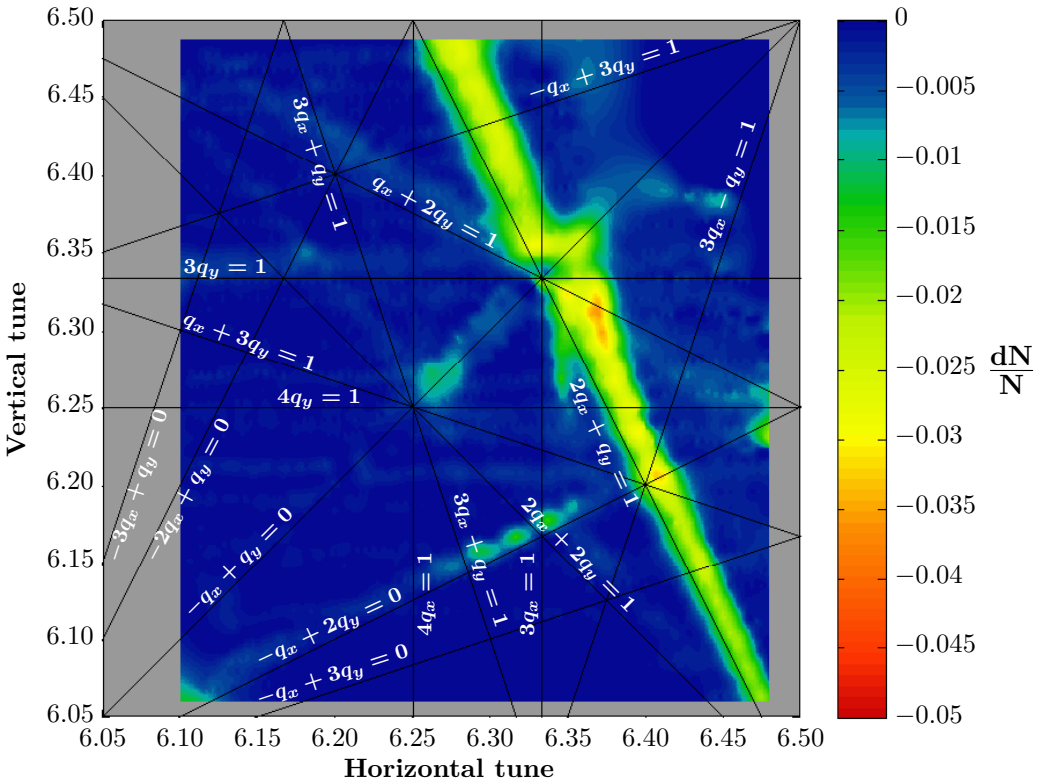

Figure 4.11: Tune diagram with fixed F8L and horizontal scan.

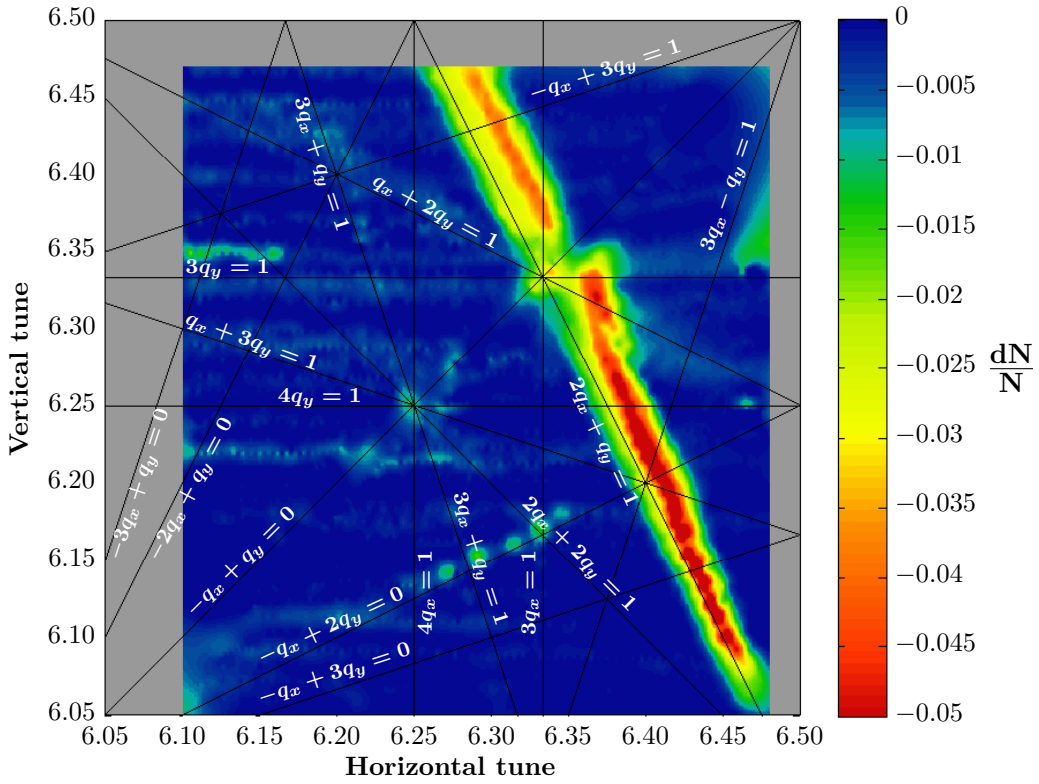

Figure 4.12: Tune diagram with fixed F8L. For this measurement a horizontal scan in the inverse direction - from 0.47 to 0.1 - was programmed.

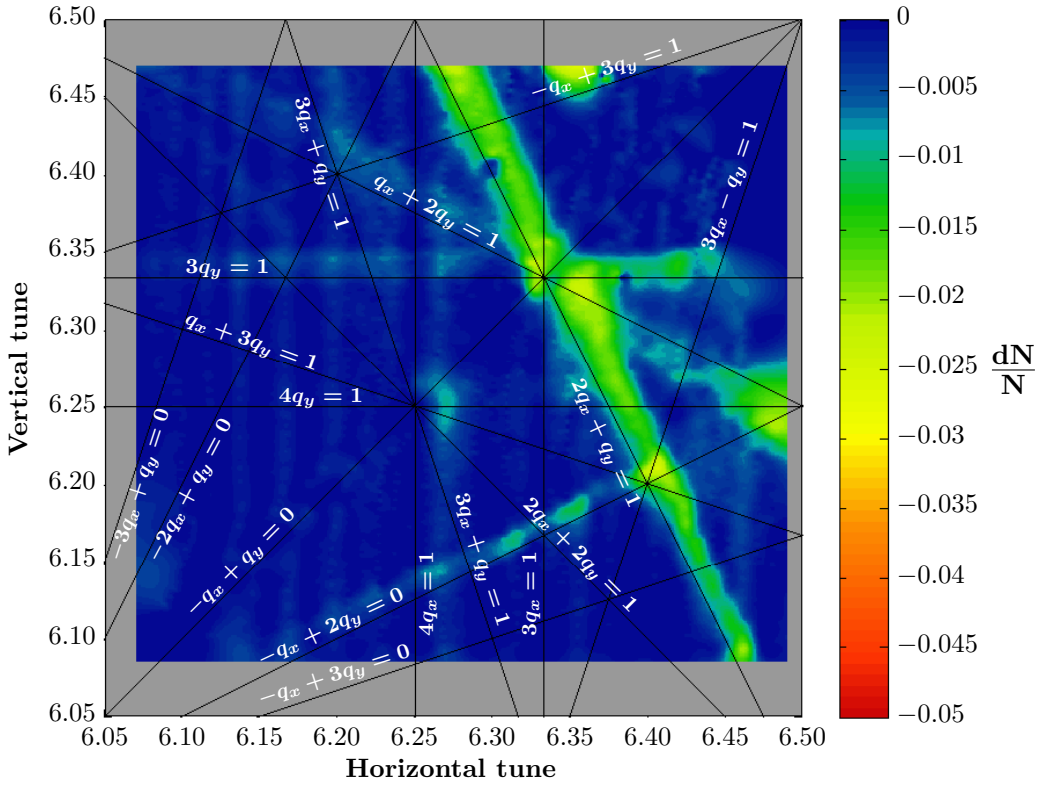

Figure 4.13: Tune diagram with fixed F8L and scan in the vertical direction.

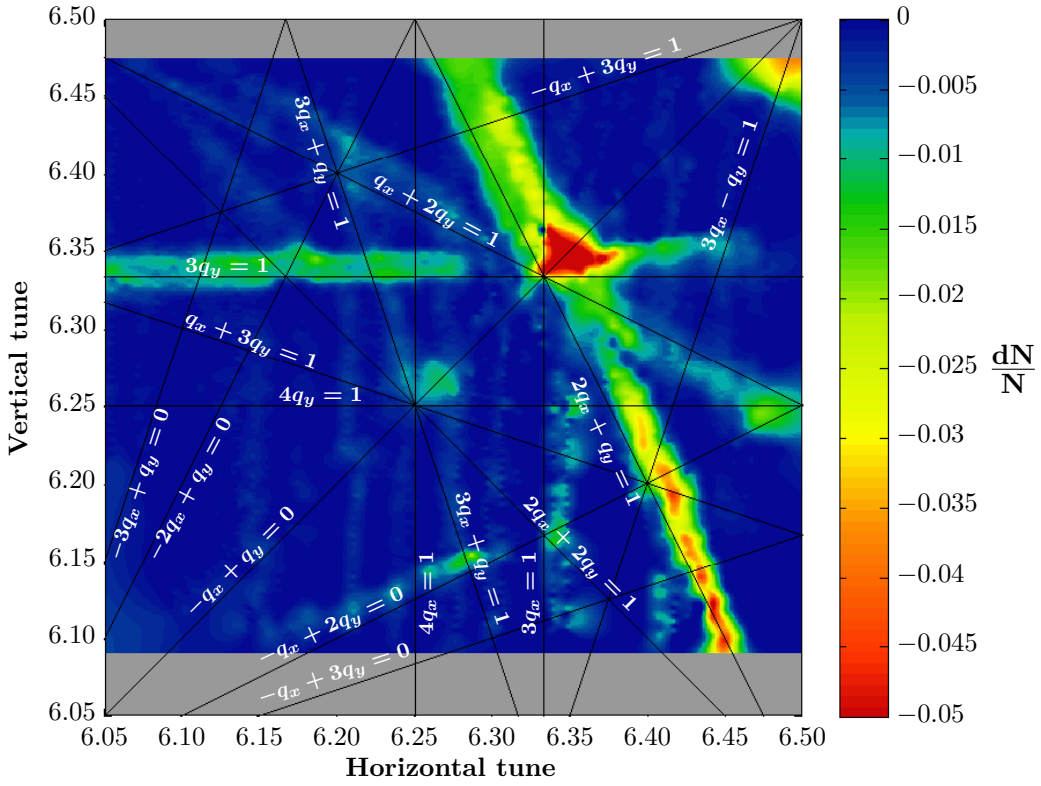

Figure 4.14: Tune diagram with fixed F8L and inverse vertical scan.

4.4 Examination of the resonance $3q_y = 1$

The scan in Fig. 4.14 clearly reveals the existence of the 3^{rd} order resonance $3q_y = 1$. To further examine whether this is an effect caused by the PFW or already present for the bare machine, an inverse vertical scan at 1.4 GeV with the LEQ has been carried out in a restricted area. Figure 4.15 confirms the presence of both 3^{rd} order lines that were already discovered in Fig. 4.14.
It is, however, astonishing that the resonance $q_x + 2q_y = 1$ appears to be stronger than in the cases when the scan was done with the PFW. One potential explanation is based on the effect of the octupole component within the magnetic field, which causes a change of the tune of a particle depending on its oscillation amplitude. In case the beam becomes transversely unstable, this amplitude dependent detuning provides a stabilizing mechanism, as the collective motion decays faster and the oscillations that could lead to beam loss are therefore damped. This effect was first described by Landau and is therefore known as Landau damping [41].

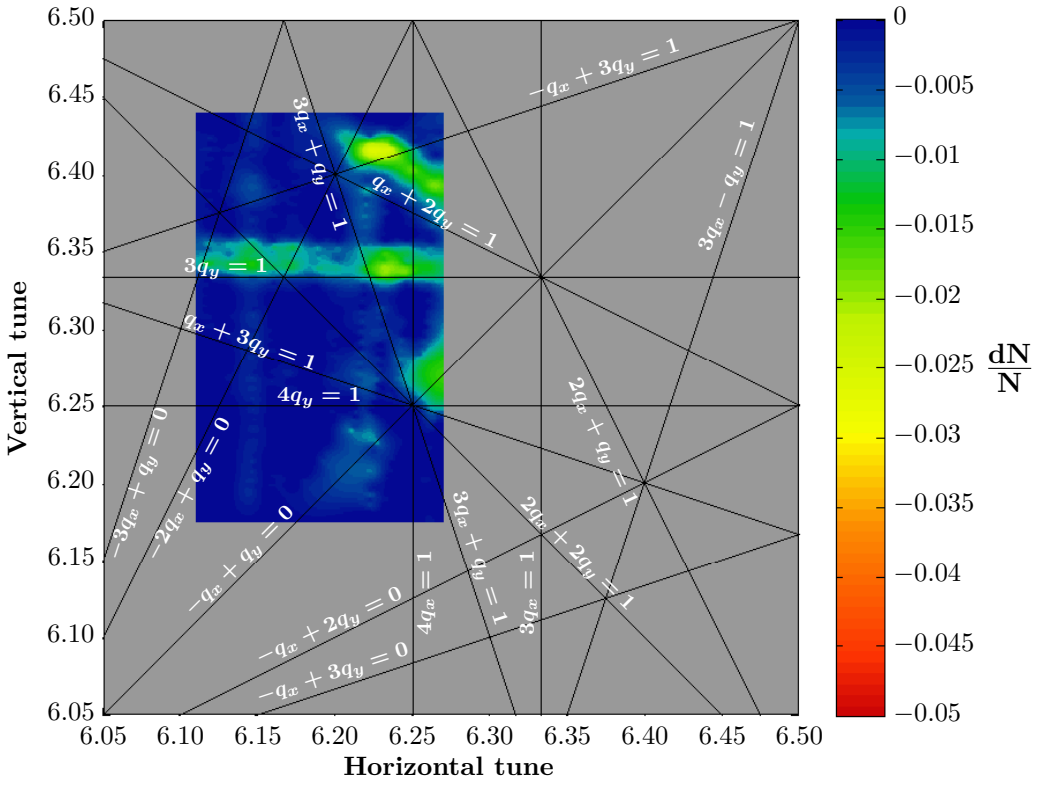

Figure 4.15: Tune diagram obtained at 1.4 GeV with the LEQ. The small area has been chosen to examine only the line $3q_y = 1$.

The appearance of the 3^{rd} order resonances depends on the direction of the scan and, therefore, indicates an intrinsic limitation of the measurement procedure.

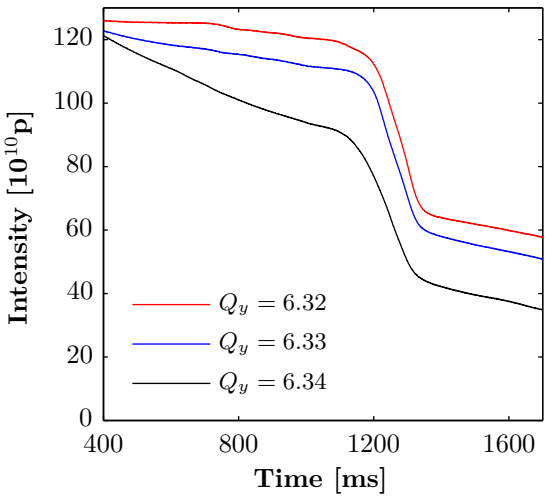

(a) Measured intensity for a horizontal scan in the normal direction. The red curve represents a working point slightly below the stop band of the resonance $3q_y = 1$. Once the resonance is touched, beam loss appears.

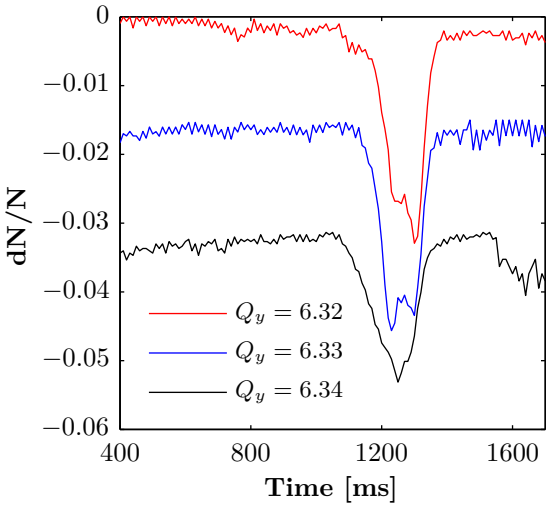

(b) Numerical derivatives of the curves in Fig. 4.16a. The peaks correspond to the skew sextupole resonance while the line $3q_y = 1$ is concealed by the noise. The curves have been offset to improve visibility.

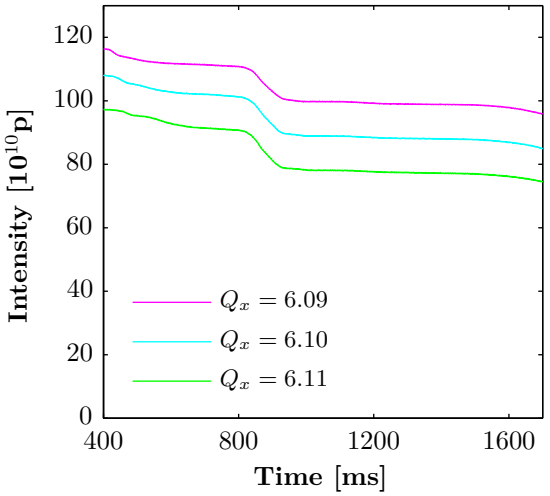

(c) Measured intensity for a vertical scan in the inverse direction. The loss at 800 ms is clearly connected to the resonance $3q_y = 1$. As all three lines almost overlap, an offset has been added.

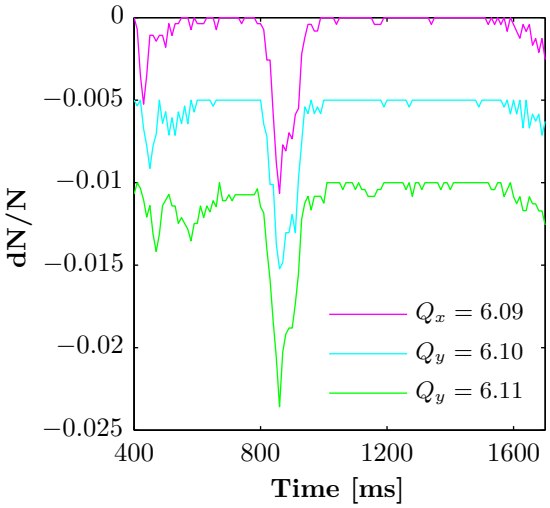

(d) Clear identification of the resonance $3q_y = 1$ is now possible. Flat parts of the derivatives are obtained when the noise level rises to positive values, which would correspond to physically impossible particle creation. These points have therefore been set to zero. Again an offset has been added.

Figure 4.16: Detailed analysis concerning the appearance of the resonance line $3q_y = 1$.

In Fig. 4.16 the origin of this limitation is explained. The calculation of the derivative is more sensitive to local beam loss and, therefore, to a vertical scan. In a horizontal scan the beam is placed on the resonance throughout the cycle and constant losses appear as a background effect.

4.5 Combination of results

The major part of the scans of the working point plane has been conducted at the future injection energy of 2 GeV, with the working point being controlled exclusively by the PFW in 4CM. Five different configurations of the PFW have been used to obtain graphical representations of the tune diagram. In all these measurements the skew sextupole resonance appeared. However, additional resonances could be observed as well, which are particularly caused by the influence of the narrow windings.

The configuration with the F8L being fixed to a current of zero ampere was subject to detailed studies, as it appeared to be almost resonance-free in the region, where the injection working points of the operational beams are situated today.

In Fig. 4.17 a combination of the horizontal scan in Fig. 4.11 and the inverse vertical scan in

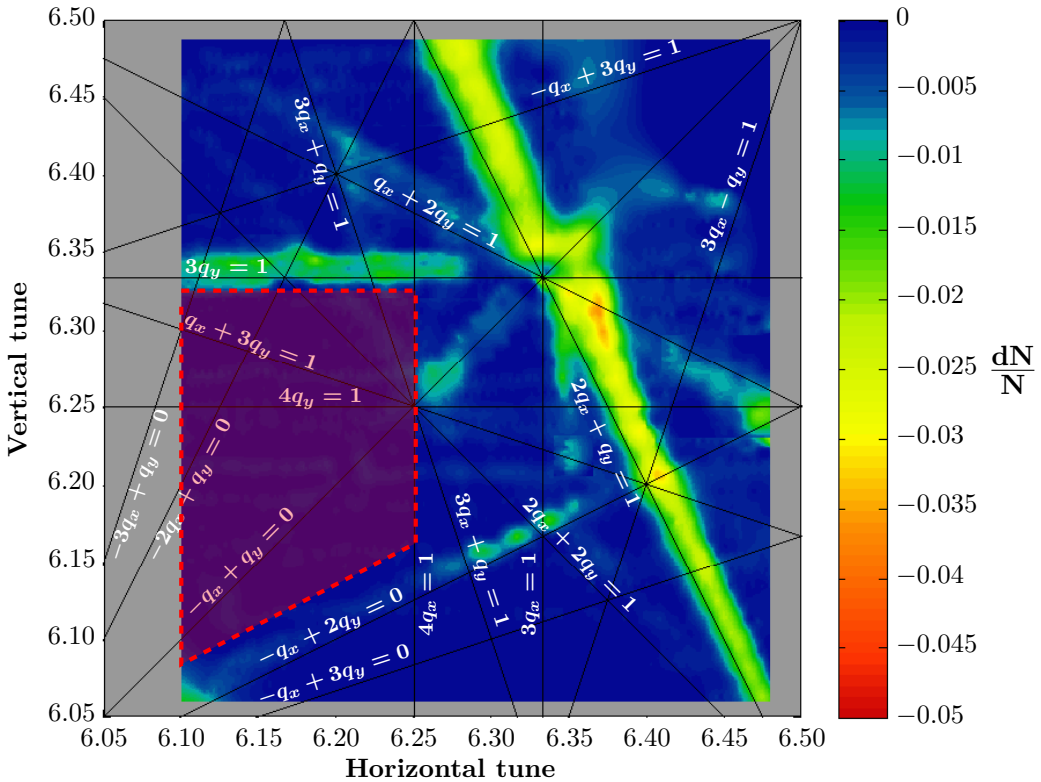

Figure 4.17: Combination of the plots in Figs. 4.11 and 4.14. The most beneficial region for an injection working point is highlighted in red.

Fig. 4.14 is shown. Within the red emphasized area no resonance lines appear to be excited, causing this to be the optimum region for working points at injection. The choice of the working point is restricted by the 3^{rd} order lines $3q_y = 1$ and $-q_x + 2q_y = 0$ and the horizontal 4^{th} order resonance $4q_x = 1$. Even though not directly visible, it is essential to consider both the horizontal and the vertical integer resonances as well.
The 50 ns LHC beam is injected at (6.235, 6.245) with a calculated Laslett tune spread of (0.19, 0.28), causing the beam in theory to cross the resonance $-q_x + 2q_y = 0$ and even the vertical integer. However, no beam loss or degradation of the beam quality by modification of the transverse or longitudinal characteristics is currently observed for this space charge dominated beam.

5 Conclusions and outlook

Depending on the energy of the circulating beam, different elements are used to control tunes and chromaticities at the CERN PS. At today's injection energy of 1.4 GeV, control of the working point is realized by the LEQ. Unlike the PFW, these magnets do not offer a possibility to correct chromaticity. Currently, this is not an issue for machine operation but it might become a limitation for future high-brightness and high-intensity beams, as a chromaticity correction scheme, together with a damper system, has a beneficial impact on curing Head-Tail instabilities. Therefore, extensive studies have been conducted within this thesis to examine the influence of the PFW on the operation of the machine.

In Chapter 3 it was shown, that independent powering of the five circuits of the PFW leads to non-linearities within the magnetic field. Based on the 5CM matrix formalism, the feasibility of influencing the different magnetic components and, therefore, the beam parameters was studied at a kinetic energy of 2 GeV.

The control of both transverse tunes was discovered to work in the expected way, while this was not the case for the linear and second order chromaticities. In order to understand this discrepancy, an improvement of the magnetic model of the PS would be highly beneficial, as by simulations matrices with far larger validity can be calculated. Experimentally it was not possible to enlarge this area as the measurement process is limited by the stability of the beam. Additionally, the 5CM matrices should be measured for a working point different from (6.10, 6.20). Ideally, one would choose the working point in such a way, that the measurements can no longer be corrupted by the presence of linear coupling around the central orbit.

The effect of the PFW on the non-linear behavior of the machine could also be studied at an energy different from 2 GeV. So far, only linear chromaticity is changed when the operational beams approach transition. These changes are programmed in 3CM and studying the influence of 5CM on the properties of the magnetic field would also lead to deeper insight of the CERN

PS.
Failing this, the approach of reducing the observed non-linearities with a linear formalism may be naïve. One could therefore try to use the two different octupole families which are currently installed - seven distributed octupoles, the ODEs, or the octupoles for the multi-turn extraction [42] - to examine their impact on machine operation in the presence of higher order magnetic fields.
The arising non-linearities are likely to cause betatron resonances in addition to the ones present in the bare machine and, therefore, scans of the working point plane have been conducted with the aim of identification of beam destructive resonances. Already for the bare machine, the skew sextupole resonance $2q_x + q_y = 1$ was found to be very strong and its origin remains to be understood. A multitude of effects such as alignment or magnet production errors or potential non-linear magnetic fields between the focusing and defocusing half unit of the main magnet could be a cause. Recently the skew errors of the magnetic field have become available by simulations, allowing to benchmark the theoretical model of the PS and ideally to reproduce this natural resonance. Additionally, skew sextupoles will be hopefully installed in the machine during the winter 2012 to investigate the feasibility of resonance compensation [43].
The measurements in Chapter 4 clearly revealed a promising candidate for tune control with the PFW at injection, namely the configuration with the fixed F8L. Based on the appearing resonances and on the fact, that for the operational LHC beams no emittance blow up is observed, one can estimate the maximum acceptable tune spread to be $\Delta Q \approx -0.35$. However, additional measurements need to be launched to determine the limitations in detail.
Therefore, beams with different Laslett tune spreads have to be injected and the working point has to be increased up to $Q_y = 6.30$ or even beyond, if possible. These measurements will provide additional information about the maximum acceptable ΔQ and the influence of the vertical integer resonance $Q_y = 6.0$. In contrast to measuring beam loss, it will then be important to examine the influence of the crossed resonances on transverse and longitudinal beam characteristics, because even without losing particles the beam quality may drastically degrade.
Additionally, tune diagram measurements should be carried out to see if controlling chromaticity with the PFW at 2 GeV causes excitation of additional resonances. This is important concerning future proton beams, which might require a chromaticity correction scheme already at injection.
The studies presented in this thesis as well as the ones additionally mentioned allow one to determine whether the CERN PS in its current shape will be able to provide the transverse beam specifications required by the HL-LHC.

References

[1] E. Wilson, *An introduction to particle accelerators*, ISBN 0-19-850829-8, Oxford University Press, United Kingdom, 2001

[2] H. Wiedemann, *Particle accelerator physics*, ISBN-13 978-3-540-49043-2, Springer, Berlin Heidelberg New York, 2007

[3] M. Giovannozzi, *Tune, chromaticity and coupling observables*, CARE NA3 Workshop, Chamonix, France, 2007

[4] K. Schindl, *Space charge*, in Proceedings of CAS - CERN Accelerator School, Basic course on general accelerator physics, Loutraki, Greece, 2000, CERN-2005-004, pp. 285-300

[5] H. Burkhardt, G. Rumolo, and F. Zimmermann, *Investigation of space charge effects in the SPS*, CERN-AB-2003-013-ABP

[6] R. Steerenberg, *Introduction to accelerator physics, AXEL 2012*, CERN-BE/OP Shutdown Lectures, Geneva, Switzerland, 2012

[7] n_TOF web page, *https://ntof-exp.web.cern.ch/ntof-exp/*

[8] S. Gilardoni (Ed.), D. Manglunki (Ed.) et al., *Fifty years of the CERN Proton Synchrotron*, CERN-2011-004, pp. 1-28

[9] M. Juchno, *Electromagnetic FEM analysis of the CERN Proton Synchrotron main magnet unit*, CERN-Thesis-2009-175, p. 21

[10] J.-P. Burnet and O. Michels, *Projet de Consolidation des Convertisseurs PFW*, CERN Note Technique AB-PO N10 (EDMS585302), 2005

[11] M. Juchno, *Electromagnetic FEM analysis of the CERN Proton Synchrotron main magnet unit*, CERN-Thesis-2009-175, p.23

[12] O. Brüning (Ed.), P. Collier (Ed.), P. Lebrun (Ed.), S. Myers (Ed.), R. Ostojic (Ed.), J. Poole (Ed.), P. Proudlock (Ed.) et al., *LHC Design Report, v.1: The LHC main ring*, CERN-2004-003-V-1

[13] M. Benedikt (Ed.), P. Collier (Ed.), V.Mertens (Ed.), J. Poole (Ed.), K. Schindl (Ed.) et al., *LHC Design Report, v.3: The LHC injector chain*, CERN-2004-003-V-3, Part 4, pp. 263-356

[14] M. Benedikt (Ed.), P. Collier (Ed.), V.Mertens (Ed.), J. Poole (Ed.), K. Schindl (Ed.) et al., *LHC Design Report, v.3: The LHC injector chain*, CERN-2004-003-V-3, Chapter 2, pp. 5-11

[15] G. Arduini and W. Venturini Delsolaro, *Summary of the limitations to the LHC performance*, in Proceedings of the 2011 Evian Workshop on LHC Beam Operation, CERN-ATS-2012-083, pp. 25-28

[16] Entry in the PSB eLogbook, *https://ab-dep-op-elogbook.cern.ch*, Morning shift, 06.09.2012

[17] M. Benedikt (Ed.), P. Collier (Ed.), V.Mertens (Ed.), J. Poole (Ed.), K. Schindl (Ed.) et al., *LHC Design Report, v.3: The LHC injector chain*, CERN-2004-003-V-3, Chapter 7, pp. 45-64

[18] Entry in the PS eLogbook, *https://ab-dep-op-elogbook.cern.ch*, Morning shift, 06.09.2012

[19] High Luminosity LHC web page, *http://hilumilhc.web.cern.ch/HiLumiLHC/index.html*

[20] O. Brüning (Ed.), P. Collier (Ed.), P. Lebrun (Ed.), S. Myers (Ed.), R. Ostojic (Ed.), J. Poole (Ed.), P. Proudlock (Ed.) et al., *LHC Design Report, v.1: The LHC main ring*, CERN-2004-003-V-1, p.21

[21] The ATLAS Collaboration, *Observation of a new particle in the search for the Standard Model Higgs boson with the ATLAS detector at the LHC*, CERN-PH-EP-2012-218

[22] The CMS Collaboration, *Observation of a new boson at a mass of 125 GeV with the CMS experiment at the LHC*, CERN-PH-EP-2012-220

[23] H. Damerau, R. Garoby, S. Gilardoni, B. Goddard, K. Hanke, A. Lombardi, M. Meddahi, B. Mikulec, E. Shaposhnikova, and M. Vretenar, *Upgrade plans for the LHC injector complex*, CERN-ATS-2012-111

[24] J. M. Paterson, *The 'Head-Tail' instability*, Stanford Linear Accelerator Center, Stanford, California, 1973

[25] R. Cappi, R. Garoby, and E. Métral, *Collective Effects in the CERN-PS beam for LHC*, CERN/PS 99-049, 1999

[26] M. Gasior, *The principle and first results of betatron tune measurement by Direct Diode Detection*, LHC-Project-Report 853, 2005

[27] R. Bartolini, A. Bazzani, M. Giovannozzi, W. Scandale, and E. Todesco, *Tune evaluation in simulations and experiments*, CERN SL/95-84 (AP), 1995

[28] M. Sands, *The head-tail effect: an instability mechanism in storage rings*, SLAC-TN-69-8, 1969

[29] P. Freyermuth, D. Cotte, M. Delrieux, H. Genoud, S. Gilardoni, K. Hanke, O. Hans, S. Mataguez, G. Métral, F. Peters, R. Steerenberg, and B. Vandorpe, *CERN Proton Synchrotron working point matrix for extended pole face winding powering scheme*, in Proceedings of IPAC 2010, Kyoto, Japan, THPE019

[30] A. Hofmann, *Present status*, in Proceedings of the First Workshop on LEP Performance, Chamonix, France, 1991, pp. 265-270

[31] M. Juchno, *Magnetic model of the CERN Proton Synchrotron main magnet unit*, in Proceedings of IPAC 2011, San Sebastian, Spain, WEPO019

[32] R. Cappi, *The PS in the LHC injector chain*, CERN-PS-97-016-CA, 1997

[33] H. Damerau, S. Gilardoni, S. Hancock, and R. Steerenberg, *Emittance growth MD at the PS*, November 2010, unpublished

[34] R. Wasef, H. Damerau, S. Gilardoni, G. Franchetti, A. Huschauer, A. Molodozhentsev, and F. Schmidt, *Space charge studies and impact on performance*, presented at the LIU Beam Studies Review Day, Geneva, Switzerland, 2012

[35] G. Franchetti, B. Franczak, and P. Schütt, *A benchmarking experiment in SIS for dynamic aperture induced beam loss*, GSI-Acc-Note-2004-05-001, Darmstadt, Germany

[36] D. Belohrad, *Fast beam intensity measurements for the LHC*, CERN-Thesis-2010-131

[37] Ch. Steinbach, *Emittance measurements with the CERN PS wire scanner*, CERN-PS-95-04, 1995

[38] C. J. A. Corsten, *Resonance and coupling effects in circular accelerators*, Doctoral thesis, Eindhoven University of Technology, 1982, Chapter 5

[39] H. Wiedemann, *Particle accelerator physics*, ISBN-13 978-3-540-49043-2, Springer, Berlin Heidelberg New York, 2007, pp. 621-630

[40] B. Goddard, *Can the proton injectors meet the HL-LHC requirements after LS2?*, presented at the LHC Performance Workshop 2012, Chamonix, France

[41] E. Wilson, *Non-linearities and resonances*, in Proceedings of CAS - CERN Accelerator School, Fifth general accelerator physics course, Jyväskylä, Finland, 1992, CERN-94-1, pp. 239-252

[42] R. Cappi and M. Giovannozzi, *Novel method for multi-turn extraction: trapping charged particles in islands of phase space*, Phys. Rev. Lett. **88** 104801, 2002

[43] P. Urschütz, *Measurement and compensation of betatron resonances at the CERN PS Booster Synchrotron*, CERN-Thesis-2004-043

Appendix

The tables in the following sections show the parameters defining the proton beams that were used to conduct the measurements within this thesis. All parameters are based on a programmed working point (6.15, 6.20), which was kept constant along the magnetic cycle and was established only by the LEQ.

A.1 Working point control

Parameter	**Timing [ms]**	
	190	400
Magnetic field [G]	1012.5	1325.4
Kinetic energy [MeV]	1.4	2
Momentum [Gev/c]	2.12	2.78
Harmonic number	8	8
Number of bunches	1	1
Number of protons per bunch [10^{10}]	55	55
Bunch length (4σ) [ns]	172	127
Relative momentum error (1σ) [10^{-3}]	0.84	0.94
Longitudinal emittance (matched area) [eVs]	1.01	1.09
Normalized horizontal emittance (1σ) [π·mm·mrad]	1.10	1.13
Normalized vertical emittance (1σ) [π·mm·mrad]	1.03	1.19

Table A.1: Beam parameters for the measurements explained in Chapter 3.

A.2 Resonance identification

A.2.1 Measurements at 1.4 GeV

Parameter	**Timing [ms]**
	200
Magnetic field [G]	1012.5
Kinetic energy [MeV]	1.4
Momentum [Gev/c]	2.12
Harmonic number	8
Number of bunches	1
Number of protons per bunch [10^{10}]	130
Bunch length (4σ) [ns]	186
Relative momentum error (1σ) [10^{-3}]	1.3
Longitudinal emittance (matched area) [eVs]	1.68
Normalized horizontal emittance (1σ) [π·mm·mrad]	12.65
Normalized vertical emittance (1σ) [π·mm·mrad]	4.20

Table A.2: Beam parameters for the measurements explained in Section 4.2.

A.2.2 Measurements at 2 GeV

Parameter	**Timing [ms]**	
	190	350
Magnetic field [G]	1012.5	1325.4
Kinetic energy [MeV]	1.4	2
Momentum [Gev/c]	2.12	2.78
Harmonic number	8	8
Number of bunches	1	1
Number of protons per bunch [10^{10}]	120	120
Bunch length (4σ) [ns]	151	117
Relative momentum error (1σ) [10^{-3}]	0.80	0.80
Longitudinal emittance (matched area) [eVs]	0.86	0.84
Normalized horizontal emittance (1σ) [π·mm·mrad]	10.30	10.40
Normalized vertical emittance (1σ) [π·mm·mrad]	7.65	7.64

Table A.3: Beam parameters for the measurements explained in Section 4.3.

A.2.3 Laslett tune spread

The calculation of the Laslett tune spread according to (1.21) leads to the following values:

- **1.4 GeV:** $\Delta Q_x = -0.051$, $\Delta Q_y = -0.094$
- **2 GeV:** $\Delta Q_x = -0.046$, $\Delta Q_y = -0.057$